EPFL

An autonomous microfluidic device for identification and analysis of individual clinically-relevant mammalian cells

Présentée le 12 novembre 2021

Faculté des sciences et techniques de l'ingénieur
Laboratoire de caractérisation du réseau biologique
Programme doctoral en biotechnologie et génie biologique

pour l'obtention du grade de Docteur ès Sciences

par

Fabien Louis Claude Robert JAMMES

Acceptée sur proposition du jury

Prof. A. Radenovic, présidente du jury
Prof. S. Maerkl, directeur de thèse
Prof. A. deMello, rapporteur
Prof. S. Reddy, rapporteur
Prof. M. Lütolf, rapporteur

École
polytechnique
fédérale
de Lausanne

2021

"Cell division allows us as organisms to grow, to adapt, to recover, to repair—to live. And distorted and unleashed, it allows cancer cells to grow, to flourish, to adapt, to recover, and to repair—to live at the cost of our living. Cancer cells can grow faster, adapt better. They are more perfect versions of ourselves."

— Mukherjee, Siddhartha. The Emperor of All Maladies: A Biography of Cancer (p. 6).

Acknowledgements

As this thesis can be considered as a keystone in my life, I would like to personally thank the many people who have contributed, helped or just motivated me during those four years and a half:

- First of all, the EPFL entity for the education I received within those walls, for the amazing people I met and all the different experiences I lived during this ten-year journey from undergrad to doctoral student.

- My professor, Sebastian Maerkl, for the warm welcome and continuous guidance he showed towards me and my project.

- My jury committee: Prof. Andrew deMello, Prof. Matthias Lütolf, Prof. Sai T Reddy & Prof. Aleksandra Radenovic, who took the time to evaluate my work.

- All of my colleagues at LBNC, most of them have become more than colleagues but real friends on and off the laboratory space. They have helped me, supported me and more importantly, provided a steady source of joy during the troubled times that can represent a doctoral thesis. A special thank you to Barbora Lavickova and Laura Grasemann, the best office colleagues there are. And a very special thank you to Evan Olson, without whom I would have probably given up on my thesis and for his invaluable help and guidance all along this project. Evan supported me in my research, helped me in time of struggle by showing me that the science I did mattered. His help cannot be overstated.

- My collaborators, Julien Schmidt, Alexandre Harari and Prof. George Coukos, who haven been of tremendous help for this whole adventure and have actively contributed to this project.

2

- My parents, who have raised me, taught me that the hardest fights are the best ones to have, and who have loved me through thick and thin all this years.

- My sister, for she represents both my mentor and mentee and has always been there for me.

- My grandparents, who have given me pure love and a motivation to exceed myself.

- My friends, who can read me like a book and have provided me with love, support and laughter during this thesis. A special thank you to Alexander Audouy, Laura and Maxime Curvat, Maelle Bezy, Lucien Trummer, Simon Schaerlaeken, Jonas Schneider, Tom Kunckler, Claire-Una Fitzgerald, Jean Troyon, Loic Sottas, Tiphaine Descombes, David Christe, Numa Piot, Harish Grandjean, Marion Badi and Johanna Chiffelle.

Abstract

Cancer represents one of the major public health challenges worldwide, representing more than 25% of all deaths in the European Union in 2014. It affects a large and growing part of the general population, with the National Cancer Institute (NCI) estimating that nearly 40% of men and women will be diagnosed with cancer at some point in their lifetimes. Cancer presents an enormous intrinsic complexity and diversity as well as a pronounced resistance to interventions. Current treatments are composed primarily of chemotherapy, surgery, radiotherapy and drug therapy. Each of these approaches has been met with restrained successes and limitations. One growing field of cancer treatments that is showing promising results is immunotherapy. An improved understanding of the cancer biology and microenvironment over the years, particularly the interactions between a tumor and the immune system, has demonstrated the capability of the host immune system to detect and eliminate malignant cells through the process of immune surveillance. However, by various mechanisms, malignant cells can stochastically "hide" from the immune system and transform into tumors. Immunotherapies intend to use the immune system to fight the tumor progression. Different kinds of immunotherapies exist: from immune checkpoint inhibitors (*e.g.* PD-1), to monoclonal antibody treatments and cancer vaccines. One interesting approach of immunotherapy is called adoptive cell transfer therapy (ACT), wherein immune cells, and more precisely, T cells, from the cancer-affected patient are extracted, allowing tumor-specific and effective T cells to be isolated, expanded, activated and re-injected into the patient's body. This type of treatment has already demonstrated great tumor clearance potential as well as the ability to induce long-term cancer immunity. However, one of the major challenges in this type of treatment is the recognition, isolation and expansion of high-affinity, effective T cells that are able to eliminate cancer cells. Several key advances in the field of genetics, sequencing, and personalized medicine have allowed for the identification of tumor-specific antigens, the unique cancer signature for a given patient and

4

a specific tumor. But there is a growing need for novel tools and platforms enabling the screening, selection and isolation of rare, naturally-occurring, high-affinity, tumor-specific T cells.

In this thesis we present a novel approach to study the affinity of CD8+ lymphocytes at the single-cell level using microfluidics technology. We demonstrate the ability of our platform to isolate single cells and evaluate their affinities towards a given antigen by using the reversible pMHC NTAmers technology developed by Julien Schmidt et al. at the Ludwig Institute for Cancer Research in Lausanne, Switzerland. The innovative platform developed here effectively alleviates some of the bottlenecks of current technologies, like flow cytometry, for affinity studies of lymphocytes at the single-cell level. This thesis represents the development from idea to proof-of-concept of this novel platform and we herein describe the origins and characterization of this technology as well as the first applications towards a personalized-medicine tool for clinical research uses.

Keywords: cancer, immunotherapy, lymphocytes, microfluidics, immunoassay, pMHC, TCR, single-cell, lab-on-chip, immunoengineering

5

Résumé

Le cancer représente l'un des principaux défis de santé publique dans le monde, représentant plus de 25% du total des décès dans l'Union Européenne en 2014. Il touche une part importante et croissante de la population. En effet, le National Cancer Institute (NCI) estimerait que 40% de la population (hommes et femmes) sera diagonistiquée d'un cancer à un moment de leur vie. Le cancer présente une grande complexité et diversité intrinsèques ainsi qu'une résistance prononcée aux traitements. Les traitements actuels sont principalement composés de chimiothérapie, chirurgie, radiothérapie et pharmacothérapie. Chacun de ces traitements présente des avantages et inconvénients mais surtout tous ne montre qu'un succès limité dans la lutte contre le cancer. Dans cette lutte, l'immunothérapie est un domaine en pleine croissance et a demontré des résultats prometteurs. Au fil des années, une meilleure compréhension des tumeurs et de leur microenvironnement, mais aussi des interactions complexes entre une tumeur et le système immunitaire, a montré la formidable capacité du système immunitaire à détecter et éliminer les cellules malignes grâce au processus de surveillance immunitaire. Cependant, de manière stochastique et par divers mécanismes, les cellules malignes peuvent "se cacher" du système immunitaire et se transformer en tumeurs. L'immunothérapie a pour but d'utiliser le système immunitaire pour lutter contre la progression tumorale. Il existe différents types d'immunothérapies allant des inhibiteurs de points de contrôle immunitaires (*i.e.* PD-1), aux traitements par anticorps monoclonaux et aux vaccins contre le cancer. Une approche intéressante de l'immunothérapie est appelée transfert adoptif de cellules T, où les cellules immunitaires, et plus précisément les cellules T du patient, sont extraites puis les cellules T, montrant une spécificité envers la tumeur et une aptitude à l'élimination de cellules tumorales, sont isolées, développées, activées et réinjectées dans le corps du patient. Ce type de traitement a déjà démontré un grand potentiel anti-tumoral ainsi que la capacité d'induire une immunité anticancéreuse à long terme. Cependant, les défis majeurs de ce type de traitement sont la reconnaissance, l'isolement et

l'expansion de cellules T efficaces et de haute affinité, capables d'éliminer les cellules cancéreuses. Plusieurs avancées clées dans le domaine de la génétique, du séquençage et de la médecine personnalisée ont permis d'identifier des antigènes tumoraux, la signature du cancer unique pour un patient et une tumeur spécifique. Mais il existe un besoin croissant de nouveaux outils et plates-formes permettant le criblage, la sélection et l'isolement de cellules T rares, naturellement présentes dans notre corps et de haute affinité contre une tumeur.

Dans cette thèse, nous présentons une nouvelle approche pour étudier l'affinité des lymphocytes CD8+, pour chaque cellule individuelle, en utilisant la technologie des microfluidiques. Nous démontrons la capacité de notre plateforme à isoler des cellules individuelles et à évaluer leurs affinités envers un antigène donné via l'utilisation des NTAmers, une technologie de protéines CMH sous formes multimeriques et reversibles développée par Julien Schmidt et autres collaborateurs au Ludwig Institute for Cancer Research à Lausanne, en Suisse. Cette technologie permet de résoudre certaines limitations rencontrées par les technologies actuelles, comme la cytométrie en flux, pour les études d'affinité des lymphocytes à l'échelle de la cellule individuelle. Cette thèse représente le cheminement de l'idée à la preuve de concept de cette nouvelle plateforme et nous décrivons ici les origines et la caractérisation de cette technologie ainsi que les premières applications vers un outil de médecine personnalisée à des fins de recherches cliniques.

Mots-clés: cancer, immunothérapie, microfluidiques, test-immunologiques, CMH, TCR, monocellulaire, automatisation, médecine, personnalisée

Contents

List of Figures

List of Tables

1

Motivations

1.1 Context of the thesis

Since I was a teenager, biology has always fascinated me. How does a single component such as a cell generate, by interactions with other cells, complex machinery such as an organ? How do complex interactions between distinctive tissues generate a functional living organism such as ourselves? The intrinsic and complex machinery that is within all of us remains a marvel to my eyes. Just like a watch mechanism slowly becoming loose and losing control, cancer can be seen as a loss of control by our organism. Cancer highlights the complexity and fragility of our being. For all those reasons and for personal ones, cancer biology has been of strong interest for me for years. I would describe myself as a problem-solver, and this trait led me to pursue a bioengineering education at EPFL rather than medical training. At EPFL, I found the perfect balance between engineering, the way to solve problems; and biology. It became clear to me that an engineering approach to biology had the potential to solve countless diseases and biological mysteries, including the scourge that is cancer.

This passion to mix biology and engineering pushed me to continue my studies after receiving my master's degree and to pursue an applied, translational project for my PhD. EPFL was naturally my first consideration and when during the EPFL Hiring Days, Prof. Sebastian Maerkl described a collaborative project between EPFL and the famed Ludwig Institute for Cancer Research, with the idea to develop a new and innovative technological tool to answer current limitations in cancer immunotherapy treatments, I realized that this project was a perfect fit for me. A collaborative, translational and applied project marrying cancer biology and a state-of-the-art engineering ap-

proach such as microfluidics technology.

During my doctoral thesis, I developed this new, innovative technology, aiming to help the fight against cancer. I hope that my modest contributions could result in a potential impact one day. Successful collaboration between biologists, clinicians, and engineers represents our best chance to tackle huge challenge such as cancer and I am humbled to have been part of this process here in Lausanne, between the CHUV, the Ludwig Cancer Research Institute, and EPFL. This project came from the fruition of thinking between Prof. Sebastian Maerkl (EPFL), Prof. George Coukos and Julien Schmidt (Ludwig Institute for Cancer Research), and was supported by a grant from BITLEMA. This project was mainly performed in Prof. Maerkl's laboratory, where I was supported by extraordinary colleagues like Evan Olson, Barbora Lavickova, Laura Grasemann, and Gregoire Michielin.

1.2 Sections of the thesis

- The first part of the thesis focuses on introducing the concept of immunotherapy in the fight against cancer, the field of microfluidics, and how single-cell immunology is benefiting from microfluidic technologies.

- The second part of the thesis is the development of a novel platform for TCR-pMHC off-rate measurements at the single-cell level and the automation of the experimental process for throughput and reliability.

- The third part of this thesis describes the measurement of dissociation kinetics of pMHC bound to TCR-expressing cells at the single-cell level, using reversible pMHC technology like NTAmers and our novel microfluidic platform. Moreover, the platform's sensitivity was assessed to demonstrate the potential of this platform for screening complex cell mixtures for clinical uses.

2

Cancer and Immunotherapy

2.1 A brief description of cancer

Cancer seems omnipresent in our society. A dark shadow ever lurking. Because of this quite recent exposure in our society, we could be deceived into thinking that cancer is a new disease that was created by our modern way-of-life, our increased longevity and exposure to harmful novel carcinogenic substances created by modern chemistry. But it would seem that cancer might be one of the oldest diseases to ever afflict mankind and even organisms which roamed the earth before us. Traces of benign and malignant tumors have been found in fossilized dinosaurs [1]. It is believed that even Imhotep, the renowned architect/doctor of the first pyramid of Djoser in Sakkara (27th century B.C.), described the first references to the diagnosis of breast cancer, and several cancerous growths were documented in Egyptian mummies [1, 2, 3]. The first mention of cancer as a disease was in 400 B.C. by Hippocrates, who described cancer as a form of imbalances between the "body humors" [2, 3] and divided tumor types into three main categories: hard, ulcerated, and hidden cancer. If cancer has been part of mankind's history for so long, it is true that its presence in our society has never been so strong. It is expected to be the leading cause of death worldwide in the 21th century [4] and represents a global health problem despite all modern efforts. But what is cancer?

Cancer is a broad family of diseases involving uncontrolled growth of malignant cells. The transformation from normal to malignant cells arises by accumulation of genetic mutations or triggered by environmental factors such as exposure to cancerous substances like UV, tobacco, and alcohol. Every day our cells are exposed to harmful substances and acquire mutations, and when a genetic

mutation occurs in a critical part of the genome coding for a protein involved in cell proliferation or survival, the cell can acquire resistance to the normal proliferation signaling. However, this is not enough to create a tumour. In order to turn into a growing tumour, malignant cells must acquire several capabilities through different mutations over time. Those capabilities were described as the hallmarks of cancer [5]. They include abilities such as sustaining proliferation while avoiding death signals, evading the immune system, tumor angiogenesis, and many others. Evading the immune system can be considered a key characteristic of cancer. It has been demonstrated over the years that, on a daily basis, the immune system is able to detect malignant cells and eliminate them through the process of immune surveillance [6, 7, 8]. However, cancer cells can acquire abilities to evade the immune system by, for example, lowering the expression of certain tumor antigens and decreasing the expression of the major histocompatibility complex (MHC class I and II). Unlike bacterial or viral infections, which can trigger a strong immune response (both innate and adaptive) due to the presence of non-self antigens, cancer arises from degeneration of our own cells and therefore tend to be less antigenic. However, due to their genetic instability, tumors can also produce specific antigens called tumor antigens (TA) that can be recognized and cleared by our immune system. Those antigens are processed like endogenous antigens, through the MHC Class I pathway. All nucleated cells express on their membranes the MHC Class I protein and load epitopes from proteolytic degradation of expressed proteins. Through this mechanisms, cytotoxic T cells (CTLs), or CD8+ T cells, can recognize viral antigens through a specific receptor called the T Cell Receptor (TCR) and kill infected or tumorous cells. In the case of cancer, the tumor antigens can arise from different mechanisms, like a point mutation leading to an epitopes slightly different from a self-antigen. Some tumor antigens present high tumor specificity and will potentially trigger a strong immune response, while other antigens such as overexpression of a non-mutated protein can also trigger an immune response but are less tumor specific. Finally, some antigens are tissue-specific and can be recognized if a tumor begins expressing them in a different tissue after epigenetic modifications (*e.g.* demethylation), such as in the case of expression of testis-specific antigens, normally not expressed in adult somatic tissues [9].

2.2 A brief history of the fight against cancer

While modern oncology can be considered to be born in the 1700s, where the effects of carcinogenic substances were first described, the evolution of cancer treatment did not change until quite recently. Until the 1900s, the main and often only way to treat tumors was surgical treatments [10, 2, 3]. Some of the surgical therapies were extremely aggressive but still often proved ineffective to fully cure cancer patients. Early 1900s was also the beginning of radiotherapy with the discovery by Marie and Pierre Curie of radiation emitted by Radium and the potential use of X-rays to treat tumors [1]. The use of radiotherapy for both diagnosis and treatment of some kinds of tumors was followed in the '40s by the first chemotherapy agents. One of the first chemotherapy agents discovered were the alkylating agents (*i.e.* nitrogen mustard) and their discoveries were a by-product of the Second World War and its race for deadlier chemical weapons. Famous pioneers followed these early uses of chemotherapy, such as Sydney Farner and his use of antifolates to treat children with acute lymphoblastic leukaemia (ALL) [11]. Later in the '80s, advances in our understanding of molecular biology revealed the different mechanisms used by cancer cells to evade control. An improved understanding of protein pathways and signaling allowed the identification of new potential molecular targets that present a modified profile in cancer cells compare to normal cells (*i.e.* overexpression, loss of signaling, *etc...*). This approach differs from chemotherapy agents that affect both normal and malignant cells and inhibit proliferation and instead targets specific proteins and proteins interactions that have been selected by cancer cells to provide an advantage [12, 3]. Those types of treatments include specific protein inhibitors designed by advances in chemical synthesis (*e.g.* tyrosine kinase inhibitor) or monoclonal antibodies produced to target specific proteins and receptors involved in the neoplastic transformation. The discovery by Köhler and Milstein of hybridomas [13], an entity resulting from the fusion of murine B lymphocytes to human myeloma cells, has enabled the large production of monoclonal antibodies and the growth of this type of treatment.

Surgery, radiotherapy and chemotherapy remained the three major cancer therapies of the 20th century, and while each of those therapies had their advantages and success, they were all met with their own limitations and failures. Surgical treatments can cure a patient of tumor but if the primary tumor has metastasized, this therapy generally fails. Chemotherapy agents often demonstrated positive results over the years but presented two major drawbacks. Firstly, as mentioned

above, chemotherapy generally affects both normal and tumor cells and therefore can lead to complications and severe side-effects. Secondly, as cancer cells can adapt to the pressures stemming from different intervention mechanisms, resistance to chemotherapy agents has been observed and sometimes leads to multi-drugs resistance from tumors, resulting in a lack of treatment options. While targeted therapies were often effective to the point of declaring patients cancer-free, relapses were observed with former patients being unresponsive to former treatments. The mechanisms of intrinsic and adaptive tumor resistance to therapies are complex but generally hindered the successes of chemo- and targeted therapies [14, 15, 16, 17]. By the end of the 20th century, the need of a new approach to fight cancer was required and lead to the blossoming of the fourth major field of cancer treatments: cancer immunotherapy. The general evolution of those major milestones in the fight against cancer are presented in Figure 2.1.
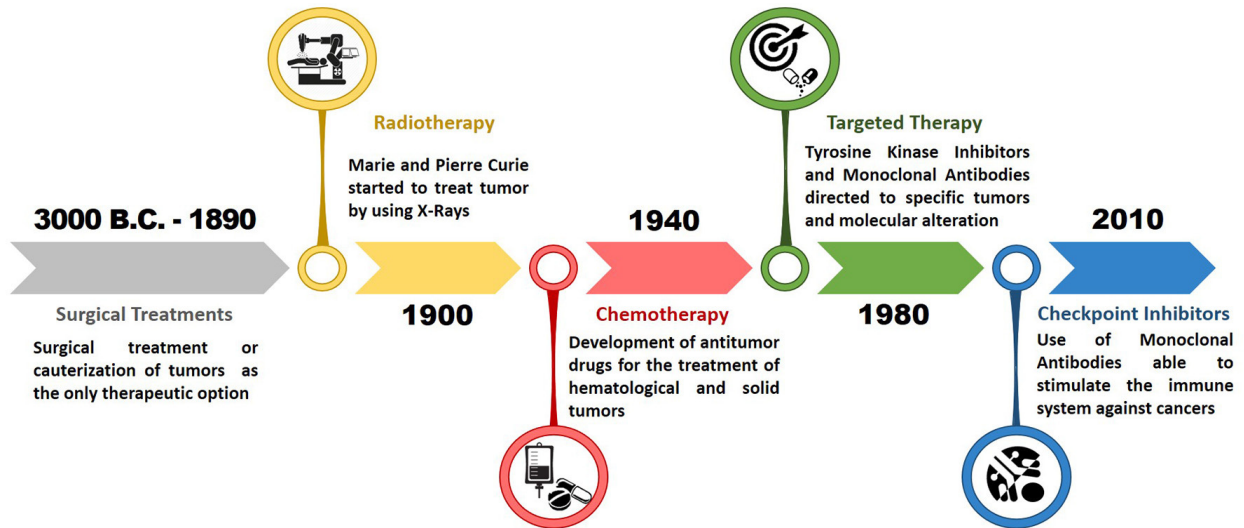
Figure 2.1: **A brief history of the fight against cancer.**
Timeline of turning points in modern oncology. The four major cancer therapies and their breakthroughs over time are presented here: surgery, radiotherapy, chemotherapy, and the beginning of immunotherapy. Reprinted with permission [3].

2.3 Cancer immunotherapy, a novel approach in the fight against cancer

In this section, I will briefly introduce the modern history of cancer immunotherapy and the main axes that compose it. I encourage the viewers to read the following work, which presents detailed reviews of the birth of cancer immunotherapy [18, 6, 19, 20, 21, 22]. The field of cancer immunotherapy is often considered as quite recent, however its roots are older. Its modern birth can be traced back to the 19th century. Where two physicians, Fehleisen and Busch, discovered that tumor regression could be observed in patients infected with erysipelas (bacterial infection of the skin). This led to the understanding that a modification in the immune response had an impact on tumor progression. William Bradley Coley, widely known as the "Father of Immunotherapy", tried, in 1891, to use this knowledge to treat various types of cancer with a mixture of heat-inactivated bacteria, famously called "Coley's toxins". Encouraging and promising results were observed but, triggering sepsis in a cancer-infected patient was bound to trigger side-effects and unwanted reactions. Therefore, until quite late in the 20th century, chemotherapy and surgery remained the main treatment strategies for cancer. It has only been quite recently, with great discoveries in the field of immunology, that the modern version of cancer immunotherapy has arisen. For instance, in 1909 when Paul Ehrlich started hypothesizing that neoplastic cells are consistently created by the human body but almost always eradicated by the immune system. This idea was further developed by Lewis Thomas and Sir Frank Macfarlane when they postulated the "cancer immuno-surveillance" hypothesis. But the real arrival of cancer immunotherapy occurred with the discovery of immune checkpoint inhibitors such as CTLA-4 and PD-1 (explained later). Their discovery led Drs. James P. Allison and Tasuku Honjo to the award of the 2018 Nobel prize in Physiology and Medicine. Nowadays, the term cancer immunotherapy includes several leading approaches such as immune checkpoint therapy, cytokine treatments, cell-based therapies, and cancer vaccines. I will briefly explain the main mechanisms of each of those approaches, their advantages, and potential drawbacks. One common advantage of cancer immunotherapy, in addition to successful clinical treatment outcomes, is the ability to trigger long-term immunity and therefore avoid relapse as is often observed with other treatments such as chemotherapy and targeted therapy. It is worth mentioning that despite this great feature, resistance to immunotherapy has been observed. The mechanisms of this resistance remain quite obscure to this day [23].

- **Immune checkpoint therapy** The immune system is a complex machine. The adaptive immune system, with powerful tools like cytotoxic lymphocytes, requires a delicate balance between over and under-activation. When the activation potential does not meet requirements, infections or cancer progression occurs. On the other hand, an immune system that is too sensitive to activation can lead to auto-immune diseases and other side effects. Therefore, evolutionarily speaking, regulatory mechanisms have evolved to keep the activation of lymphocytes in check. The activation of effector cytotoxic T cells (CD8+) is thoroughly controlled and balanced by inhibition mechanisms coming from either intrinsic signals (*e.g* expression of PD-1 molecules by activated T cells in peripheral tissues) or external via regulatory T cells (Tregs) [21]. The main protagonists of this regulation are the CTLA-4 and PD-1 proteins. Targeting those proteins (or their ligands) by using blocking antibodies showed encouraging results like the successful treatment of melanomas by the first approved anti-PD1 monoclonal antibody (nivolumab and pembrolizumab, 2014 [21]). It is worth mentioning that correlations linking the expression level of PD-1 ligand (PD-L1) and survival chances in patients have been observed. Therefore, the PD-1/PD-L1 complex can be seen as both a biological marker and a cancer immunotherapy target. An excellent illustration of the molecular mechanisms in place to regulate the activation of lymphocytes is depicted in Figure 2.2. Immune checkpoint therapy has demonstrated extremely encouraging results in clinical trials but was followed with cases of acquired resistance.

- **Cytokine therapies** As the importance of checkpoint inhibitors to regulate lymphocytes became clearer, another key player came into view: the importance of cytokines for the activation and maturation of lymphocytes. Injection of cytokines like IL-2 and IFN-γ have been approved as immunotherapeutic treatments to activate T cells for anti-tumoral activity. However, the systemic infusion of cytokines in patients was met with side-effects, sometimes severe, such as systemic inflammation known as cytokine release syndrome (CRS) [24]. Different innovative methods have been explored to help activation of T cells in the tumor vicinity and overcome cancer-driven suppressing signals (*e.g.* PD-L1 overexpression by cancer cells), while reducing the risks of CRS and other complications. A worthy example is the concept of "cytokine-backpacks", where activating cytokines were encapsulated in protein nanogels, and released locally upon T cell activation [25].

22
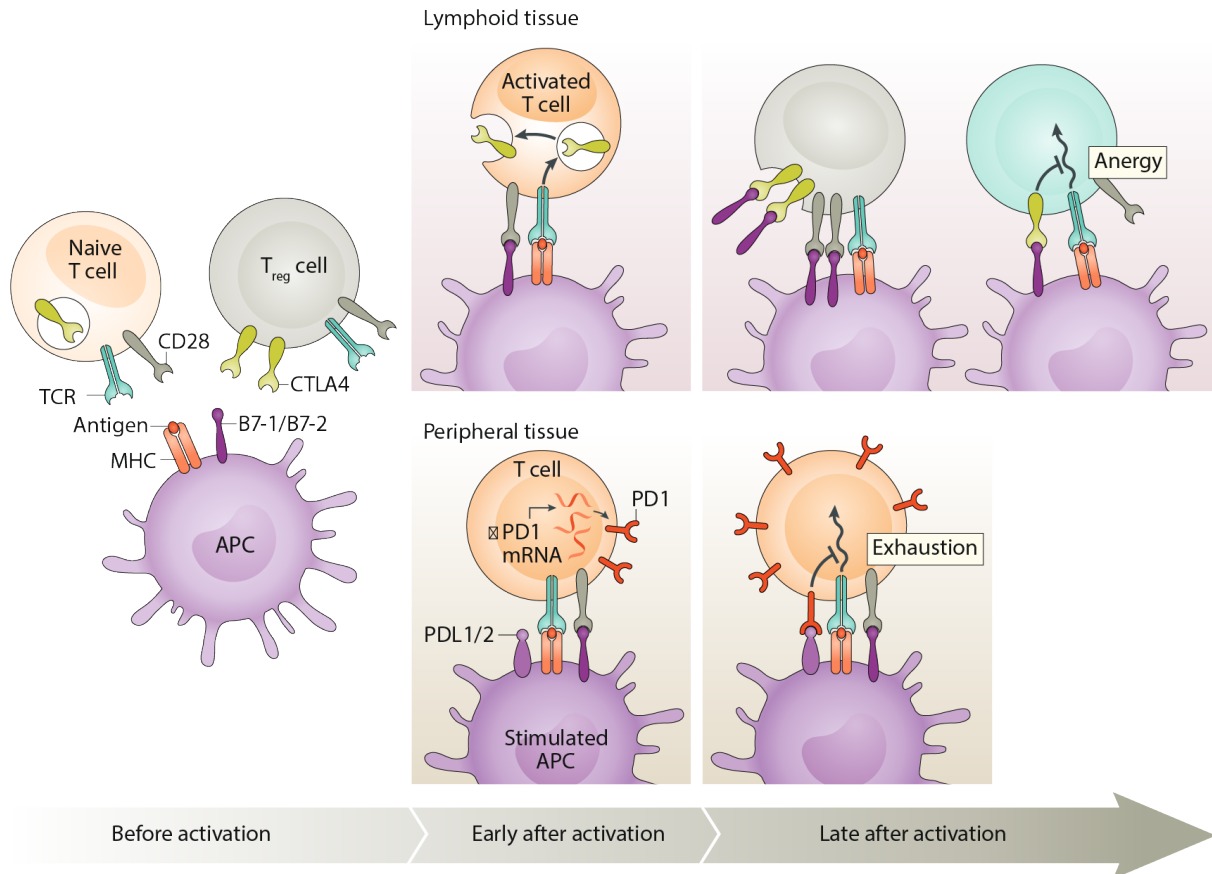
Fig. 2 | Mechanisms of T cell activation and regulation. Before activation, antigen-presenting cells (APCs) load antigen onto MHC molecules to prepare for contact with a T cell that displays a cognate T cell receptor (TCR) while also providing necessary co-stimulatory ligands B7-1 and B7-2. The inhibitory molecule cytotoxic T lymphocyte antigen 4 (CTLA4) is contained within intracellular vesicles in naive T cells, whereas it is constitutively expressed on the cell surface of CD4$^+$CD25$^+$ regulatory T (T$_{reg}$) cells. Both classes of T cells express the co-stimulatory receptor CD28. Early after activation, generally in the lymphoid tissue, T cells are activated when their TCRs bind to their cognate antigen presented by APCs in conjunction with CD28 binding to B7-1/B7-2. Also, the activated T cells begin the process of displaying CTLA4 on the cell surface. T cells within peripheral tissues upregulate PD1 at the mRNA level early after activation. Late after activation, in lymphoid tissue, CTLA4 expressed by activated T cells binds to the B7-1 and B7-2 molecules on APCs, thereby preventing their binding to CD28 and promoting anergy by decreasing the T cell activation state. At the same time, constitutive expression of CTLA4 on T$_{reg}$ cells leads to trans-endocytosis of B7 ligands and interferes with the CD28 co-stimulatory ability of APCs. Late after activation in peripheral tissues, PD1 is further upregulated transcriptionally, leading to greater surface expression of programmed cell death 1 (PD1), which binds to its ligands PDL1 and PDL2, thereby promoting T cell exhaustion at sites of infection or when confronted with neoplasms. Image courtesy of the National Institute of Allergy and Infectious Diseases.

Figure 2.2: **Mechanisms of T cell activation and regulation.**
The role of CTLA-4 and PD-1 in the activation and regulation of cytotoxic lymphocytes. Reprinted with permission [21].

- **Cell-based therapies: Adoptive Cell Therapy (ACT) and CAR-T Cells** The main principle of cell-based therapies is to identify, isolate and extract tumor-specific lymphocytes.

23

Then, those isolated cells can be studied, modified and expanded for further injection back into the cancer patients. The studies of those cells mainly consist of extracting the T Cell receptor (TCR) sequence, the source of the lymphocyte's specificity. Several modifications can be performed on isolated T cells. These can range from cytokine activation to genetically engineered T cells, the most famous example being CAR T-cells. Initially, chimeric antigen receptors (CARs) used the variable region of an antibody (targeting a tumor-specific antigen) as an extracellular component that was linked to an intracellular signaling domain (CD3). Several new generations of CAR-T cells followed and efficiency of treatment over time has improved. CAR-T cells have shown extremely encouraging results in clinical trials. For instance CAR-T cells with engineered specificity towards the surface molecule CD19 (constitutively expressed by B cells) have led to long-term, durable responses in certain forms of leukaemia [26, 27, 28]. While CAR-T cells have demonstrated interesting, long-term results in some variety of tumors, they present two major drawbacks. Firstly, by virtue of their biology, CAR-T cells are restricted to recognize tumor cell-surface antigens, limiting the spectrum of their applications. Secondly, and more importantly, CAR-T cells have shown dangerous, sometimes fatal side-effects like CRS and off-target toxicity [29, 30]. A notoriously sinister example was the death of two patients treated with CAR-T cells engineered to recognize the MAGE-A3 testis antigens, expressed in some types of melanomas. Those cells unfortunately showed off-target reactions to myocytes and led to the death of both patients [31, 32]. However, there have been recent exciting approaches to tackle toxicity and off-target reactions [33]. On the other hand, using naturally-occurring, rare, effective, and tumor-specific T cells would decrease the chances of off-target reaction but require highly effective screening technologies.

- **Cancer vaccines** Cancer vaccines are mainly divided in two categories. The first, called prophylactic have been used for a while and mainly target viruses with an oncogenic, pro-tumoral potential. Examples of such vaccines, already used in the general population, are hepatitis B and papilloma viruses [18, 20, 21]. A new approach, called therapeutic vaccine, aims to enhance the immune response towards cancer-related antigens. Those antigens are mainly tumor-associated antigens (TAAs) or tumor neoantigens. Early efforts to trigger an immune response to cancer antigens mixed extracted tumor cells with viruses to elicit a polyclonal response [21]. However, it is not always easy to extract tumor cells and this approach mainly target TAAs that are often also expressed in normal tissues. However, thanks to recent

major advances in next-generation sequencing, an exciting new field is growing rapidly. Personalized recombinant tumor vaccines are based on the sequencing of tumor tissues compared with healthy ones to extract good immunological candidates (TAAs and neoantigens). This method is highly personal and relies on complex and ever-growing computational pipelines [34] (Fig. 2.3). Early clinical trials with personalized cancer vaccines were met with great successes. However, several key limitations needs to be addressed. In addition to high time and cost requirements due to the personalized nature of this approach, this method relies heavily on computational pipelines that sometimes appear to be more art than science [35, 21]. Also, differences in reactivity between the two MHC types (Class I and II) showed that immune response were elicited differently between CD4+ and CD8+ T cells [36]. There is still a strong need for better predictive algorithms for both MHC types.
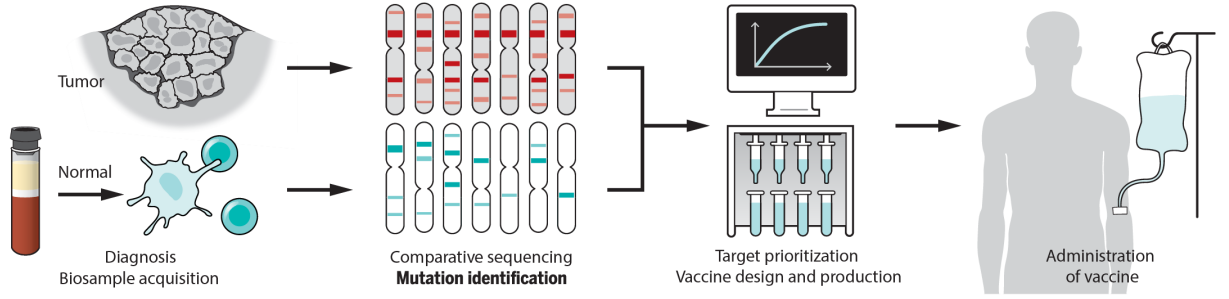
Figure 2.3: **Creation of a personalized recombinant cancer vaccine.**
Thanks to next-generation sequencing, a comparison between healthy and tumor tissues is performed and enables the identification of potential tumor-associated antigens (TAAs) or tumor neoantigens. Those peptides are then examined by computational pipelines for selection and prioritization of good candidates (*e.g.* affinity binding to HLA). Reprinted with permission [34].

2.4 The importance of the TCR-pMHC interaction and the tools to study it

2.4.1 The T cell Receptor (TCR)

Lymphocytes are a key components of an immune reaction. Cytotoxic T cells (CD8+) rely on the T cell receptor for recognition of viral and tumoral antigen. The T cell receptor is made of a heterodimers of α- and β-chains (Fig. 2.4) [37]. This formation allows specific binding to a peptide-MHC complex. The TCR lacks direct signal-transducing activity but relies on other subunits like the CD3 complexes to relay the signal to the nucleus through different signal pathways (e.g. NF-κB, Fig. 2.4). Each cell express an unique TCR generated by VDJ recombination of germline TCRα and TCRβ genes [37]. The generated cells undergo a selection process in the thymus called 'thymocyte selection' that will select cells that are between a minimum and a maximum affinity range of self-peptides loaded on MHC molecules. Effectively, TCRs that do not recognize pMHC complexes will undergo apoptosis (positive selection) and cells recognizing self-peptides with high-affinity will be removed by apoptosis (negative selection). This selection process results in a mature TCR repertoire that is both self-tolerant and minimally self-reactive [38, 37]. The adaptive immune system possesses a large number of T lymphocytes ($\succ 10^{11}$) with a mature TCR repertoire diversity still unknown but estimated to be over 10^8 [39, 40].

2.4.2 The peptide-MHC complex

Antigen presentation by major histocompatibility complex (MHC) proteins is an important part of the lymphocyte-derived immune response. Peptide are loaded onto MHC molecules in the endoplasmic reticulum are arose from the translational machinery of the cell by breakdown of generated proteins (via cytosolic and nuclear proteasomes). MHC molecules are subdivided into two classes, class I and class II [41]. Both classes share the same function for displaying peptide for recognition by T cells. All nucleated cells express the peptide-MHC class I complex and target primarily CD8+ T cells, whereas the class II complex is expressed by a subset of specific cells (e.g. macrophages, dendritic cells and B cells) and target the activation of CD4+ T cells. Additionally, both classes share a similar structure made of two domains composed of heavy chains (only one α chain for class I or two chains, α and β for class II) and light chain (β2m) [41]. Loading of peptides onto the
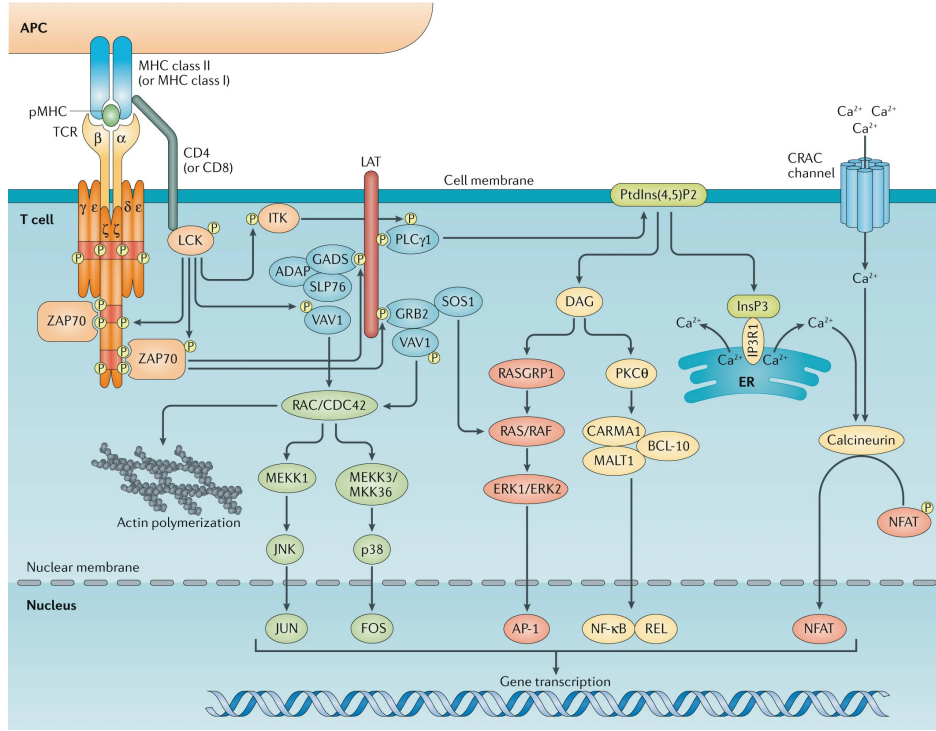
Figure 2.4: **Overview of the TCR structure and signaling pathways.**
T cell receptor (TCR) is made of heterodimers (α- and β-chains) with CD3 signaling subunits (including CD3γ, CD3δ and CD3ϵ) transferring the activation signal downstream in the cell by three main pathways: Ca^{2+}-calcineurin, mitogen-activated protein kinase (MAPK) and nuclear factor-κB (NF-κB) signaling pathways to relay the the signal into the nucleus. Reprinted with permission [37]

.

MHC molecules stabilize the pMHC structure but remains a dynamic and selective process, which allows recycling of presented peptides [42, 41]. The generated pMHC class I on nucleated cells are the key targets of the TCR receptors on CD8+ T cells. The strength of this interaction represents one of the key components for T cell activation and further antigen clearance. It is therefore quite important to study this interaction at the molecular level.

2.4.3 How to study of the TCR-pMHC interaction

The interaction between the T cell receptor present on lymphocytes (CD8+ T cells) and a peptide loaded on the major histocompatibility complex (pMHC) is one of the key components in

immunology. It represents the way lymphocytes "scan" cells to detect virus-infected or tumoral cells. Since the discovery of the structure of the TCR-pMHC interaction in 1996 [43], important knowledge has been gained regarding the role of this interaction in the activation of lymphocytes as well as its role in cancer immunotherapy. The interaction between a TCR and a pMHC molecule is dynamic and complex [44]. Extensive work has been done to better understand this interaction at the molecular level [45, 46, 47, 48]. A better understanding of both the TCR-pMHC interaction and the antigen-presenting machinery [48] has highlighted the importance of this interaction in the fight against cancer [49]. Therefore, two parallel hunts have been triggered. First, the hunt to find the best tumor-specific peptides and to better understand which antigens are processed and displayed on MHC proteins as well as their dynamics (also vital for the design of cancer vaccines 2.3). Secondly, the hunt to better understand and isolate exciting TCR receptors, that is those that show great activation potential towards a given antigen. This feature is of great importance not only for adoptive T cell transfer therapy and the development of CAR-T cells [31] (see 2.3), but also for improving our understanding the toxicities related to such treatments [32].

However, in order to better recognize and isolate tumor-specific T cells, new tools needed to be created in order to recreate the TCR-pMHC interaction *in vitro* but this interaction is fragile and dynamic. Different approaches have been used to study this interaction. They can be divided into two main families: antigen-directed approach or TCR-directed approaches [50]. TCR-directed approaches rely on the creation of large libraries of pMHC complexes (e.g. through surface expression on yeast [51]) for the screening of a defined TCR. The other approach, antigen-directed, can be assessed either through functional testing of lymphocytes after exposure to given antigens (e.g. co-culture with antigen-presenting cells) and measure T cells proliferation, survival or pro-inflammatory cytokine production (among other readouts) [50]. Another approach rely on the study of the structural affinity of the TCR-pMHC interaction. Since the discovery that multimeric pMHC molecules provided sufficient binding to TCR receptors [52], several technologies have been developed to re-create multimeric pMHC molecules like dextramers. Dextramers and tetramers are molecules covalently joining several pMHC monomeric units together, hence greatly increasing the total avidity for this complex to cells expressing TCR receptors [53, 54]. They can be used for screening of antigen-specific T cells via flow cytometry [55, 50] or adapted to different techniques as explained in Figure 2.5.
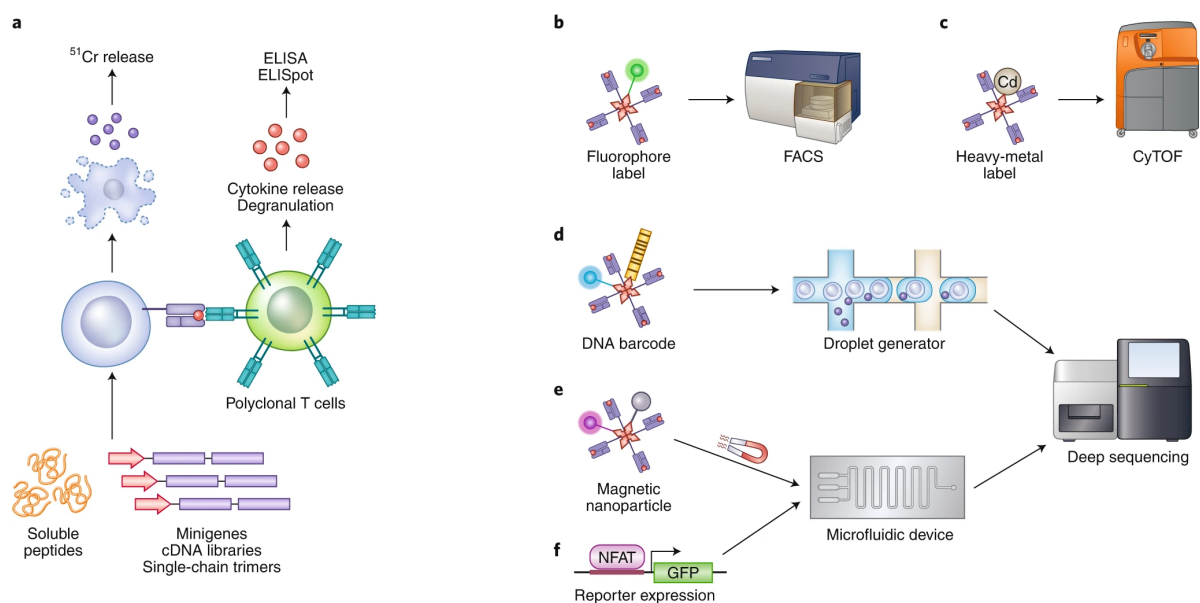
Figure 2.5: **Antigen-directed approaches for antigen T cell discovery.**
a Functional readout of TCR–pMHC interactions via detection of cytokine release and/or cytotoxicity. **b** Flow cytometric identification of antigen-specific T cells via staining with fluorescently labeled pMHC multimers. **c** Mass cytometry (CyTOF)-based identification of antigen-specific T cells via heavy-metal-labeled pMHC multimers. **d** Identification of antigen-specific T cells via DNA-barcoded pMHC multimers followed by deep sequencing. **e** Microfluidics-based identification of antigen-specific T cells via magnetic nanoparticle-barcoded nucleic acid cell sorting (NACS). **f** Microfluidics-based identification of antigen-specific T cells via the NFAT reporter system. Figure and caption reprinted with permission [50]

.

The correlation between the structural affinity of the TCR-pMHC interaction and the resulting functional affinity of a CD8+ T cell to become activated and clear away tumoral antigens has been heavily studied and represents a key pillar of how to screen and isolate relevant lymphocytes for a given tumor [56, 57, 46, 58, 59, 60]. Dextramers and tetramers are now widely used in cancer immunotherapy, as they provide a wealth of information and furthermore enable screening of antigen-specific CD8+ T cells (Fig. 2.5). However, based on their multivalent formation, they are associated with various drawbacks. Mainly, they represent a non-reversible binding of monomeric pMHC units, therefore the total avidity can lead to a TCR-induced activation of the lymphocytes

and often can lead to TCR-induced cell death. Also, only few details can be obtained on the binding kinetics, as tetramers do not provide off-rate information for monomeric pMHC. To alleviate those shortcomings, the technology of reversible multimers was developed and two new approaches were made. Firstly, streptamers [61] are molecules based a streptactin-streptag scaffold that can be dismantled by the introduction of biotin, which binds with greater affinity to strepactin than streptag. Similarly, another approach is NTAmers [62], which use a Ni2+-NTA-Histag link that can be disrupted when adding imidazole. Both reversible pMHC multimer technologies enable the isolation of "untouched" antigen-specific CD8+ T cells while avoiding over-activation and apoptosis of rare clones triggered by conventional multimers [63]. The evolution of soluble pMHC complexes and their use are described in Figure 2.6.

Reversible multimers technologies represent a major step forward in screening not only antigen-specific CD8+ T cells but also provide new ways to screen, among antigen-specific cells, the best potential candidates with high-affinity (and therefore potential functionality) against a given tumoral antigen. Those technologies, however, heavily rely on readouts like flow cytometry. Despite providing high-throughput, flow cytometry technology can only provide a singular temporal data point for a given cell. As each T cells presents an unique TCR, affinity studies through flow cytometry can only be achieved through clonal expansion of each clonal cells to reach sufficient numbers (e.g. 200'000 copies) for use with flow cytometry. Flow cytometry can be therefore considered as a limiting factor for single-cell analysis as explained later (Section 3.2).

A

2012	NTAmer, reversible multimers for sorting of "untouched" CD8 cells Cytometry by Time Of Flight (CyTOF) using tetramers
2010	Immunopure class II tetramers
2009	Combinatorial staining with pMHC class I tetramers
2006	Conditional peptide ligand for high throughput synthesis of pMHC tetramers
2005	Dextramer
2003	Well defined pMHC dimers, tetramers and octamers
2002	Streptamer and DTB-based multimers, reversible pMHC multimer
2000	Pentamer
1998	pMHC class II tetramer
1996	pMHC class I tetramer
1993	pMHC monomer and dimer binding studies

B

biotin

streptavidin

Tetramer

Pentamer

strep tag

multimerized
stept actin

Streptamer

NTAmer

dextran

Dextramer

Figure 2.6: **Evolution of soluble pMHC complexes and their applications for T cell analysis and sorting.**

Taken from [63]. **(A)** Chronological listing of milestones in the use of pMHC complexes for the detection and analysis of antigen-specific CD8+ and CD4+ T cells. **(B)** Schematics of the most frequently used pMHC oligomers; the red oval represents PE. Reprinted with permission [63].

3

Microfluidic technologies applied to single-cell immunology

The section 3.1 is adapted from a recent review written by myself and Prof. Maerkl. All figures used in this review were approved by their original publishing journals.

3.1 How single-cell immunology is benefiting from microfluidic technologies

3.1.1 Abstract

The immune system is a complex network of specialized cells that work in concert to protect against invading pathogens and tissue damage. Imbalances in this network often result in excessive or absent immune responses leading to allergies, autoimmune diseases, and cancer. Many of the mechanisms and their regulation remain poorly understood. Immune cells are highly diverse and an immune response is the result of a large number of molecular and cellular interactions both in time and space. Conventional bulk methods are often prone to miss important details by returning population-averaged results. There is a need in immunology to measure single cells and to study the dynamic interplay of immune cells with their environment. Advances in the fields

of microsystems and microengineering gave rise to the field of microfluidics and its application to biology. Microfluidic systems enable the precise control of small volumes in the femto- to nano-liter range. By controlling device geometries, surface chemistry, and flow behavior, microfluidics can create a precisely defined microenvironment for single-cell studies with spatio-temporal control. These features are highly desirable for single-cell analysis and have made microfluidic devices useful tools for studying complex immune systems. In addition, microfluidic devices can achieve high-throughput measurements, enabling in-depth studies of complex systems. Microfluidics has been used in a large panel of biological applications, ranging form single-cell genomics, cell signaling and dynamics, to cell-cell interaction and cell migration studies. In this review, we give an overview of state-of-the-art microfluidic techniques, their application to single-cell immunology, their advantages and drawbacks, and provide an outlook for the future of single-cell technologies in research and medicine.

3.1.2 Introduction

3.1.2.1 Microfluidics

Microfluidics, the science of manipulating fluids on the microscale, has had considerable impact on biology, both in research and industry. Microfluidics significantly evolved over several decades and it is now used in almost all biological fields including biochemistry, cell signaling, drug testing, genomics, and proteomics. This success can be explained by various advantages microfluidic based approaches have over conventional technologies such as precise spatio- and temporal control of extremely small volumes, reducing costs and required sample volumes, while providing sensitivity and throughput.

The immune system is a complex system consisting of a variety of cell types that work in synergy to protect against invading pathogens and control infected and mutated cells. In addition to the diversity of cell types constituting the immune system, each cell type can present distinct features or can be genetically unique. For instance, macrophages can present several different phenotypes, ranging from anti- to pro-inflammatory. Cells from the adaptive immune system (T and B cells mostly) are genetically unique due to VDJ recombination and clonal selection. These unique features are often missed by conventional, bulk measurements that usually provide population level averages. Single-cell technologies present considerable advantages that can overcome the limitations

33

of bulk measurements and can help achieve a better understanding of immune mechanisms, which in turn is expected to lead to efficient, personalized immune treatments for complex illness like autoimmune diseases and cancer.

In this review, we explore the growing field of microfluidics and present an up-to-date overview of the different approaches and techniques used for single-cell applications in immunology. We will briefly present the origins of microfluidics, focusing on the advantages this technology can bring to single-cell analyses and why reaching single-cell resolution is often a necessity in the study of the immune system. We will then briefly explain how microfluidics can be used to separate immune cell populations into more defined subsets; as the first necessary step to enable single-cell analyses. Finally, our main focus will be microfluidic techniques used in research to manipulate and study single immune cells covering active, passive, and droplet microfluidics.

3.1.2.1.1 Origins of microfluidics

Microfluidics originated in the microelectronics industry. In the late 20th century, the field of microelectronics advanced with improved silicon-based micromachining and photolithography techniques. While microelectronics dates back to the 1970s, it was not until the 1990s that microfluidic devices started to be developed and applied to biological applications. With advances in liquid and gas chromatography, microfluidic devices were first used for biological separation using electrophoresis. For instance, Woolley *et al.*[65] developed a microfluidic capillary gel electrophoresis system for DNA analysis with a considerable decrease in separation time. Since then, microfluidic techniques and devices are now used in a variety of biological applications covered in detailed reviews [66, 67, 68, 69].

3.1.2.1.2 Unique properties of microfluidic systems

Microfluidic technologies allow for the manipulation of fluids down to the micron and sometimes nanometer length scale and femto to microliter volumes. This entails several advantages that we briefly tabulate below as a non-exhaustive list.

- **Volume reduction:** Biological reactions often require expensive and/or rare molecules / cells (*e.g.* antibodies). Compared to conventional methods, microfluidics can achieve orders of magnitude reductions in volumes.

- **Laminar flow:** One key aspect of the microfluidic world is the laminar flow regime that prevails at these length-scales. Low Reynolds number flows reduce flow dispersion and allow for precise control of flow behavior. Mixing of molecules between solutions is mostly due to diffusion at this length scale and therefore can be controlled by design.

- **Parallelization:** Microfluidic experiments can often be parallelized and multiplexed. By enabling spatial and temporal control of fluids, microfluidic devices can run several parallel biological reactions simultaneously.

- **Integration and automation:** Microfluidic devices are often made of materials with appealing properties (*e.g.* gas permeable, transparent, elastic), that are compatible with different readouts such as fluorescence microscopy and can even incorporate microelectrodes for bio-electrical applications. In addition, on chip fluid shunting can be computer controlled in order to create automated systems.

3.1.2.1.3 Materials used in microfluidics

In the early days of microfluidics, channels were directly etched into silicon wafers. However, glass soon became the new standard as it presented several advantages over silicon. Glass is relatively cheap, resistant, and transparent with good optical properties, making it a suitable material for biological applications involving microscopy[67]. However, at the beginning of the 21$^{\text{st}}$ century, another material quickly prevailed over glass and silicon[70], namely silicone. Polydimethylsiloxane (PDMS) is an elastomeric polymer with excellent properties for microfluidics. PDMS, like glass, is transparent but also permeable to gases unlike glass and silicon. PDMS can be poured on a mold containing features on a silicon wafer, cured, peeled off the mold and bonded to another material such as glass. The master mold can be reused many times. This molding process drastically simplified the process of making microfluidic devices and reduced fabrication costs considerably. PDMS is therefore a suitable material candidate due to its inherent properties as an elastomeric, transparent polymer but also because of its molding microfabrication process that allows for fast, cost-efficient prototyping [71]. PDMS, while being one of the most commonly used materials, is not the only polymer used for microfluidic applications. Polymethylmethacrylate (PMMA) and Polycarbonate (PC) are also good candidates and typically used with injection molding methods for chip fabrication, albeit these two materials are not elastomeric. Glass and silicon are still used

for certain applications as they do present specific advantages over polymers (*e.g.* better thermal resistance and conductivity).

3.1.2.2 Immunology & single-cell analysis

While most bulk measurements obtain the average phenotype of a population of cells, they advanced the field of immunology and immunoengineering to a great extent: production of specific antibodies in large-scale, detection of viruses in blood samples, analyses of vaccine-induced T cells, *etc.* However, conventional technologies are inefficient in handling rare subsets of cells (such as antigen-specific T cells or B cells) because of their requirements for relatively large volumes and, as mentioned earlier, their inherent property of giving an average response of a population rather than returning specific, individual cell characteristics. Especially in the case of lymphocytes which are genetically unique, being able to specifically measure single-cell phenotypes is required for advanced immunologic treatments such as autoimmune disease and cancer immunotherapy. Single-cell measurements are difficult to achieve with conventional techniques, hence the need for novel single-cell analysis tools in immunology. As a prominent example of a single-cell measurement, we will examine flow cytometry. Flow cytometry and more specifically fluorescence-activated cell sorting (FACS) have been incredibly useful tools in biology. Those technologies have allowed the detection and enrichment of specific immune populations in samples (*e.g.* isolate CD4+ or CD8+ T cells among a tumor sample). However, in FACS, each cell is only "a dot in a plot". Features like affinities, secretion dynamics, and cell-cell interactions over time are not easily attainable by FACS. Recent advances enhanced the optical resolution of flow cytometry, such as polychromatic flow cytometry (PFC)[72] and imaging flow cytometry[73], but these technologies still lack temporal resolution for single-cell analysis. Microfluidic techniques make this additional dimension now accessible. We will describe how microfluidics can address single-cell analyses for immune cells and how this technology already had an impact on the field of immunology. We would like to mention a review by Chattopadhyay[74] on single-cell technologies for monitoring immune cells, which covers the shortcomings of bulk measurements and the need of single-cell resolution techniques.

3.1.2.3 Enriching immune cell subpopulations

While the focus of this review is on single-cell techniques for immune research, we believe that a short description of microfluidic techniques used to sort entire immune populations and enrich

specific subsets can be useful as it is generally the first necessary step to obtaining single-cell measurements.

Microfluidic devices often use mechanical filters for sorting cell populations based on their physical properties (size, shape, etc.) in a label-free manner. As extensively described by Gosset *et al.* [75], mechanical filters come in different shapes including weir-style filters, where a small planar gap is created allowing small cells to pass while retaining large cells. These type of filters have been used to filter white blood cells (WBCs) from whole blood samples [76]. Another type of sorting relies on pillar arrays to divert a cell's flow path based on its size or trap large cells while letting small ones pass. This technique was used by Jiang and Aceto to extract WBCs and circulating tumor cells (CTCs) from whole blood samples [77, 78]. More recently, groups including Chronis *et al.* [79] used similar approaches for trapping WBCs. Arai and his group used pillar arrays to isolate and detect T and B cells from whole blood [80, 81] with specifically designed pillars of various geometries.

Another technique for filtering cells under constant flow is called hydrodynamic filtration. This technique relies on the laminar flow regime and specific channel geometries [82, 75, 83] to achieve cell filtration in a passive, constant flow [75]. Another hydrodynamic method to separate cells based on their size is pinched flow fractionation [84, 85]. The technique uses different inlets to pinch the sample flow against the microfluidic wall with another flow. In the process, small particles reach flow profiles closer to the wall than large particles. The pinched segment is then followed by a sudden widening of the channel with several branches. The particles follow the streamlines they were forced into during the pinching and the streamlines are then separated into the different branches. Therefore, large particles will end up in a different branch than small ones. Another technique relying on hydrodynamic filtration is called deterministic lateral displacement (DLD)[75] and uses micropillar arrays. DLD allows for separation of particles based on their size. Small particles will flow through a micropillar array with their streamlines unchanged and therefore will follow a straight course. The larger the particle gets, the more likely it will hit a pillar and its course will change into a different streamline. Therefore a correlation is observed between the size of the particle and the angle of its final streamline compared to the original one [75]. DLD was successfully used to filter whole blood samples and to separate WBCs from red blood cells (RBCs) and platelets [86, 87].

3.1.2.4 Single immune cell analyses using microfluidics

As described above, microfluidic devices are useful tools to filter and sort subpopulations of cells, often without the need of fluorescent tags as required by FACS. In addition, microfluidics is ideally suited to study single cells. We will describe how different research groups over the years have used microfluidic techniques to study immune cells on the single-cell level. We will divide those techniques into three main microfluidic categories: passive devices, active devices, and droplet microfluidics. For each category, we will describe how these technologies were used in biological applications such as genomics, proteomics, and cell-cell/cell-environment interactions.

In this review, we will not cover microfluidic devices that use integrated electrodes, rely on electrophoresis, magnetophoresis, or other more specialized techniques. Our list is not exhaustive and there are several excellent reviews that have been published on microfluidic systems applied to single-cell analysis, including immune cells. We recommend several technical reviews describing single-cell techniques [88, 89, 90, 91, 92]. Our focus here is on single-cell microfluidic techniques for immune applications, this topic has also been described by excellent reviews. We strongly suggest our readers to complement their readings with those reviews [93, 94, 74, 95, 96, 97].

3.1.3 Passive microfluidic devices

Passive microfluidic devices do not rely on active on-chip control elements for flow handling and regulate flow behavior by their inherent design. Fluids are driven through such chips either by capillarity or by applying a pressure source. Flow rates can be tuned by adjusting the design of the microfluidic chip or by adjusting the pressure source. Microwell and microtrap arrays are common approaches to isolate individual cells. Although glass microwell arrays generated by microengraving glass substrates have been around for a long time, one of the earliest uses of microwells in PDMS for single-cell isolation was performed by Rettig *et al.* in 2005 [98]. Similarly, microtrap arrays are often used to isolate individual cells for different applications. The works of Di Carlo *et al.*[99] in 2005 and Faley *et al.*[100] in 2009 are early examples of hydrodynamic cell traps for cell applications.

3.1.3.1 Genomics

The ability to measure the transcriptome of individual cells is highly desirable, especially for immune research. One key aspect to better understand the immune system is to unravel the heterogeneity

of immune cells. Adaptive immune cells are genetically unique. But in addition, each immune cell (both innate and adaptive) is at a given time and space polarized. Immune cells can be in a pro- or anti-inflammatory state; they can be idle or activated. The ability to identify the states of single immune cells is of great importance to understand an immune response. Single-cell RNA sequencing (scRNA-seq) technologies have allowed a breakthrough in this respect [101]. Although scRNA-seq can be performed in "bulk" with the use of small tubes and vials, this technology requires precise control of small volumes down to the picoliter scale. Requirements that microfluidics can achieve and therefore represents a good candidate for scRNA-seq technologies for immune cell studies. Several groups implemented different approaches to isolate individual cells for scRNA-seq. An early example was the work of Love's group [102], where they developed a microfluidic platform with a microwell array of subnanoliter wells. Their platform was used to isolate individual B cells in microwells, filled with a RT-PCR solution before the entire chip was sealed to a glass slide. The amplification was performed after thermal lysis on a thermocycler (Fig.3.1A). This technique was then combined with image-based cytometry and another process pioneered by Love's group, called microengraving, which enables the capture and quantification of single-cell secretomes (we will explain this process just below). While not providing a quantitative gene expression platform, the approach of Gong *et al.* provided insights into the relationship between target gene transcription and protein expression / secretion levels. Other groups used microwell arrays to perform scRNA-seq [103, 104]. While Yuan and Sims did not focus on immune cells but rather on gliomas, the microfluidic platform they developed is of interest for immune applications. They designed a high-throughput microwell array (up to 150'000 microwells) and isolated individual cells by gravity trapping. Then, polymer beads with attached oligo(dT) primers were trapped in the same microwell in order to obtain a cell-bead pair. Each bead contains sequences for amplification of captured mRNA as well as a unique barcode for identification. The team was able to successfully sequence RNA in a high throughput manner with single-cell resolution. In 2015 Kimmerling *et al.*[105], designed a microfluidic chip with single hydrodynamic traps to isolate individual CD8+ T cells. Through their design, they were able to trap and culture individual cells under defined conditions. The design enabled the capture of daughter cells from proliferating trapped cell. Single-cell release and recovery was performed and cells were analyzed by off-chip scRNA-seq. Thanks to this design, the team was able, by comparing intra- and inter-lineage expression of specific genes, to create a link between gene expression profiles and cell-division cycles. This type of platform has great

potential for any studies on heterogeneous populations of cells with different clonal histories, as is the case for adaptive immune cells (B and T cells) and could be used to study the evolution of inflammatory states of a given clonal population and their progeny over time and under different stimulants.

3.1.3.2 Proteomics & cell signalling

While passive microfluidic systems have been used for RT-PCR, they are generally more popular for proteomics applications. As briefly mentioned above, the microengraving technique (Fig.3.1B)) is nicely suited for single-cell secretome screening. This process relies on sequestration of individual cells into microwells where their secretome can be captured by antibodies immobilized to the glass surface used to seal the microwells. Microengraving can effectively screen specific protein secretion down to the single cell level. This process was pioneered by Love's group and was used to actively study cytokine secretion profiles in lymphocytes[106, 107, 108, 109, 110]. For example, Varadarajan *et al.* in 2012 incubated mononuclear cell populations with a specific antigen, followed by single-cell isolation by microwell trapping[109]. Microwells containing CD8+ T cells were identified and their pro-inflammatory cytokine profiles (IFNγ, IL-2 and TNF) were quantitatively analyzed (Fig.3.1B). Cells showing increased pro-inflammatory cytokines, and therefore providing a potential effective immune response, can be retrieved through micromanipulation and expanded *in vitro* for further analysis. Their method was able to successfully establish clonal CD8+ T cell lines with high specificity for HIV antigen in a rapid, cost-effective process while requiring 100- to 1000-times less cells than conventional methods and without the need of sequencing. Similar microengraving techniques were used on B cells to identify specific antibody-producing cells among a heterogeneous population[111, 112, 113, 114] and even on macrophages[115]. Microwells were also used to monitor long-term survival and proliferation rates of isolated T cells subjected to different culture conditions[116].

3.1.3.3 Cell-cell & cell-environment interactions

Another popular application of passive microfluidic systems is for cell-cell interaction studies. The ability to isolate pairs of cells in a defined environment and to monitor their interactions spatially and temporally is a key aspect in immune research. Immunotherapies are a new approach for cancer treatment and rely on using the immune system to fight tumors. A promising approach for

immunotherapies is to isolate and enrich antigen-specific T cells and screen for the most potent ones, which show the highest anti-tumor activity. The process of T cell activation is a complex mechanism involving the screening by T cells of potential antigen peptides. While T cells (especially CD8+ T cells) can be screened for antigen presence in stromal cells (through t cell receptor (TCR) - peptide major histocompatibility complex (pMHC) interactions), immune reactions often rely on phagocytic uptake of antigens by dendritic cells (DCs) (*e.g.* virus-infected cells ultimately dying and releasing viral antigens that are phagocytosed by DCs). The DCs will then display the antigen and travel to a lymph node where a high concentration of lymphocytes (B and T cells) are present. When a defined peptide antigen matches the specificity of a given T cell clone, this clone will activate and expand in order to eliminate the antigen's source. Therefore, the ability to understand and create DC-T or B-T cell interactions is of great importance in immunotherapies. However, each T cell clone is genetically unique, and therefore such interactions should be handled at the single cell level. Several research groups have used passive microfluidic systems to isolate individual T cells and match them with different cell types to monitor their activation and proliferation potential. Dura's group[117, 118] created a microfluidic system with hydrodynamic traps able to capture pairs of immune cells (Fig.3.1C). Their system uses specifically designed traps to capture single cells, transferring them into larger trapping areas where single cells from a second cell type can be loaded and trapped. Dura's group and others used this system to profile lymphocyte interactions between an antigen-loaded B cell and a T cell[118, 119] but also between other types of immune cells such as natural killer (NK) cells[120]. Dura's group was able to monitor early activation dynamics of single T cells and to study the heterogeneity of T cell activation. Compared to conventional approaches, this platform offers the advantages of precise spatial and temporal control over single cell pairs. This platform also allows control over cell culture conditions with the possibility of adding reagents to test different microenvironmental conditions without losing cell pairs and is well suited for samples with low cell numbers, that are insufficient for analysis using conventional techniques such as flow cytometry.

After an encounter with its specific antigen, a T cell will proliferate and activate. Then, the T cell will migrate towards the source of antigen. T cells can follow inflammatory signal gradients throughout the body in a process called chemotaxis. T cell migration is an important step and many immunotherapeutic approaches for cancer treatment aim to maximize T cell chemotaxis. Passive microfluidic systems have been used to recreate inflammatory gradients to study how T

cells migrate. In 2006, Lin *et al.*[121] created a microfluidic device able to generate precise gradients of chemokines, both in time and space to study the migration of lymphocytes towards different chemokine gradients and were able to identify potent candidates (CCL19 and CXCL12). Another example of T cell chemotaxis in a microfluidic device was performed by Jain et al[122] in 2015, where they created a microfluidic maze with pro-inflammatory cytokine gradients to study patterns between activated and unstimulated lymphocytes. In cancer research, passive microfluidic systems with gradient generators or with migration chambers are good tools to study immune response against tumor cells[123, 124, 125, 126].

3.1.4 Active microfluidic systems

While passive microfluidic systems provide significant advantages over conventional methods for single-cell applications, it is often difficult or impossible to perform complex fluidic manipulations. Certain applications require dynamic inputs during the experiment or testing of many different reagents or conditions in parallel. In 2000, Quake's group[127] developed a process called "multi-layer soft lithography" (Fig.3.2), by bonding multiple patterned layers of PDMS elastomer together. PDMS and other elastomers are soft materials that can be deformed elastically with small actuation forces. This property can be used to fabricate on-chip valves by stacking microfluidic channels and pressurizing the control channel. In response to the pressure increase, a membrane separating the two channels will deflect and reversibly pinch off the flow channel (Fig.3.2). The actuation of such valves is a fast process and the response time is on the order of milliseconds[127]. By combining multiple valves, the group fabricated functional elements including peristaltic pumps and multiplexers. The use of valves enables precise flow control on-chip. By combining valves in specific manners, highly complex flow paths can be controlled with a relatively small number of control inputs[128]. Microfluidic Large-Scale Integration (mLSI) has become a useful tool in biological research. In this review we will focus only on their uses for single immune cell studies. Other applications and uses of active microfluidic systems can be found in several reviews[93, 94, 74, 95, 96, 97].

3.1.4.1 Genomics

Active microfluidic systems have been used for single-cell genomics for the past decade. Their ability to isolate small volumes (using valves) and to mix different reagents are useful functions for transcriptome analysis. The use of a ring mixer has been a popular method for single-cell RT-
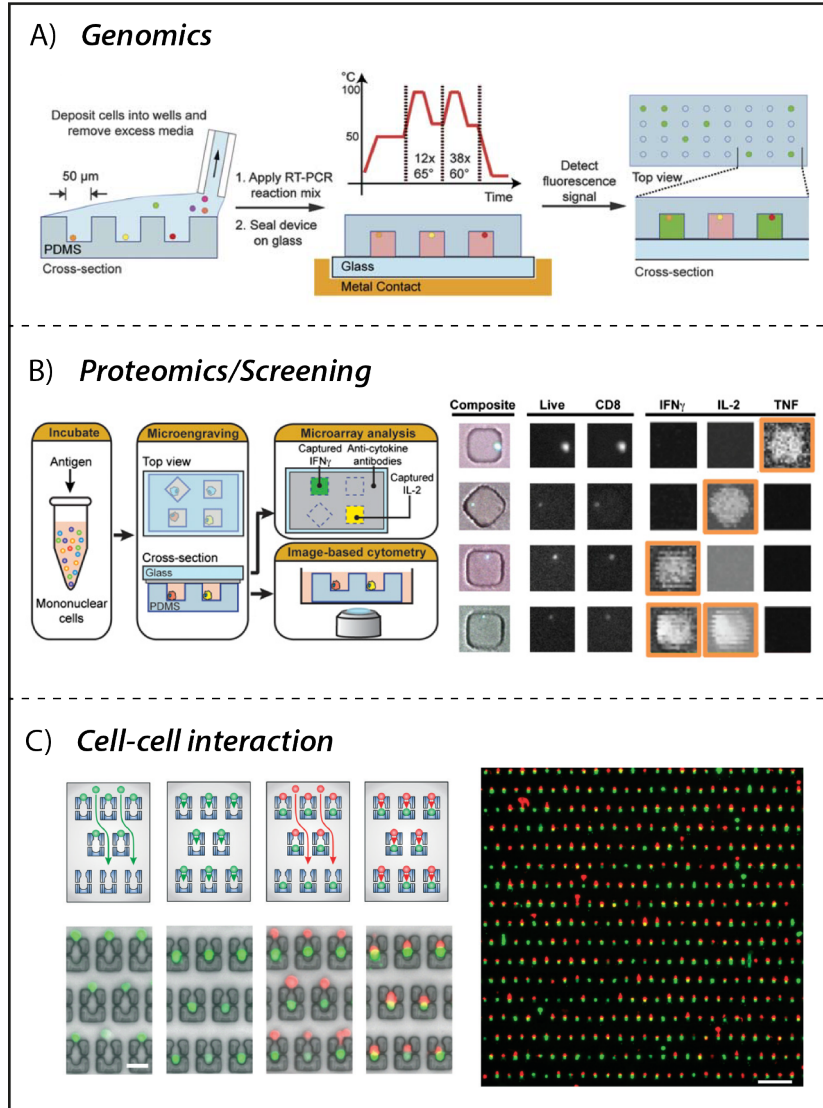
Figure 3.1: **Passive devices for single-cell analysis.**
A) Single cells can be trapped in microwells that can be sealed with RT-PCR solution and thermocycling will trigger the amplification reaction. **B)** Microengraving is a useful tool for studying immune cell secretion at the single-cell level. **C)** Interactions between immune cells can be studied at the single-cell level by trapping cell pairs using hydrodynamic traps. Reprinted with permission [102, 109, 117], adapted with permission from [64].

PCR[129, 130, 131]. A study even combined a microfabricated capillary electrophoresis separation channel for product analysis [132]. In 2011, White *et al.*[133] designed a fully-integrated single-cell RT-qPCR microfluidic platform performing on-chip cell capture, cell lysis, reverse transcription
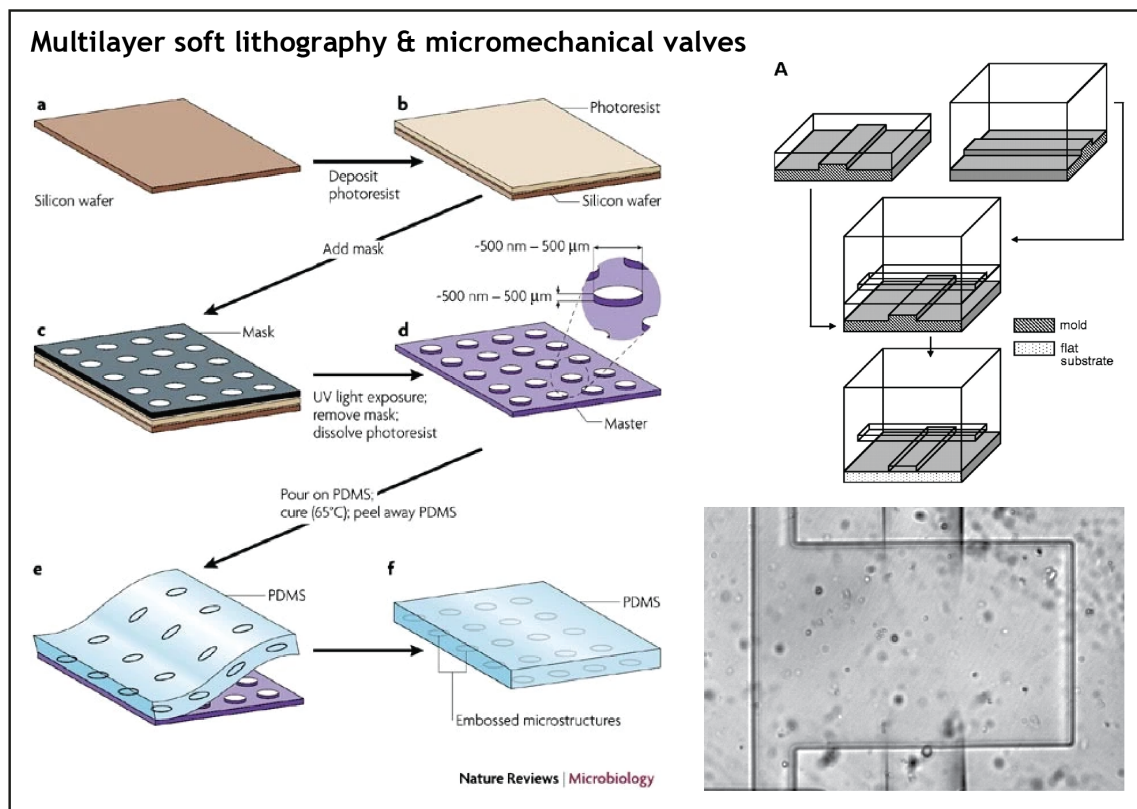
Figure 3.2: **Multilayer soft lithography.**

Multilayer soft lithography allows for microfabrications of creation of micromechanical valves on chip. The process of multilayer soft lithography is described here as well as an example of multilayer PDMS chip for micromechanical valves. A sample image of an actuated valve closing the flow channel underneath is depicted. Reprinted with permission [71, 127], adapted with permission from [64].

followed by off-chip quantitative PCR (Fig.3.3A). To achieve such designs the team combined the use of hydrodynamic traps to isolate single cells and the use of valves to create dedicated chambers for cell lysis, loading of reagents and mixing. This platform was applied to measure more than 3000 single-cell miRNA expression profiles. This type of platform has great potential for single immune cell genomics. By enabling isolation and transcriptome analysis of single T cells, such platforms could greatly enhance the study of immune cell heterogeneity. While active microfluidic systems are well-suited for single-cell genomics, droplet microfluidics has become more popular and suitable as we discuss in the droplet microfluidics section.

3.1.4.2 Proteomics & cell signaling

Compared to passive devices for proteomics such as microengraving, microfluidic devices involving active systems possess certain advantages. Using valves, such systems can isolate small volumes in which single cells are contained. The concentration of secreted molecules will increase over time and therefore the sensitivity of detection is higher. Several research groups have used active valve-based devices to study single cell secretion. Ma *et al.*[134] in 2011 created a microfluidic system containing arrays of different capture antibodies. Using valves, they achieved single-cell separation and measured, for each cell, more than 10 different proteins. Another approach with active valves was achieved in 2010 by Singhal *et al.*[135], where they created a microfluidic device for studying antibody-antigen binding kinetics on beads and single-cells. While elastomeric valves can, as described above, collapse the flow channel, their geometry can be adapted to produce sieve valves. A sieve valve is an actuated valve that doesn't fully collapse the lower channel but leaves a narrow opening on the sides (a leaky valve). This feature can be useful when cells need to be trapped and retained in a microchamber while different reagents need to be added to the cell culture condition. Singhal *et al.* used sieve valves to trap beads coated with antibodies to study association and dissociation rate measurements of antigens to their specific antibodies. The use of active systems enabled the ability to isolate beads and to control the fluidic operations required to study protein interaction kinetics. The group also focused on capturing antibodies produced by hybridoma cells by pairing a single hybridoma cell with antibody capture beads, followed by antigen loading. This technique facilitated single cell screening of antibody-producing cells for a specific antigen by providing full spatial and temporal control over flow behavior, tracking of capture beads and antigen-producing cells using sieve valves and sensitive fluorescent readouts. Quite similarly, Tay's group[136] in 2016 used active microfluidic systems to create a platform combining nanoliter immunoassays, microfluidic input generation, and time-lapse microscopy to measure time-dependent cytokine secretion and transcription factor activity from single macrophage cells under different inputs. Their work is a sophisticated example of a fully-automated, multiplexed platform capable of trapping and isolating single macrophages while detecting cytokine secretion with capture beads downstream. By using traps and valves, the device can trap and isolate single cells but also different types of cytokine-specific beads for multiple readouts. This system can manipulate single beads to sequentially expose them to the trapped cell secretome for cytokine

capture in a controlled manner. In this study, Junkin *et al.* looked at the dynamics of TNF secretion and NK-κB expression under foreign antigens (*e.g.* LPS). The same team further improved on their integrated platform[137] by removing the use of antibody capture beads by the use of on on-chip antibody patterning developed previously by our group for large-scale protein interaction studies[138, 139] and molecular diagnostics [140, 141]. This protocol allows the immobilization of antibodies to the chip surface using a MITOMI "button" [142]. MITOMI buttons were used to functionalize the chip surface for capture of antibodies at precise locations and allowed the multiplexing of antibody types. The platform by Tay *et al.* works as follows: a single macrophage cell is trapped via a hydrodynamic trap in a chamber. This chamber is then isolated via valve actuation and the macrophage, cultured with foreign antigens, will activate a pro-inflammatory transcription factor (NK-κB) and secrete inflammatory cytokines (*e.g.* TNF) that can be both analyzed through the cytokine-specific, spotted antibodies and through the use of reporter genes for the transcription factor. These two studies are good examples of the advantages of active microfluidic systems. Because of active valve-based control, such systems can provide a fully-integrated, large-scale analysis of cell secretion and proteomics while retaining single-cell resolution and limiting cross-contamination between cells.

3.1.4.3 Cell-cell & cell-environment interactions

Like passive systems, active microfluidic systems are good candidates to study cell chemotaxis. As already discussed, chemokine gradients can be generated on-chip and T cell migration towards certain chemokines can be recorded and quantitated. Active systems can provide better flexibility in flow and cell handling than passive systems. In 2015 Mehling *et al.*[143] developed an automated microfluidic cell culture system with stable, diffusion-based chemokine gradients. Their device enabled the precise placement of cells in the migration chamber and single-cell displacement could be tracked by fluorescence microscopy. The chip also provided several outlets along the migration chamber to extract lymphocytes based on their migration speeds for further off-chip analysis. With this system, the team studied migration of individual human primary T cells towards a CXCL12 gradient[143]. In physiological conditions molecules that are involved in cellular locomotion are not only soluble, they can also be attached to the extracellular matrix (ECM). To recreate this complex network of bound and unbound chemokines, Tay's group[144] designed a microfluidic device generating a gradient of soluble chemokine through the use of active fluidic controls combined

with patterned chemokine gradients immobilized to the chip surface. To achieve chemokine immobilization, they used a technique called Laser Assisted Protein Absorption by Photobleaching (LAPAP)[144]. They used their device to track DC migration towards bound CCL21 and soluble CCL19 chemokines.

Overall, in this section, we looked at how the implementation of active systems have boosted the use of microfluidics for single-cell applications. Active systems enabled precise spatial and temporal control of the flow within microfluidic chips. Large-scale integration enabled parallelization and increased the throughput of experiments. Single immune cell research took advantage of active microfluidic systems for controlling and analyzing cells in defined, dynamic microenvironments.

3.1.5   Droplet microfluidics

In order to obtain information about a single cell and to study the heterogeneity of a cell population, confinement of single cells is essential. Advances in microfluidics and microengineering have enabled the confinement of single cells to picoliter-sized water droplets contained in an oil phase. Droplet generation frequency can be tuned and can vary from slow dripping to frequencies of several kHz[145]. Those droplets can encapsulate cells or biological materials, and therefore have the potential for high-throughput single-cell studies. Although water-in-oil droplets have been used since the 1950s, recent advances in droplet microfluidics have greatly increased their uses in single-cell analysis[146]. Our review is focused on droplet microfluidics for single immune cell applications, thus we will not describe the history and advances of this field extensively. We recommend our readers to read dedicated reviews covering droplet microfluidic technologies[147, 146, 148]. Here, we explore how droplet microfluidics has been used in research to tackle the various challenges that single-cell immunology presents. Examples of droplet microfluidics applied to genomics, proteomics, and cellular interactions are described below.

3.1.5.1   Genomics

Single-cell RNA sequencing (scRNA-seq) was achieved by Tang *et al.* in 2009 [149]. This technology allowed the study of the heterogeneity and diversity of gene expression among a cell population. However, using conventional techniques usually leads to low throughput for scRNA-seq. Moreover, certain studies require sequencing of rare samples with few cells. Droplet microfluidics enables the isolation of cells in picoliter sized droplets, where appropriate chemistry can be added to achieve
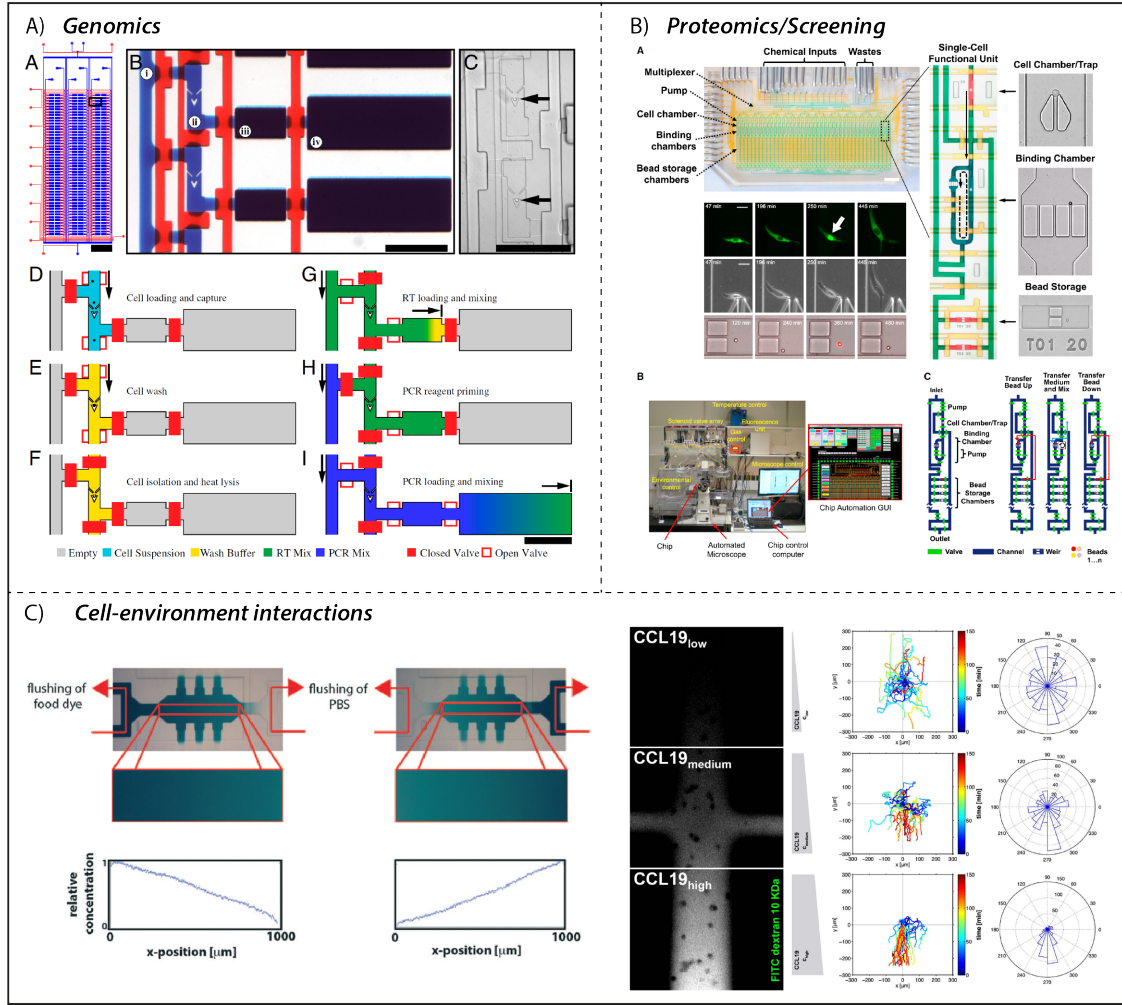
Figure 3.3: **Active devices for single-cell analysis.**
A) The use of valves allows compartmentalization of small volumes, which is an useful for performing on-chip single-cell RT-PCR. **B)** Compartmentalization can be used to isolate single-cells and study their secretion dynamics over time. **C)** Active systems can precisely control flow patterns, enabling the creation of protein gradients in time and space. Immune cell migration towards different cytokine profiles can be studied at the single-cell level. Reprinted with permission [133, 136, 143, 144], adapted with permission from [64].

RNA-sequencing with high sensitivity. Recently, several groups achieved high-throughput scRNA-seq systems using commercial droplet technology, including inDrop[150], Drop-seq[151] (Fig.3.4A) and the 10X systems [152]. All these systems are described and compared in a recent review by Zhang *et al.* [153]. Single-cell RNA sequencing provides profiling of cellular mRNA expression and

also enables analysis of the transcriptional state of single cells such as splice variants. Genome-wide expression profiles of single cells was achieved by Macosko *et al.* in 2015[151], with their Drop-seq platform. It allows for single cell mRNA extension through PCR combined with molecular barcoding for single-cell tracing. They used their platform to analyze the transcriptome of almost 50'000 mouse retinal cells and were able to identify several transcriptionally different populations. One big advance in the field of single immune cell analysis was the sequencing of both immune receptor chains from millions of lymphocytes at the single-cell level by McDaniel *et al.* in 2016[154]. They encapsulated cells with lysis reagents and magnetic beads in droplets. The lysed cells release their mRNA which are captured by the magnetic beads. Then emulsions are broken and the beads are separated, purified, and mixed with RT-PCR solutions with the final products submitted for sequencing. This platform allows a single researcher to achieve T cell receptor (TCR) sequencing within a day[154]. The sequencing of variable domains of immune receptors (antibodies and TCRs) has enormous potential for cancer research and personalized medicine as a whole. While the field of droplet microfluidics for single-cell sequencing, both genome-wide and RNA-sequencing, is quite young, it promises to improve our understanding of the immune repertoire at the single-cell level. Such technologies also have the potential to help identify rare immune cell populations and to develop personalized, immune cell-based therapies as potent new standards for complex diseases like cancer.

3.1.5.2 Proteomics & cell signaling

As we discussed in the previous sections, secretion of cytokines by immune cells is a powerful readout. It provides information about the specificity and the function of immune cells. However, bulk experiments lack single-cell resolution and average the cytokine secretion of an entire immune population. Single-cell technologies aim to study the heterogeneity of immune cells. Single-cell cytokine secretion studies are important for isolation of rare, antigen-specific T cells and could lead to improved immunotherapies. As observed with active microfluidic systems, the confinement of single cells with capture beads for cytokine secretion are useful approaches. Droplet microfluidics offers the advantages of increasing the sensitivity and throughput of the experiments, while retaining isolated single cells in droplets. In 2013, Chokkalingam *et al.*[155] presented a droplet microfluidic platform to detect cytokines (IL-2, IFN-γ, TNF-α) secreted from single, activated T cells over time. Their approach relies on the use of agarose-gel droplets encapsulating a single T

cell with different cytokine capture beads. During the incubation, the activated T cell will secrete cytokines that will be captured by the capture beads in the near vicinity within the droplet. The droplets can then be separated, washed and incubated with secondary fluorescent antibodies for quantification of cytokine presence and analyzed by flow cytometry[155]. Their method allows high-throughput detection of T cell activation heterogeneity and allowed to define subsets of cell populations based on their function. Droplet microfluidics has the ability to isolate single cells in defined microenvironments, while retaining high-throughput. Similar approaches for cytokine detection in single T cells in droplets were designed [156, 157, 158], such as the work of Konry *et al.*[156] (Fig.3.4B), where IL-10 cytokine secretion was studied in droplets containing single T cells. The group added the secondary antibody to the droplets to achieve, after incubation, on-chip sorting between cytokine producing cells and the rest. The same group used similar designs to study cytokine secretion in dendritic cells[157]. Also using droplet microfluidics, Qiu *et al.*[158], designed a T-cell surface aptamer sensor for measuring cytokine secretion at the single-cell level through single-cell isolation in droplets. Their aptamer probe can be anchored onto the cell surface and upon cytokine binding to the aptamer, a fluorescent signal will be emitted that can be analyzed by fluorescence microscopy and flow cytometry. In addition to cytokine analysis, droplet microfluidics was used for single-cell phenotyping of antibody-secreting cells. Eyer *et al.*[159] designed a droplet microfluidic system combined with a sandwich immunoassay for IgG phenotyping. They used nanoparticles pre-coated with antibodies to capture secreted immunoglobulin. Using a magnetic field, the nanoparticles can form an aggregate, observable by microscopy. Those are only a few examples where droplet microfluidics was used for proteomics applications for single immune cell research highlighting the advantages of this technology. Whether it is cytokine secretion from T cells or screening of antibody-producing B cells, droplet microfluidics provides a high-throughput, sensitive platform to study immune cell functions at the single-cell level.

3.1.5.3 Cell-cell & cell-environment interactions

Droplet microfluidics can also be used to encapsulate cell pairs and study their interactions. This feature has great potential for single-cell immune analysis as it allows direct observation of immune cell interactions and their outcome on cell survival, proliferation and activation. Konry *et al.*[157, 160, 161] encapsulated single pairs of T cells and dendritic cells into droplets, which were arranged into microarrays for monitoring of T cell activation (Fig.3.4C). Using this setup, they suggested

that activation of single T cells is more rapid and efficient if T cells are in contact with DCs. Another example of encapsulating immune cells in droplets for cell-cell interaction studies is the work of Segaliny *et al.* [162], where they trapped specific T cells with target cells (*e.g.* tumor cells) to monitor T cell activation. T cells were engineered to express eGFP upon encounter with their specific antigen. Engineered T cells were then co-encapsulated into droplets with antigen-presenting cells. Then, the droplets were trapped using a microwell array for monitoring. The setup also allows for specific recovery of individual droplets. By heating the oil around a trapped droplet with a laser, a bubble forms and pushes the cell-containing droplet away from the trap and back into circulation. Recovered droplets can then be processed for TCR sequencing. The described setup provides a fully-integrated solution for T cell screening, isolation and recovery on the single-cell level and can be linked to downstream genomic analysis. The ability to isolate a single T cell based on its specificity for an antigen and the ability to sequence its TCR receptor to extract information about this specificity is important for cancer immunotherapy treatments. While conventional bulk assays would require T cell clonal expansion to reach sample numbers sufficient for analysis by flow cytometry, which is a time-consuming and expensive step, microfluidics can provide single-cell methods sensitive enough to eliminate the need of clonal expansion while retaining high-throughput. While requiring some cell engineering beforehand, which can be difficult for some applications, Segaliny's work demonstrates the potential of droplet microfluidics for immunological cell-cell interaction studies.
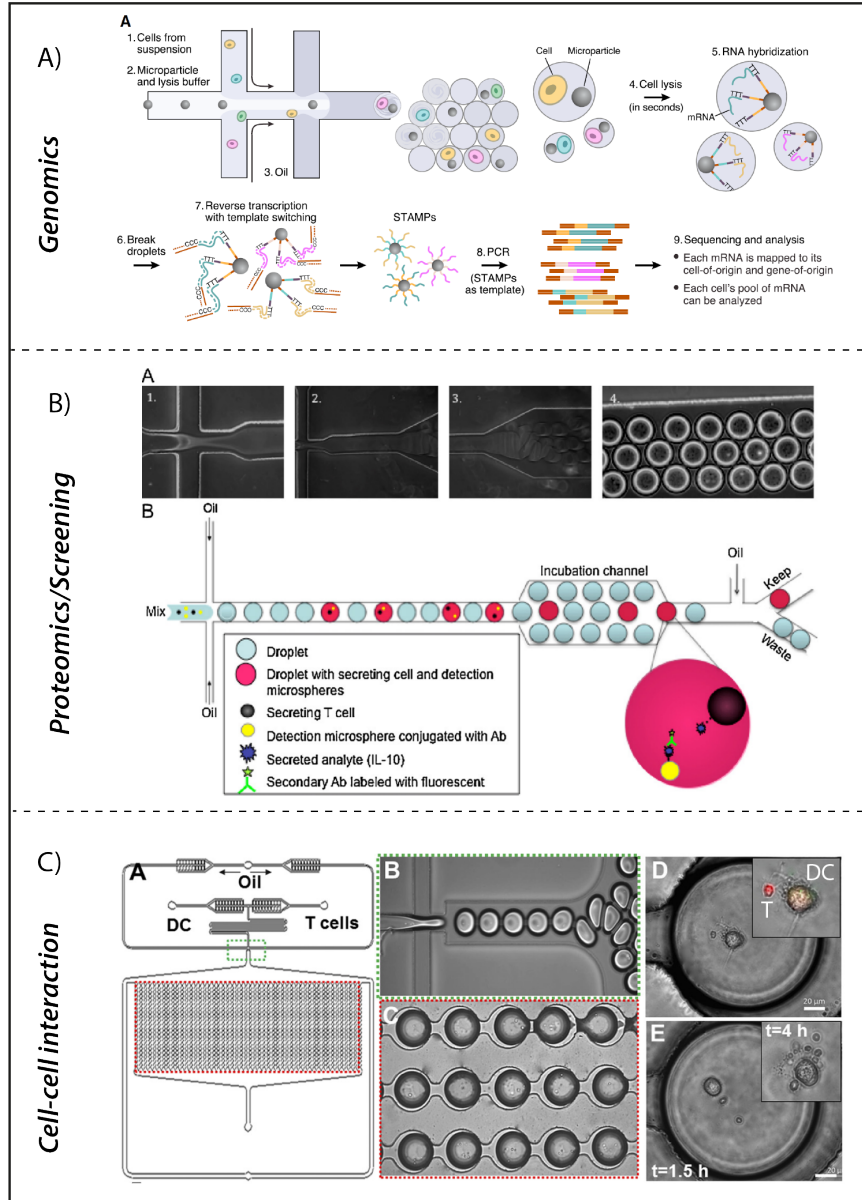
Figure 3.4: **Droplet microfluidics for single-cell analysis.**
A) Drop-seq technology allows for lymphocytes receptor sequencing and entire transcriptomes. Cells are co-encapsulated with lysis buffers and DNA-capture beads with unique barcode. **B)** Single lymphocyte encapsulated in droplets containing cytokine-capture beads and secondary antibodies for cytokine secretion analysis. **C)** Interactions at the single-cell level between antigen-presenting cell (DC) and a lymphocyte (T) can be recorded through droplet encapsulation of cell pairs. Reprinted with permission[151, 156, 161].

3.1.6 Discussion

The immune system is very complex and involves the intertwined network of several cell types. In addition to complex interactions between cells, certain immune cells are genetically unique. The ability to separate and study cell behaviors in controlled environments is required to deepen our understanding of the immune system and help regulate cases where the immune system machinery is broken or ineffective, such as autoimmune diseases and cancer. The behavior of single immune cells is the result of highly complex networks that involve a delicate balance between intracellular and extracellular signaling. Immune cells can be considered as a black-box that integrates internal and external triggers into a proper response. In order to comprehend an immune cell response, the complex mechanisms that regulate an immune cell must be unraveled. Understanding single-cell specificity and dynamics require appropriate tools that conventional, population-based methods cannot deliver. Microfluidic devices have reached single-cell resolution and, because of their increased throughput, helped achieve multi-parameter measurements. Microfluidics enabled researchers to create controlled, dynamic microenvironments where single cells can be interrogated. Advances in different areas of immunology have been made because of microfluidic systems such as advances in single-cell genomics, proteomics, secretion dynamics and signaling as well as advances in cell interactions with their environment and between themselves.

However, due to the complexity of the immune system, much remains to be done. Immune cells are highly responsive to a multitude of complex signals from their environment, both in time and space. Experiments measuring only few parameters are often not adequate for deepening our understanding of how the immune system works. In order to further decipher the complexity of the immune system, multi-parameter experiments should be conducted on single-cells in a precisely defined, dynamic microenvironment. Microfluidic systems have been used successfully to recreate complex environments for single-cell analysis and have enabled studies of single-cell dynamics from genomics, proteomics to cell-cell interactions.

The integration of multi-parameter experiments on single immune cells will enable the acquisition of large datasets that, through the use of machine learning and other artificial intelligence methods, train and create computer models of immune cells and immune responses [163]. We believe that microfluidics can play a key role in achieving that goal through automation. Integrated microfluidic systems can be automated through computer-controlled interfaces. By controlling a

microfluidic chip, as well as data acquisition and analysis, automated microfluidic systems can create a closed-loop system with real-time data acquisition and analysis with potential decision-making abilities. Advances in machine learning and artificial intelligence will strengthen the potential of automated microfluidic systems and could lead to fully integrated measurement and screening devices. Microfluidics, however, is not without drawbacks. One weakness of microfluidic systems is reliability. Indeed, microsystems are often prone to clogging by dust or small debris. Intelligent systems must be developed to ensure reliability and robustness. Despite those weaknesses, we believe that microfluidic devices also will have an important role to play as point-of-care applications for immunology. Integration of microfluidic systems in clinical pipelines could help reduce time and cost for personalized treatments including immunotherapy. Personalized cancer treatments based on modified T cells with high anti-cancer specificity, either by immunoengineering CAR-T cell technologies [164] or by isolating naturally-occurring, rare anti-tumor T cells, are already under clinical trials, including immune checkpoint blockade (PD1-PD-L1) trials [165] that involve T cell engineering for immunotherapy, and show great promise for personalized cancer treatments. Immunotherapies present the advantages of greatly reducing the probability of tumor relapse by creating memory T cells. However, extensive, laborious, time-consuming and expensive protocols are currently needed to manipulate single T cells for personalized treatments. Clinics need more effective and high-throughput platforms for single immune cell genomics and proteomics to identify and address potential targets on a patient-to-patient basis. Microfluidic systems have the potential to cut the cost and analysis time required to achieve single-cell analyses as an integrated aspect of the clinical pipeline. Some start-ups have already successfully implemented microfluidic devices for single immune cell analysis such as the C1™system by Fluidigm, or the Chromium™system by 10x Genomics. Given the rapid technological advances in the past 1-2 decades it seems very plausible that in the near future single-cell techniques are used routinely, from check-up diagnostics at the pharmacy to highly-complex single-cell tools used in clinics for personalized treatments in the field of cancer or autoimmune diseases.

3.2 The need of a novel approach to study lymphocytes affinities at the single-cell level

As explained briefly in 2.3, while CAR-T cell therapy have shown great potential for adoptive T cell transfer for cancer immunotherapy [166], they however display several disadvantages like the targeting of tumor cell-surface antigen only but more importantly CAR-T cells therapies have shown toxicity, sometimes fatal, with toxic levels of cytokine release and severe immune reactions observed [167, 168]. Side effects like cytokine-release syndrome (CRS) or macrophage activation syndrome (MAS) have been observed in clinical trials with CAR-T cell therapies. Similarly, engineered TCR-based cell therapies have shown toxicities and on-target off-tumor effects for several shared antigens (*e.g.* engineered TCR against MART-1 antigen [166]). Another approach is to use naturally-occurring TCR receptors recognizing either shared antigens or tumor neoantigens. This approach reduces the probability of toxicity as the CD8+ T cells with T cell receptors of interest are already present in the body. However, naturally-occurring TCRs tend to present lower avidity compared to CAR-T cells [166]. Therefore, the importance of identifying adequate TCR receptors for a given tumoral antigen cannot be overstated and relies on the study of the TCR-pMHC interaction.

As described in the sections 2.3 and 2.4, the role of the TCR-pMHC interaction for cancer immunotherapy is of great importance. By using this interaction, through the use of soluble pMHC monomers (*e.g.* dextramers, NTAmers, etc...), the specificity of a given lymphocyte and its TCR receptor can be studied. But more importantly, its affinity towards a specific antigen can be studied. As described in section 2.4, a link exists between the physical structural affinity of the TCR-pMHC interaction and the potential of a lymphocyte to get activated upon encounter of this specific antigen. Therefore, in the field of cancer immunotherapy and more precisely, adoptive T cell transfer with naturally-occurring T cell transfer, which presents several advantages on the field of CAR-T cells (mainly safety and less cross-reactivity), there is a need for identification of rare, high-affinity, tumor-specific T cells and their potential isolation for further analysis and uses. This is currently done by several scientific groups who have shown the potential clinical benefits that can be obtain when such rare cells are found and exploited. Studying the affinity of a given lymphocyte is different than studying if its TCR recognizes a given antigen. It represents another level of complexity as the structural affinity of this interaction can only be studied with kinetics (on-rate/off-rate). It has been shown that off-rate measurements and affinity analysis are good indicators of the potential of

55

T cells towards a given antigen [169, 170]. The identification of such rare cells is usually performed by using reversible multimers of soluble pMHC complexes. The technologies of Streptamers and NTAmers (already introduced in 2.4, Fig. 2.6) have helped to reach such goals.

However, as each lymphocytes are unique and present distinct TCR receptors, identifying rare, high-affinity lymphocytes for tumor-specific antigens requires, therefore, to work at the single-cell level. Current technologies (*i.e.* flow cytometry) used with reversible multimers often requires clonal population of each unique lymphocytes as they do not provide temporal single-cell resolution. Such clonal expansion relies on cumbersome cell culture procedures that yield poor results (few clonal population survive expansion *in vitro*) and can lead to a biased final, cultured and expanded population. Moreover, the current clinical and experimental pipelines using clonal expansion for flow cytometry analysis require extensive time and cost due to such elaborated cell cultures procedures. As we discussed in Section 3.1, the field of microfluidic technologies have distinctive advantages over current technologies when it comes to reach single-cell level as well as time and cost benefices. Microfluidics have been used extensively in the field of immunology and have enabled great advances in clinics for cancer immunotherapy.

In this project, we propose to use an innovative microfluidic design, combined with the technology of reversible pMHC multimers (*i.e.* NTAmers [62]) to study, identify and isolate rare, high-affinity, tumor-specific T cells by studying the dissociation kinetics and affinities of the TCR-pMHC interaction for a given tumor-specific antigen. By combining those two innovative technologies and using fluorescent microscopy, machine automation and image analysis we aim to develop a new platform that could enable the identification and recovery of such rare cells that could lead to better personalized, cancer immunotherapies clinical treatments. The origins and aims of this project are illustrated in Figure 3.5.
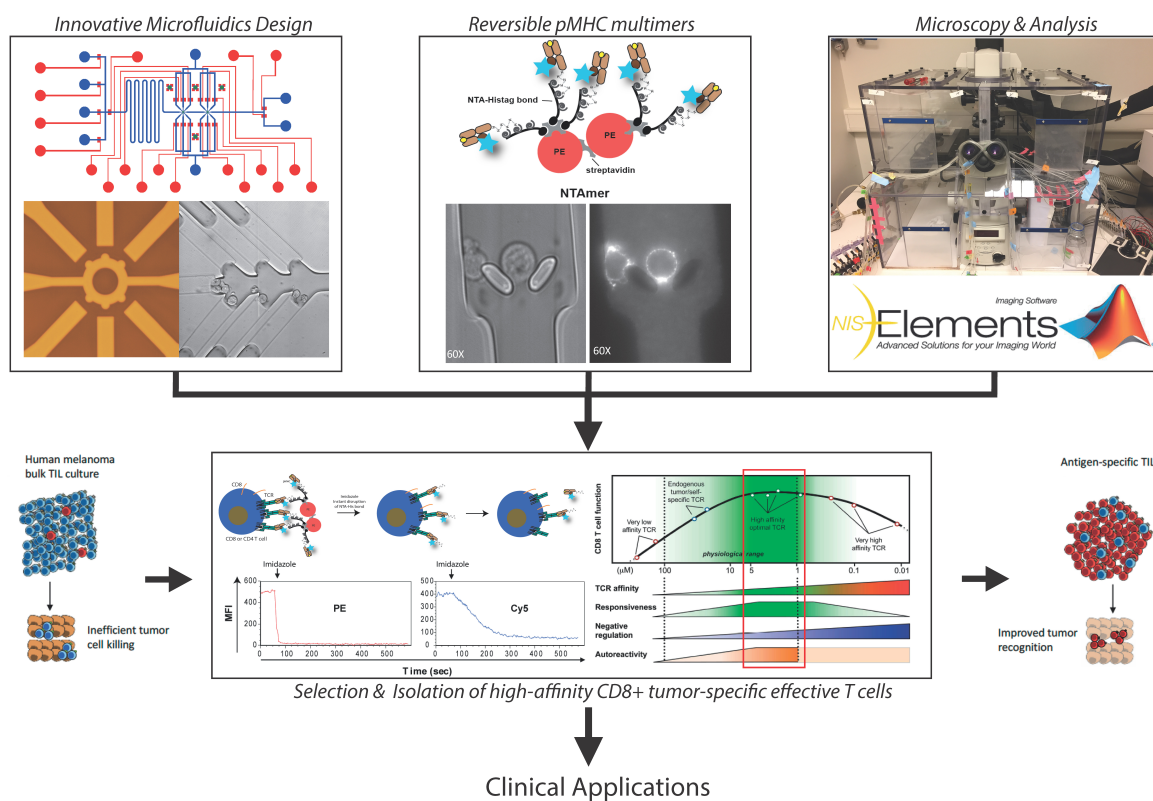
Figure 3.5: **The origins and aims of this project.**

By combining innovative microfluidics designs with the technology of reversible pMHC multimers and adapting those technologies to fluorescent microscopy, we aim to enable the identification of high-affinity, tumor-specific T cells by studying their affinities towards a given tumor-specific antigen. Adapted with permission from [171].

4

A new microfluidic platform for studying the pMHC-TCR interactions at the single-cell level

4.1 Specifications and requirements

The primary goal of this project was to bypass the limitations found in a pMHC-TCR interactions study by our collaborators resulting from using flow cytometry as a readout. By preparing the cells in the desired concentration in buffer and adding imidazole immediately before loading the cell in the flow cytometer, our collaborators at CHUV recorded dissociation kinetics of target cells labeled with NTAmers (reversible pMHC multimers). However, this approach is not truly a single-cell approach as flow cytometry provides single-event data for a single temporal point per cell (*e.g.* size, granularity, fluorescent signals, etc...). As each TCR sequence is unique, the study of dissociation kinetics via flow cytometry requires single clonal population presenting the same TCR receptor. This results in the requirement of working with a single clonal population presenting the same TCR receptor, which in turn requires single-cell dilution to isolate each CD8+ clones separately, followed by clonal expansion to reach numbers sufficiently high for flow cytometry experiments (*e.g.* 100'000 clonal cells). These cumbersome steps, which present the disadvantages of being costly, time-consuming, and furthermore introduce a potential important bias of *in vitro* culture selection, can be avoided by working, in time and space, at the single-cell level. The field

of microfluidics possesses several qualities to achieve such goals. However, a microfluidic design for such experiments should fulfill the following requirements:

- **Adaptability:** This microfluidic technology should work in tandem with fluorescence microscopy as a readout. Therefore the design should be able to adapt the current NTAmers technology (used mainly with flow cytometry) to work adequately (*i.e.* signal strength, resolution, etc...) with fluorescent microscopy.

- **Cell loading:** The device should be able to receive and load cells, while keeping them alive for the duration of the experiment.

- **Single cell isolation:** The device should be able to isolate cells individually or track them in order to reach single-cell level resolution.

- **Flow exchange:** The device should be able to transfer the cells from an imidazole-free to an imidazole-rich buffer on-chip in order to trigger the switch to monomeric pMHC state and record the dissociation kinetics.

- **Temporal resolution:** The device should enable us to study dissociation kinetics of the pMHC-TCR interactions at the single-cell level, with enough details and data to fit an exponential decay and extract a key parameter of the pMHC-TCR interaction, the half-life of dissociation, the link between structural, and functional affinity of the T cell.

- **Recovery:** The device should, if possible, be able to recover cells of interest based on their affinity towards a given antigen (extracted from the half-life of dissociation). This means being able to recover a given cell compared to another in a controlled way.

- **Throughput:** The throughput should reach the order of hundreds to thousands of cells analyzed per experiment to effectively be able to isolate rare, high-affinity T cells in a mixed population of cells.

In order to achieve these requirements, the microfluidic device was selected to be an active microfluidic system with the integration of mechanical valves on the chip for precise control (spatial and temporal) of flow. The description of such types of active microfluidics can be found in section 3.1. The cells used in this work are SupT1 cell lines developed previously and described here [172]. Here, two clones were used: WT (with the WT TCR sequence) and DMβ with increased affinity

59

compared to WT, both TCR receptors recognizing the same cancer antigen, same antigens loaded on the NTAmers (see Materials & Methods 7.2).

4.2 Adapting the reversible pMHC NTAmers technology for microfluidic technology

One of the key points of this work is to adapt the NTAmers technology from flow cytometry to microfluidics technology. NTAmers are reversible pMHC multimers. Effectively, an antigen of interest (in this project we used the analog NY-ESO-1157-165 [SLLMWITQA] tumor antigenic peptide), is loaded onto His-tagged HLA-A*0201 monomers containing an Cy5/Alexa647-labeled β2m (see 7.2). The monomers are then mixed at a 10-fold ratio with Streptavidin-Phycoerythin (SA-PE) cores with four Ni2$^+$ -nitrilotriacetic acid (NTA4) in order to assemble into stable multimers (Fig. 4.1). Addition of imidazole will create competitive inhibition of the His-tagged links on the monomers, effectively dissociating the monomers form the SA-PE core within seconds (5s), which can be easily observed as a fast and sharp decrease in PE signal (Fig. 4.1). Therefore, when the NTAmers technology is used to label TCR-expressing cells, after addition of imidazole, single pMHC monomers will remain bound to TCR receptors. Their dissociation kinetics, intrinsically linked to the structural affinity of the pMHC-TCR interaction, can be observed as the decay in Cy5/Alexa647 fluorescence of the cell membrane over time (Fig. 4.1).

However, it is worth noticing that the NTAmers technology was initially designed for use with flow cytometry. In this project, we first investigated the potential use of the NTAmers technology for microfluidics and fluorescence microscopy. Initially, the NTAmers used were made with Cy5 fluorophores. Signal strength was originally found to be too weak to use with lower magnifications such as via a 20X objective (Fig. 4.2). As the microfluidic design iterated (see later), the need for a stronger signal for single-cell analysis pushed the use of higher magnifications like 40X. A high bleaching rate and low signal strength were still observed. Cy5 was substituted for Alexa647, which presents a higher signal-to-noise ratio and a better stability against bleaching. Upon final iterations of the microfluidic design, as well as the study of the NTAmers signals with fluorescence microscopy, it was decided that the use of Alexa647 as fluorophores with the use of a 60X objective (oil) were the most suitable options (Fig. 4.3).
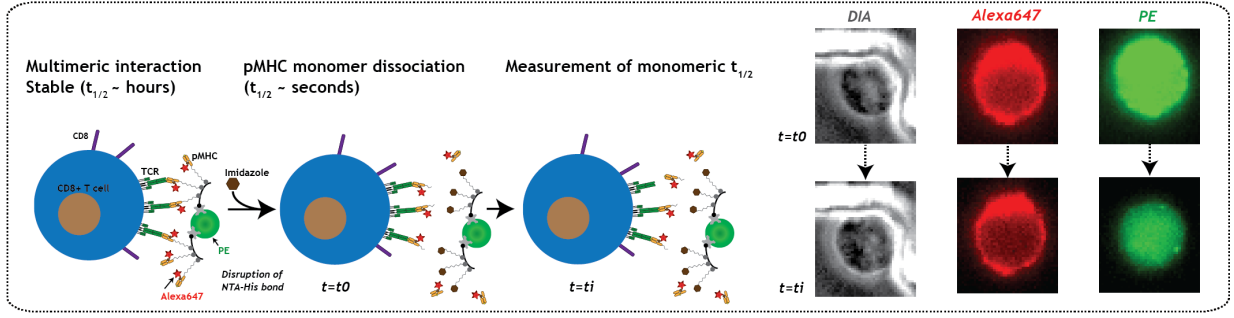
Figure 4.1: **The NTAmers technology: reversible pMHC multimers.**
Peptide-MHC complexes are labeled with Alexa647 fluorophores and modified to display His-tag links. A multimeric core, labeled with PE fluorophore is then used to aggregate several pMHC molecules (10-12 per multimeric core). The reversibility of this technology is achieved when adding imidazole, which disrupts by competitive inhibition the links between the multimeric core and the pMHC monomers, effectively leaving pMHC monomers bound to TCR receptors on the cell surface.

4.3 Design iterations and final design

In order to tackle the requirements described above, the microfluidic device needed to have precise temporal and spatial control of the cells and their handling on chip. While flow cytometry technology provides great analytical throughput, this technology is unable to perform single-cell off-rate measurements. Previous attempts showed the potential of studying single-cell off-rate measurements via fluorescence microscopy but the throughput of analysis was low [169]. Therefore, it was decided in this project that throughput would represent an important parameter. During this project, several design iterations were performed to achieve the best compromise between throughput and resolution, while maintaining single-cell handling capability. As described above, adaptation of the NTAmers technology to fluorescence microscopy led to the requirements of higher resolution objectives. This evolution was reflected on the iterations of the microfluidic designs. A brief description of the main iterative steps is described in Figure 4.4. Three main design types were assessed during this project ranging from a microwell array to single independent chambers. For each design, technical challenges were encountered, which had to be addressed.
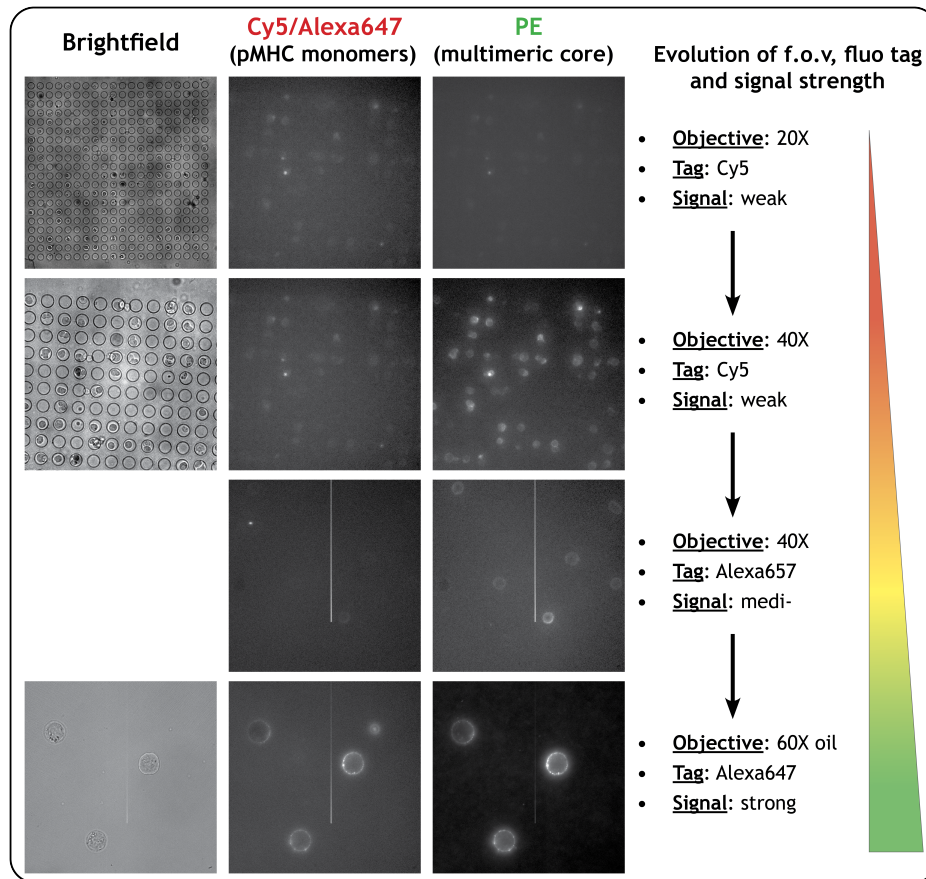
Figure 4.2: **Evolution of the required f.o.v and fluorophores for signal strength.**

Initially, the NTAmers technology presented Cy5 tags on monomeric pMHC units but the signal strength observed by fluorescence microscopy was revealed to be too weak for lower magnifications such as that from a 20X objective. In order to increase the strength of the fluorescent signal, the desired magnification was increased from 20X to 60X and the fluorophore was changed from Cy5 to Alexa647. Theses decisions impacted the design and geometry of the microfluidic device as observed in Fig. 4.4

4.3.1 Microwells and microtrap arrays

The initial design idea was inspired by the work previously done by Kristina Woodruff, a former PhD student at LBNC. She designed a microfluidic platform for high-efficiency and high-throughput transfection and culturing of mammalian cells [173]. The first design trial adapted her approach, but instead of culturing cells the idea was to trap cells and maintain them on-chip for flow exchange

Figure 4.3: **Adapting the NTAmers technology to fluorescence microscopy: Signal strength.**
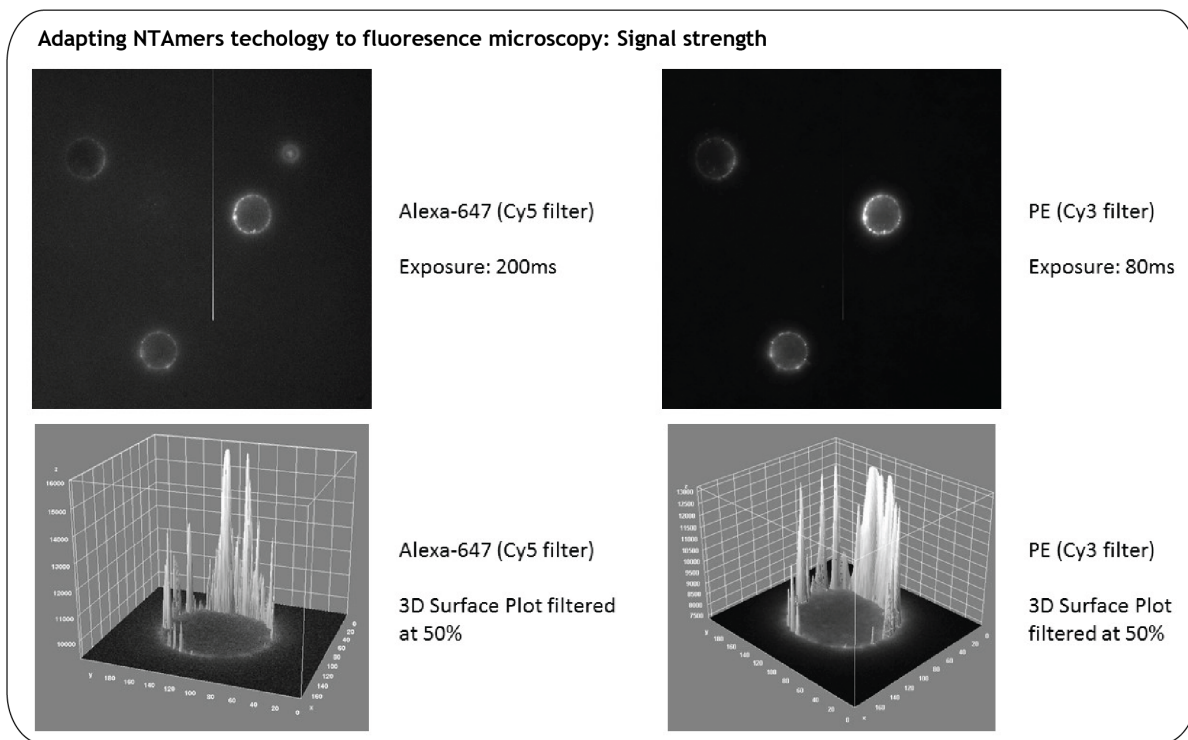
Signal intensity was found to be sufficient and acceptable when using a 60X oil objective magnification coupled with the use of Alexa647 as fluorophores for the pMHC monomers instead of Cy5, due to a stronger signal-to-noise ratio and better bleaching resistance.

with imidazole while recording dissociation kinetics with the NTAmers technology. The first cell-trapping idea was to use a third, separate PDMS layer consisting of a microwell array. The design presented four independent rows with five chambers each for a total of 20 individual chambers (Fig. 4.4). Each chamber presented 400 microwells. The microwells were made to be between 20 and 40μm in depth and 20μm in diameter. The initial idea of this design would be to capture cells in the microwells. Upon cell capture, flow exchange with imidazole-rich buffer would be triggered in a single chamber. Dissociation kinetics for the entire chamber would be recorded via a low resolution objective (*e.g* 20X) and after analysis, cells of interest would be registered in the corresponding microwells. The chip would then perform dissociation kinetics in the others chambers. At the end, the chip would be unplugged, and the interface between the microwells layer and the rest of the chip would be dismantled. Selected cells would be recovered individually in each microwells by a
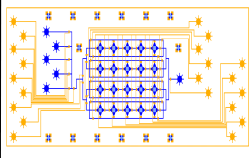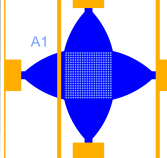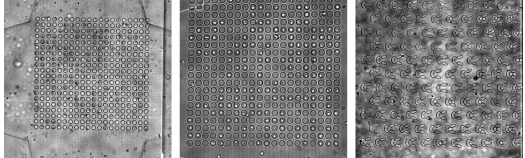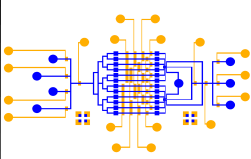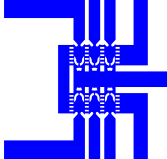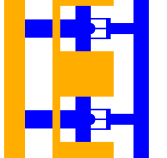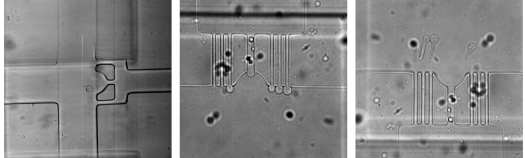
Type of design	Design layout	Close-up	Sample images
Micro-wells/traps: • 3 layers PDMS Chip (control, flow, wells/traps) • 20 individual chambers • 400 microwells per chamber • 116 microtraps per chamber • Chamber size: 620x620um			
Trapping areas: • 2 layers PDMS (control & flow) • Trapping areas with independent lanes for recovery • Multiplexor • Fit for 40X objective			
Independent chambers: • 2 layers PDMS (control & flow) • Up to 16 isolated chambers • Multiplexor • Fit for 40X-60X objective			

Figure 4.4: **Main iterations of designs.**

Early approaches to the microfluidics platform. Initially, the main idea was to use relatively big chambers with arrays of microwells or microtraps which can be flooded independently with imidazole. Potential recovery was envisioned by peeling apart the PDMS layers and micropipetting out the cell(s) of interest. Another approach was to create condensed trapping areas to visualize several trapped cells with higher resolution (40X or 60X objective). Separated channels grouped in a common trapping area while allowing for independent trapping and recovery of single cells. The final approach was to create independent chambers able to trap single cells and address each chamber individually for flow exchange as well as cell recovery.

micropipette. While this design was successful in trapping cells in the microwells with relatively high efficiency (up to 33% of filled microwells, Fig. 4.5b), it presented several drawbacks. Mainly, when flowing imidazole-rich buffer into the chambers, loss of cells was observed. In addition to cell loss, cells required a significant amount of time to settle at the bottom of the microwells, which impacted the potential throughput of the approach. To circumvent those issues, an alternate version of the des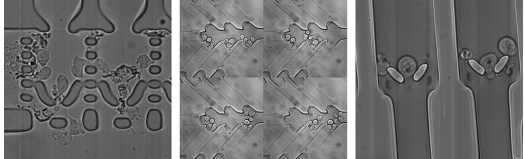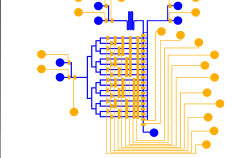ign was developed with microtraps instead of microwells. Microtraps (Fig. 4.5c) presented the advantage of removing settling time and keeping the cells in the same optical plane as the flow layer. It presented however a smaller trapping efficiency than observed when using microwells (16% vs 33%). It was concluded finally that a device with three PDMS layers was not optimal for microfabrication, practicality, and potential future cell recovery. As the adaptation of

the NTAmers technology for fluorescent microscopy pushed the project to use higher magnification objectives (*e.g.*40X or 60X instead of 20X, Fig. 4.5a), the design of the chip evolved to accommodate a smaller field of view.
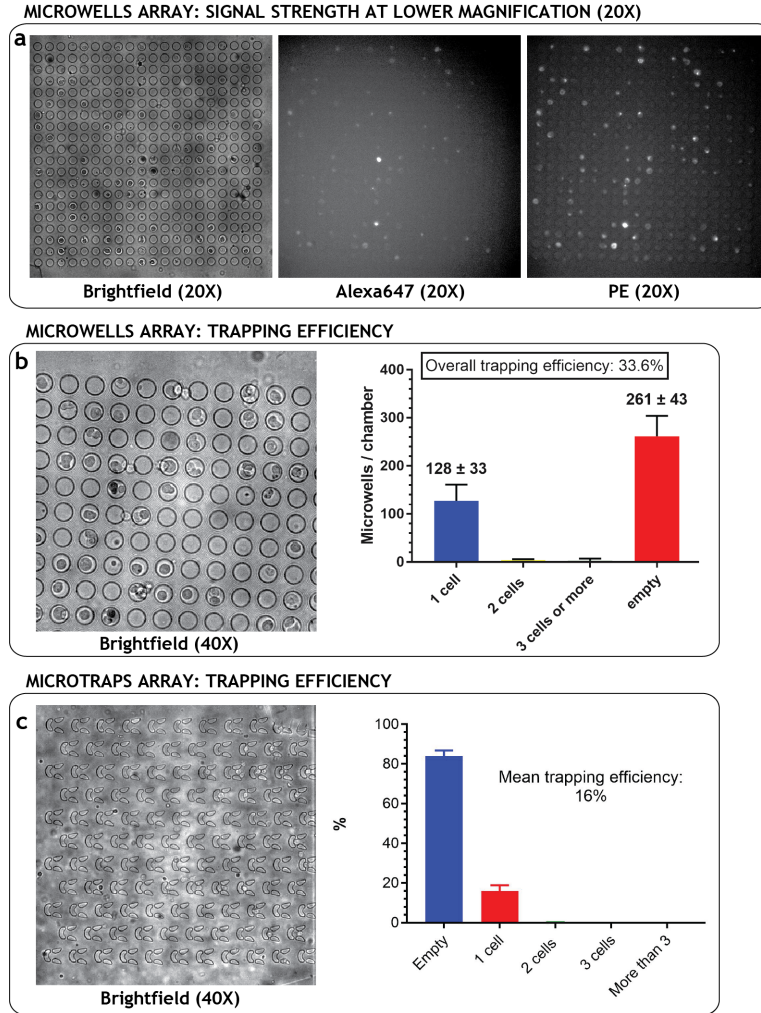
Figure 4.5: **Microwell- & Microtrap-based microfluidic approach.**
a Signal strength for NTAmers-labeled SupT1 cells (DMβ) trapped in microwells with a low magnification objective (20X). **b** Assessing trapping efficiency (33%) with microwells. Image of trapped cells (40X, brightfield) with microwell count for presence of single or multiple cells as well as empty chambers. **c** Similar approach for microtrap-based microfluidic variant with lower trapping efficiency (16%).

4.3.2 Trapping areas

To accommodate higher magnification while maintaining high throughput, microfluidic designs were then adapted to trap single cells within defined areas. Each trapping area would be connected by different independent lanes, which could ensure selectivity of cell loading and recovery (Fig. 4.4). This approach aimed to trap cells from different independent lanes in a small and confined area, which could then be imaged through a high-resolution objective like 40X or 60X. The chip was composed of two PDMS layers (Fig. 4.6a). The first one, the control layer for pneumatic valve actuation, was made out of SU-8 at a height of 30μm. The flow channels were composed of a single layer of AZ 9260 (height of 15μm), which was annealed in order to reach a rounded profile required for lane closure. The cell traps were made by creating gaps in the flow channels that were filled by PDMS during chip microfabrication. The design proved to be successful at loading cells on chip and effectively trapped cells in the trapping areas (Fig. 4.6b). However, cells were often observed to squeeze out of the traps when under flow either from loading or flow exchange (Fig. 4.6b). This resulted in loss of cells, mixing of cells between what should have been independent lanes, and accumulation of cell debris (due to squeezing) in the trapping areas. Cell loss by trap avoidance was a recurrent problem in this project. This issue was attempted to be addressed several times and by different approaches, which eventually led us to abandon trapping area-based microfluidic designs in favor of independent chambers. These chambers could be isolated by micromechanical valves actuations and were better suited to handle flow exchange while minimizing shear stress on cells.

4.3.3 Independent chambers

Isolating individual cells in a confined area can be achieved quite straightforwardly thanks to the integration of micromechanical valves in an active microfluidics system (see 3.1). However, the requirements of this project demand not only single-cell isolation, but for the cells to receive and handle flow exchange as well in order to introduce imidazole in the cell vicinity. This requirement has been challenging and cells squeezing out of traps were regularly observed with the two previous approaches. It was observed that the use of the positive photoresist AZ 9260, which allows for rounded microfluidics channels required for closure upon valve actuation, presented the drawback of a lack of precision for cell traps. Rounded channels are indeed required for valve closure and are
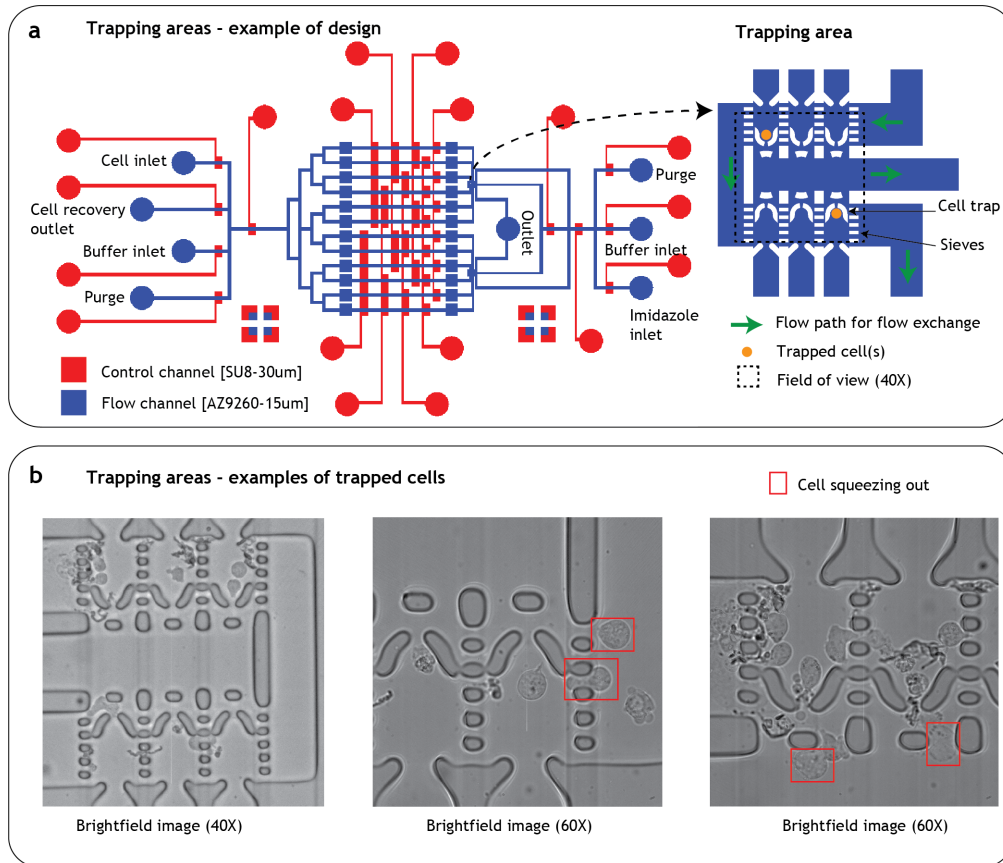
Figure 4.6: **Trapping area-based microfluidic approach.**
a Example of a tested design based on a shared trapped area that allowed for independent lanes to aggregate in a common areas which could be imaged with high resolution (*e.g.* 40X). A close-up portion of the trapping area is depicted with trapped cells and the flow path of the required flow exchange (see specifications above) with imidazole for NTAmers technology. **b** Brightfield images of SupT1 cells on-chip in trapping areas. Close-up views highlight a technical problem encountered with this type of design, which was cell squeezing out of traps into other trapping or flow lanes.

obtained by annealing of the flow channels at a high temperature which transforms a rectangular channel into a rounded one (Fig. 3.2). While being a desirable feature it presented the side effects of lacking resolution for small features like cell traps. In addition, lymphocytes are, by nature, designed to migrate all over the human body, including small capillaries. Therefore, it could be argued that cell extraction and mobility is high for this cell type. To prevent cell squeezing, it was decided to refine the cell traps by not only creating thin cell traps but by changing the

height of certain part of the trapping section. This lead to a new approach (Fig. 4.7) of trapping cells in independent chambers that are interconnected during cell loading but can be isolated by micromechanical valves. Each chamber would represent an intersection between a cell loading path and a buffer exchange path (Fig. 4.7a). To ensure that cells will remain in the chamber while under flow exchange, an additional flow layer was created with a smaller height. This resulted in the introduction of sieves as cell traps. While the main flow layer was typically 15μm high, the sieves portion were designed to be between two and four microns high (Fig. 4.7a). While the frequency of cell squeezing during flow exchange was greatly reduced with the use of sieves, it was not completely removed during the first iterations of designs that incorporated sieves. As observed in Figure 4.7b, cell squeezing was still observed, and in other instances, instead of cell squeezing, cells were deformed by protrusion into the sieves part (red rectangles).

Overall, the results obtained with this type of microfluidic device was encouraging. While the general principle of connected chambers that can be loaded with a continuous flow of cells and then isolated by valves actuation was showed to be a viable option for single-cell analysis, the necessity of performing flow exchange on chip in the isolated chambers presented several problems. Mainly, shear stress on cells exerted by the imidazole-rich buffer flowing into a chamber was sufficient to trigger cell squeezing through the sieves, and often resulted in cell death and creation of cell debris in the sieves area. In addition to cell squeezing, cells were observed to be damaged during flow exchange, with protrusion of the cell membrane into the sieves being observed. This lead to the development of innovative solutions to reduce local shear stress in the chamber area for isolated cells. Those solutions were implemented in the final iteration of the design presented below.
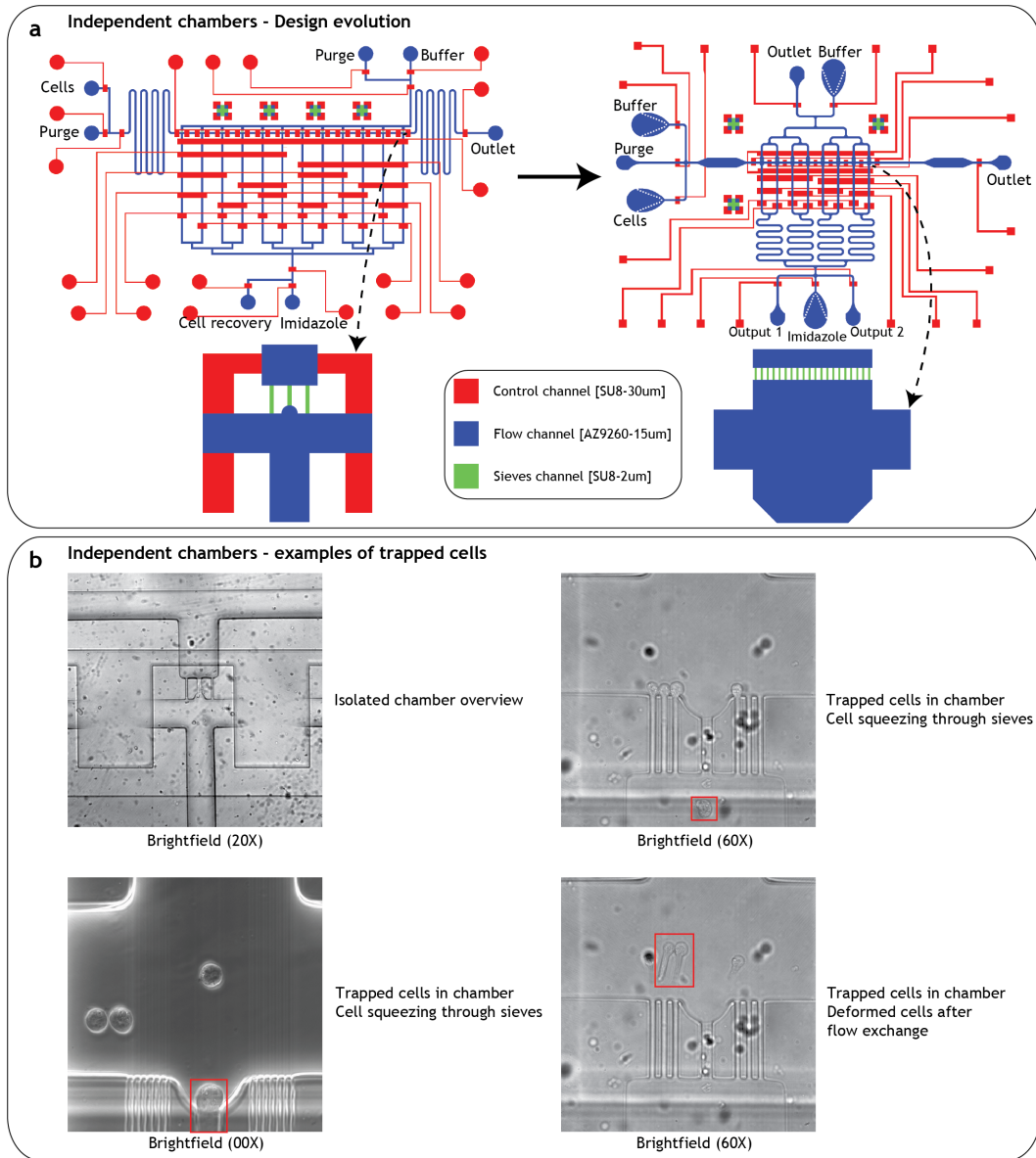
Figure 4.7: **Independent chamber-based microfluidic approach.**
a Examples of the evaluated designs based on independent chambers. By using micromechanical valves, small areas defined as cell chambers can be isolated. The use of a second thin layer (2-4 μm) in the flow channel allows for better control of cell squeezing during flow exchange. **b** Brightfield images of trapped cells in independent chambers. An overview of an isolated chamber (valves actuated) is depicted. Cell squeezing and deformation were observed under the sieves (red rectangles).

4.3.4 Final design

In order to reduce shear stress on cells during flow exchange, several innovative solutions were implemented on chip. Those solutions mainly targeted the chambers part of the microfluidic device. A brief descriptions of the the implemented solutions is presented here:

- **A new chamber channel:** As mentioned before, the positive photoresist AZ9260 presents the advantage of forming a rounded fluidic channel that is suited for valve closure. However, it usually presents lower resolution for small features than the negative photoresist SU-8. This lack of resolution was observed when using trapping areas, as the cell traps made in AZ9260 were unsuccessful in trapping cells consistently. In the final design, the chamber part was replaced with SU-8 with a height of 10μ (Fig. 4.8a), which will ensure better resistance of the fluidic channel during flow exchange. The removal of the round fluidic channel allows for better precision of the chamber geometry.

- **Partially-closing valves:** The use of SU-8 in the chamber area brought another advantage. If valves are placed above an SU-8-made flow channel, valves closure cannot be complete because of the lack of rounded features (characteristic of AZ9260 photoresist). Therefore, when valves are actuated on a rectangular channel, the channel only partially closes. This feature was used to increase flow resistance by placing partially-closing valves before and after chamber areas in the design (Fig. 4.8a).

- **Smaller sieves:** Sieves were also redesigned to be smaller and shorter with a width of 3μm and a height of 1.5μm. Smaller sieves ensured to lower the probability of a cell squeezing through.

- **Flow bypasses:** In order to further reduce flow velocity locally, bypasses were installed for each chamber (Fig. 4.8a) so that the velocity of fluids coming for flow exchange in a chamber (*e.g.* imidazole-rich buffer coming from bottom inlet to a specific chamber) will be divided and locally reduced in the chamber. By placing valves on the bypasses, it was ensured that cells could not go through bypass lanes during cell loading (Fig. 4.8a).

This resulted in a better control over cell squeezing and deformation. The design was still able to load and isolate single cells in the different chambers (Fig. 4.8b, red arrows). But more importantly, cells remained in overall good shape under flow exchange and the number of cells squeezing out of

70

chamber was reduced to an insignificant level. Cell deformation was still observed regularly but in a more gentle way than previous designs (Fig. 4.8b, orange arrows). When observing cells over time during flow exchange (montages in Figure 4.8b), cells behave properly in the cell pockets that were added to the chamber design. Those results were encouraging, and it was decided that this design was sufficiently successful at the tasks of loading and isolating single cells, performing flow exchange, and pushing cells out of the chip (see later).
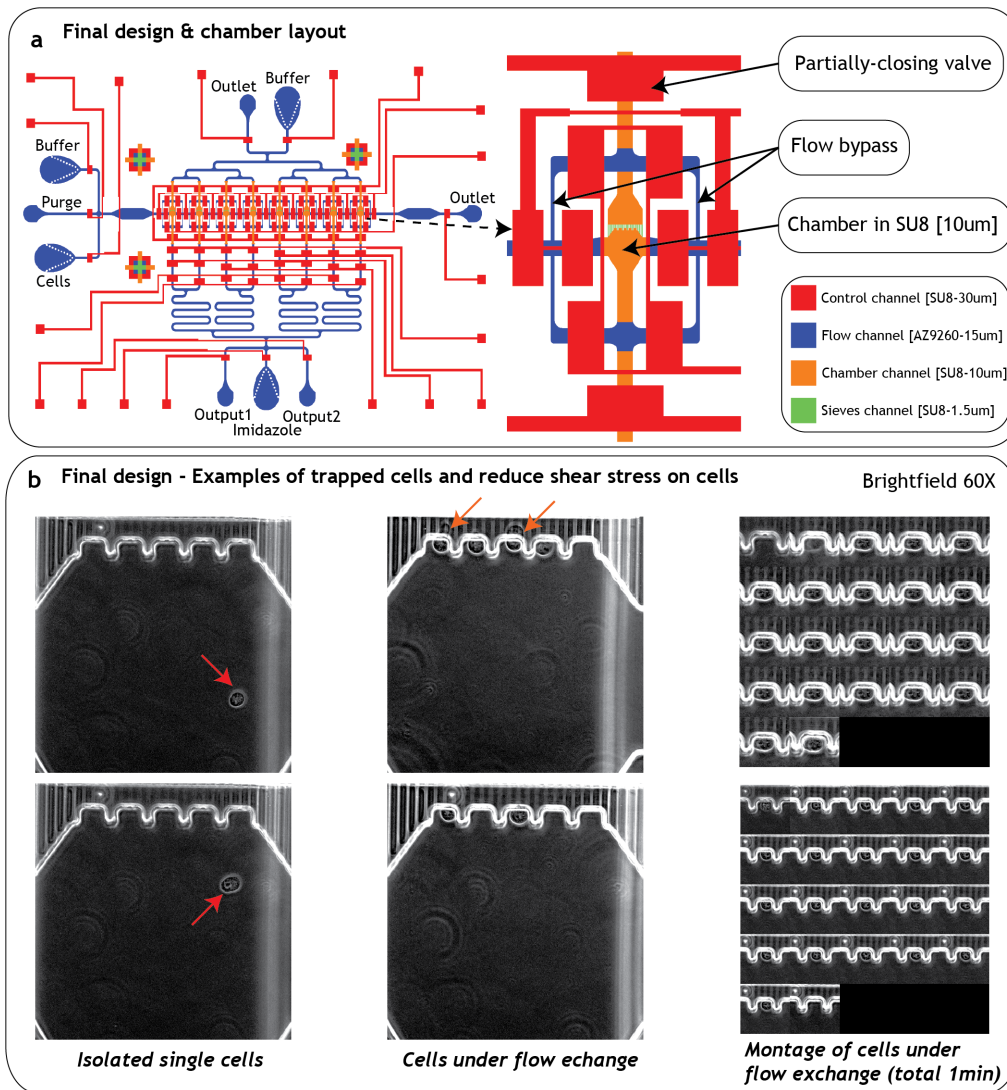
Figure 4.8: **Final microfluidic design.**

a Several changes were implemented upon the first design with independent chambers. First, SU-8 was used to create the chamber area instead of AZ9260 for better precision. Second, the sieves were redesigned to be thinner and shorter (1.5μm high). Third, flow bypasses were introduced for flow to circumvent the chamber area when performing flow exchange. Lastly, by using SU-8 in the chamber area, a partially-closing valve was introduced before and after the chambers in order to increase flow resistance when performing flow exchange. **b** Brightfield images of isolated cells in chambers (red arrows). Cell deformation and squeezing was overall greatly reduced with small protrusions observed occasionally (orange arrows). Montages of cells under flow exchange (time-lapse of 1min, 3s interval) show cell behavior during flow exchange.

4.4 Evaluation of the design & main challenges

During the different iterations of the devices, several challenges were identified. One of them was cell deformation and squeezing and was described in the previous section. The challenges encountered were primarily related to cell behavior within the chip. I would like to describe the main difficulties encountered and the solutions that were put in place to address these challenges.

4.4.1 Cell deformation and squeezing

As already described in details during the iterations of the device, cell squeezing and cell deformation have been recurrent problems. The necessity to keep cells in a defined environment while meeting the demands of the buffer exchange experiments that were selected in this project (*i.e.* use of NTAmers technology and the need to introduce imidazole around trapped cells) have proven to be difficult tasks to accomplish, in particular with the cell types used in this project (SupT1 cells). As mentioned in the previous section, the different innovations included in the final design allowed us to accommodate proper flow exchange within chambers with isolated cells, while reducing shear stress on them.

4.4.2 Fast flow exchange

As explained before, the NTAmers technology requires the fast introduction of imidazole-rich buffer to trigger the switch from a multimeric to monomeric conformation. This switch is realized by competitive inhibition of imidazole with the His-tagged monomeric pMHC molecules. The introduction of imidazole was performed conventionally by mixing imidazole-rich buffer with the cell solution before injecting it in the flow cytometer. Microfluidic technology presents the advantages of performing flow exchange on chip for better temporal and spatial control of the experimental setup. By controlling precisely when and where the imidazole-rich buffer can be introduced to the isolated cell in the microfluidic chamber, this approach presented a non-negligible advantage over conventional techniques, wherein often the first seconds of reactions are lost due to human manipulations. The flow exchange, however, is best if performed in a fast and sudden manner so that the switch for NTAmers from multimeric to monomeric conformation is fast and abrupt. Therefore, a compromise had to be found between fast flow exchange and reduced cell squeezing and deformation. The speed of flow exchange within a chamber was characterized by flooding chambers with a fluorescent

reporter diluted in buffer (*e.g.* FITC molecules in PBS) originating from the bottom inlet (Fig. 4.8a, imidazole inlet). The chamber was then washed with non-fluorescent buffer originating from the top buffer inlet. Fluorescent intensity variations were measured over time in the chamber (Fig. 4.9, ROI as yellow square) to determine how long it would take for a chamber to fully exchange its buffer content. It was observed that less than 5 seconds was required to fully exchange the buffer content in a chamber with sieves (Fig. 4.9), which represents an acceptable delay for flow exchange on chip and a good indicator that fast flow exchange was obtained on-chip.
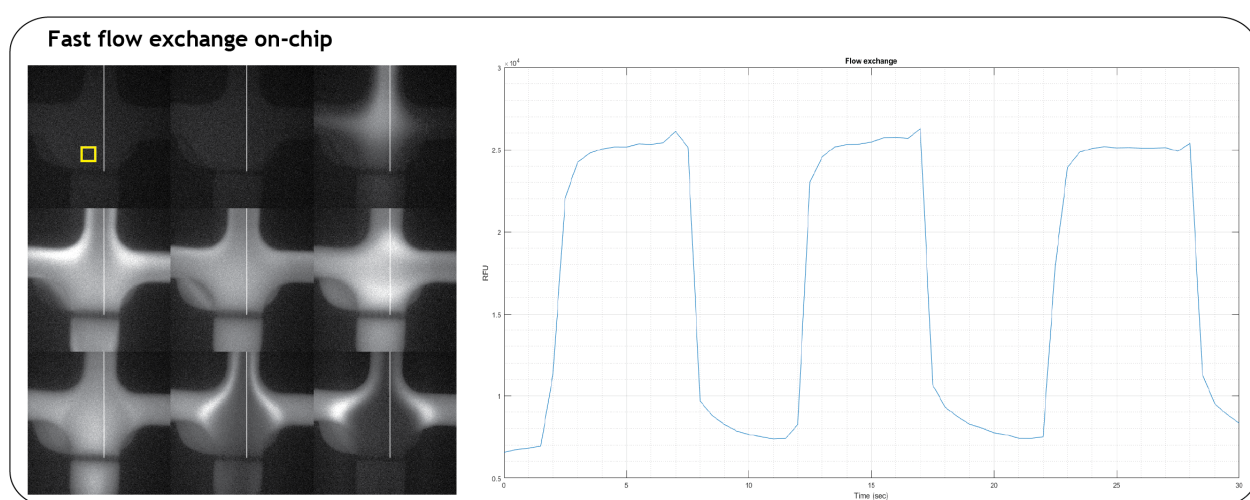

Figure 4.9: **Characterization of flow exchange on-chip.**
Duration required for flow exchange within a chamber was assessed by flowing FITC-rich buffer into the chamber via the bottom inlet and then washing the chamber with buffer from the top inlet. Montage of images of the different steps is displayed as well as the evolution of mean intensity of a selected ROI (yellow square) over time.

4.4.3   Chip clogging and cell debris

Microfluidic devices have been used to load cells previously (see 3.1). One of the common challenges encountered is cell adhesion to the surface. In this case, adhesion can occur to either PDMS or glass as the microfluidic channel is composed of boundaries with both. Priming of the device is typically achieved by flowing buffer (PBS) with high concentration Bovine Serum Albumin (BSA). In this project, the microfluidic design was initially primed with BSA in PBS and no intact cells were observed to bind to the fluidic channels. However, it was observed that when cells are damaged on-chip, it would result in the released cellular material binding and sticking to the fluidic channel. This was observed in the cell inlet (Fig. 4.10, first image) as the bottleneck between punched inlet and fluidic channel was sometimes generating enough shear stress for cells to burst open and slowly create a clog. This issue was addressed by integrating built-in filters for each inlets on chip (see inlets design in Fig. 4.8a).

However, clogging of the fluidic channels was a recurrent issue, which in some cases would trigger the abortion of the experiment. It was observed that clogging happened within fluidic channels underneath valve actuation, often under the valves between the chambers (see flow channels under valves in Fig. 4.8a). It was observed that when isolating chambers, cells could be partially retained underneath the valve and closure of the valve would result in cell death by bursting. Cellular material would then slowly aggregate in the fluidic channel, creating a partial clog (second image in Fig. 4.10), which would lead to a full clog and interruption of the flow (third image in Fig. 4.10). This resulted in "cell traffic jam" on-chip (fourth image in Fig. 4.10), that could not be addressed other than interrupting the experiment and discarding the microfluidic chip.

Three key parameters were found to reduce the probability of clogging by cell debris under valve actuation:

- **New buffer formulation:** A new buffer formulation was created to reduce binding of cellular material to the fluidic channels. In addition to BSA (4%), Pluronic F-127 (2%) was added, as Pluronic F-127 has been used to reduce unspecific cell and protein adhesion to PDMS. Furthermore, Pluronic F-68 was also added to the custom buffer mixture (2%). Pluronic F-68 is a non-ionic surfactant used to reduce shear forces in suspended cells as well as binding of cells to glass surfaces. Finally, Penicillin-Streptomycin (2%) was added to the buffer in order to prevent bacterial growth on-chip during experiments (rare but already observed, data not

shown).

- **Reduced cell concentration:** It was observed that the probability of cell clogging correlated with cell density on-chip. To reduce clogging probability, the cell concentration was reduced twofold from 10^6 cells per mL to 5×10^5 cells per mL.

- **Specific valve closure sequence for chamber isolation:** A specific sequence was defined when isolating chambers. This issue will be addressed in the next chapter, but briefly, it was observed that simply closing the valves that divide the different chambers had a tendency to push the cells under the valves. This could be explained by the sudden peak in pressure observed in a chamber, a small confined area filled with liquid, when two nearby valves are actuated. This spike in pressure was resolved by opening the top outlet so that any pressure spike could propagate out of the chip as well as concentrating cells towards the sieves part of the chambers. In addition, it was observed that closing the cell loading outlet (right outlet, Fig. 4.8a), followed by a small pause (0.5s), then closing the cell inlet valve, followed by opening of the top outlet, and finally closing of the cell dividing valves, would ensure the best probability of avoiding cell accumulation under valves. For more details, please see Figure 7.4.

By combining those three different solutions, clogging on-chip was greatly reduced and did not occur in the final design of the microfluidic device.
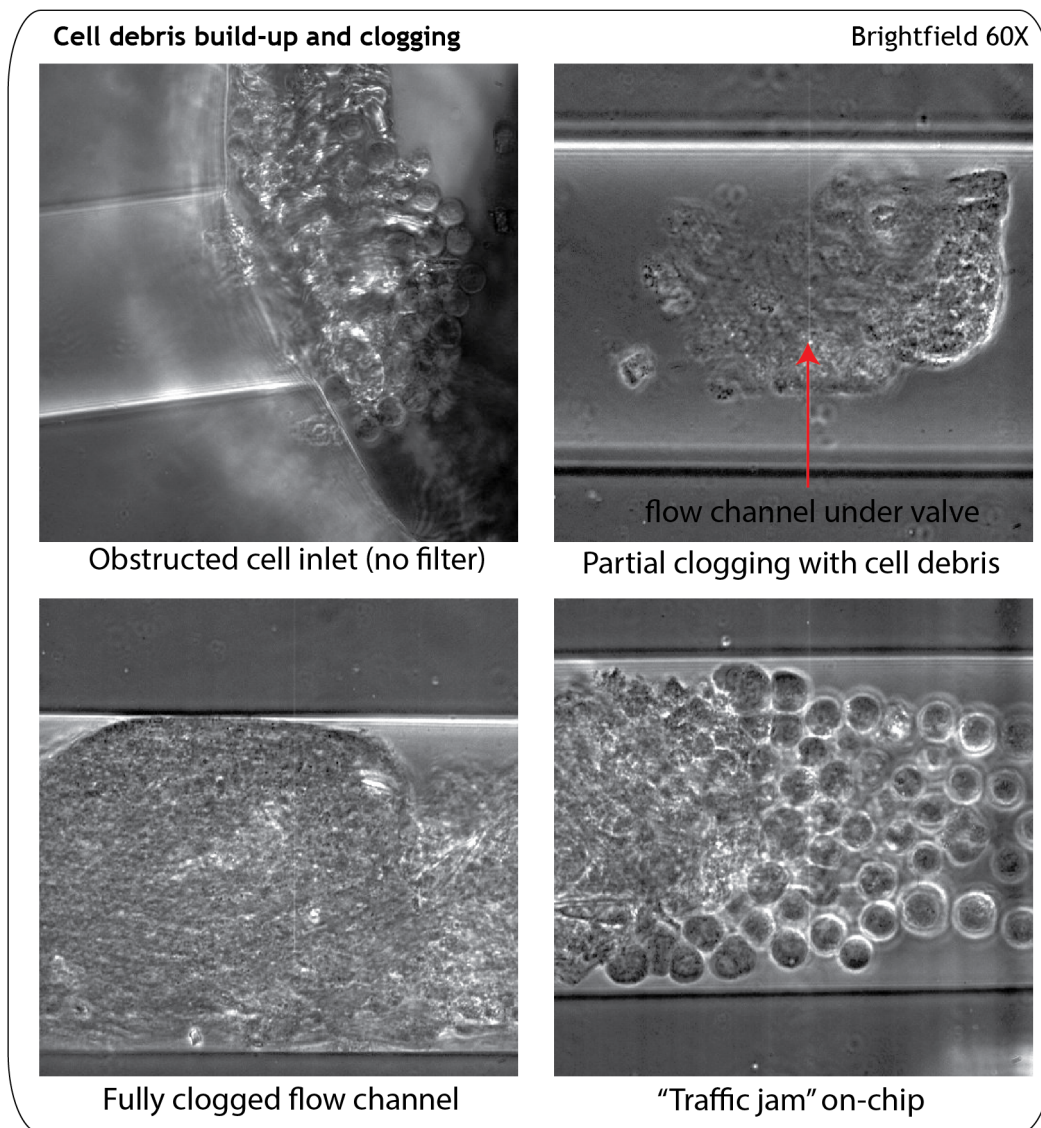
Figure 4.10: **Cell debris build-up and clogging.**

Examples of clogged microfluidic channels. Sample image of an obstructed cell inlet, before the addition of built-in filters at inlet. Cell debris that created clogs was often observed under valves. Actuation of valves was observed to trigger bursting of nearby cells. Cell-derived materials would then adhere to the fluidic channel and lead to complete clogging of the channel as observed. It would result in a "traffic jam" on chip and the necessity to stop the experiment.

4.4.4 Continuous cell loading

The approach of this work was to sequentially load and analyze cells on-chip in a continuous cycle. The need of continuous and steady cell loading on chip was therefore a requirement to achieve decent analysis throughput. It was observed however that cell loading efficiency decreased over time and remained inconsistent (Fig. 4.11a).

As this work's approach aimed at a consistent cell loading cycle over a long duration (6 hours or more), cell loading's efficiency needed to be constant for this time period. Several innovative implementations were selected to ensure a proper cell loading over time for a long period (Fig. 4.11b).

- **Glass vial with micro-magnet:** The cell solution was kept in a glass vial on ice for viability (and also to prevent temperature reaching 15°C and above to prevent NTAmers internalization by the cells, more detailed in Chapter 5). A micro-magnet (Fig. 4.11C, first point) was introduced in the glass vial, which was put on a micro-stirrer for constant stirring of the cell solution mixture. This solution prevented cell sedimentation in the vial. Cell viability in the glass vial under stirring was assessed over time and showed that cells were viable for more than four hours in those conditions (Supplementary Figure 7.1).

- **PEEK tubing for cell loading:** Tygon tubing was chosen for all control lines as well as for buffer loading because of its general characteristics (*i.e.* cost, transparency and flexibility). However, Tygon tubing presents an inner diameter of around 900μm, which is two orders of magnitude bigger than a single-cell diameter (10-15μm). Cell sedimentation within the tubing was therefore hypothesized as a potential source for inconsistent cell loading on-chip. Tygon tubing was replaced for cell loading by thinner tubing (PEEK, 125μm; Fig. 4.11C, second point).

- **Interfacing the PEEK tubing into the chip:** While PEEK tubing helped prevent cell sedimentation, it did not share the same flexibility as Tygon, which led to problematic insertion into the punched inlet on the chip. To mitigate this issue, a combination of a metal pin (see Methods), small Tygon part for flexibility and PEEK tubing plugged into Tygon was selected (Fig. 4.11C, third point).
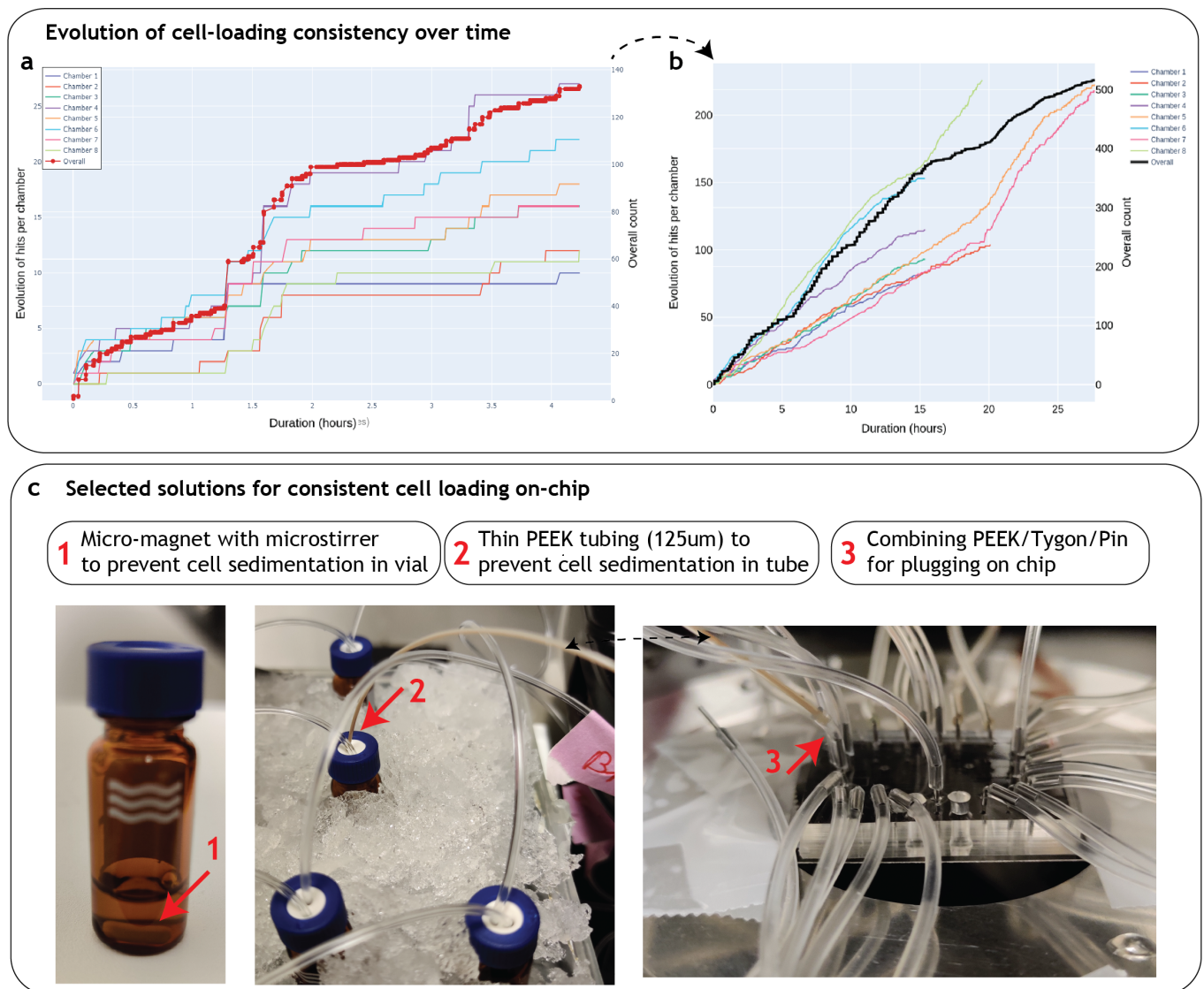
Figure 4.11: **Consistent cell loading on-chip.**

a Early assessment of cell loading on-chip revealed that loading was inconsistent and decreased over time. **b** Cell loading per hour was increased and more stable after implementation of selected solutions. **c** Three main solutions were selected to fix the cell loading issue. 1) Cell solution in a glass vial with a micromagnet and micro-stirrer combination to prevent cell sedimentation in the vial. Similarly, a thin PEEK tubing (125 μm ID) was chosen over Tygon to prevent cell sedimentation in tube. Finally, to ensure proper chip attachment, a combination of pin and small piece of Tygon tubing to join with the PEEK tubing was found to be ideal for the interface.

4.5   Image analysis & cell detection

Adapting reversible pMHC multimers technology from flow cytometry to fluorescent microscopy and microfluidics technology revolved around three main axes. The first challenge was adapting the NTAmers technology (Fig. 4.1) to fluorescent microscopy, which was covered in the section 4.2. The second was to design an innovative microfluidic device able to isolate single cells and accommodate proper buffer exchange for fast introduction of imidazole in the cell surrounding, which was covered in the sections 4.3 & 4.4. The third main goal was to trigger, record and analyze dissociation kinetics of the TCR-pMHC interactions on-chip. It required isolation of single cells in chambers (saturated with NTAmers during loading on-chip), fast flow exchange with imidazole, and a constant acquisition via fluorescence time-lapse imaging for Alexa647 (pMHC monomers) and PE (multimeric core) as represented in the montage in Figure 4.12. Dissociation kinetics of single-cells aimed to characterize the structural affinity the TCR-pMHC complex. This characterization can be read by extracting the half-life of the dissociation kinetics. Extraction of half-life of dissociation is possible with the NTAmers technology by fitting the decay of Alexa647 fluorescent signal of the monomeric pMHCs detaching over time from the TCRs receptors on the cell surface. To extract such data, several requirements have to be met:

- **Extracting cell location within the chamber:** Extracting the Region-of-Interest (ROI), which is the region corresponding to cell-containing pixels within the chamber, is required to properly study the cell-derived signal without introducing noise from the chamber.

- **Extract mean fluorescence intensities:** The mean fluorescence intensity for each fluorophores and for each frames must be extracted in order to analyze the decay in signal.

- **Identify shoulder point of PE signal:** As mentioned earlier, the multimeric signal PE serves to identify the switch from multimeric to monomeric forms of the pMHCs. Only the kinetics of the monomeric pMHCs are of interest as multimeric dissociation is correlated to the total avidity of the interaction. As observed in Figure 4.12, the PE signal decreases quickly. The point in time were the PE signal drops and forms a shoulder point (or knee-point) in curve is a signal of the switch and needs to be identified for proper cropping of the signal. This time point represents the adjusted initial time (t0) of the dissociation.

- **Exponential fit of Alexa647 signal:** After proper spatial (ROI) and temporal (adjusted

t0) cropping, the decay in the mean fluorescence intensity of the Alexa647 signal needs to be fitted with an one-phase exponential decay, corrected for fluorophore bleaching. The equation used in this work is the following: $(A * e^{(-(k+k_{bleaching})*t)}+B)$, where A represents the initial intensity at t0, B the plateau or background signal, k is the rate constant and $t_{1/2}$ is equals to $1/k$; and $k_{bleaching}$, the rate constant for bleaching-related decay.
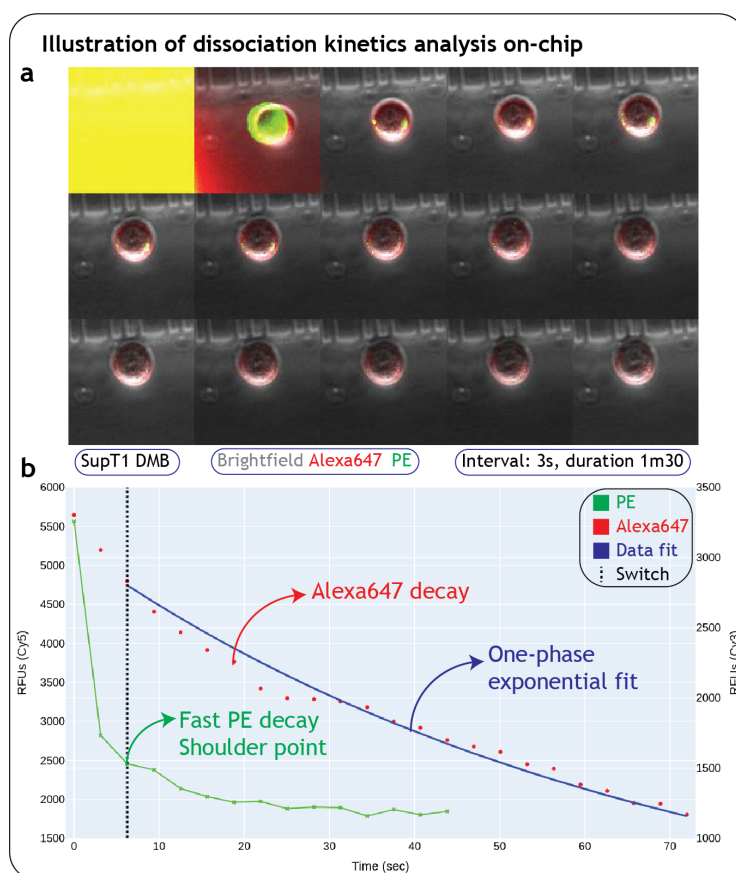
Figure 4.12: **Illustration of dissociation kinetics analysis on-chip.**
a Montage of timelapse images (brightfield, Alexa647 and PE) recorded every 3 seconds for a total of 75 seconds. A sudden decrease in PE signal is observed after flow exchange (triggered at first frame). **b** Example of extracted signals. A fast decrease in PE signal, with an identified shoulder point in curve (black dotted line), represents the switch to monomeric form. Alexa647 signal is fitted with an one-phase exponential decay equation to extract the half-life of dissociation.

In this section, the main different approaches for image analysis used in this work will be described.

4.5.1 Cell detection strategies

This section of the project focuses on characterizing dissociation kinetics of SupT1 cells (WT and DMβ) on-chip. As the design of the chip evolved, the different strategies to identify and analyze cells evolved as well.

4.5.1.1 Manually-created ROIs

The first approach was to manually generate ROIs around cells when performing buffer exchange (Fig. 4.13a) and extract mean fluorescence intensity of the different ROIs along the different frames of the time-lapse. This approach was successful at extracting half-lives of dissociation as observed in Figure 4.13b, where WT cells showed half-lives of 30.4s and 27.5s respectively. However, this approach showed two drawbacks. First, if cells were in close proximity, creating separate ROIs was problematic. The second issue encountered is described in Figure 4.13c. Cells were often found to move during the time-lapse sequence (usually around 1min-1min30 long), which led to the initial ROIs becoming inaccurate. Manually adjusting ROIs for each frame became a cumbersome task and another approach became necessary.

4.5.1.2 Automated cell detection based on fluorescence images

Manually-created ROIs proved disadvantageous as they were static. To address this issue, dynamic ROIs, adapting to each frame over time, were required. Initial work focused on using Alexa647 fluorescent images to create dynamic ROIs. Three main image analyses were tested to effectively create masks that isolated single cells from the rest of the chamber. All of the image analyses performed in this work were done in MATLAB. The different approaches focused on ways to effectively threshold the image to isolate cell ROIs and create binary masks based on fluorescence intensity. After thresholding, binary images were analyzed to find connected components (*bwconncomp* function in MATLAB) with morphological operations applied afterwards (*e.g.* dilation and erosion).

- **Top 1% pixels selection:** As NTAmers-labeled cells represented the brightest pixels in each frame. Isolating the top 1% pixels of each frame was tested as a method to effectively select the cell surface area with the bound NTAmers (Fig. 4.14a). This approach proved to be to selective for proper ROI continuity between frames.
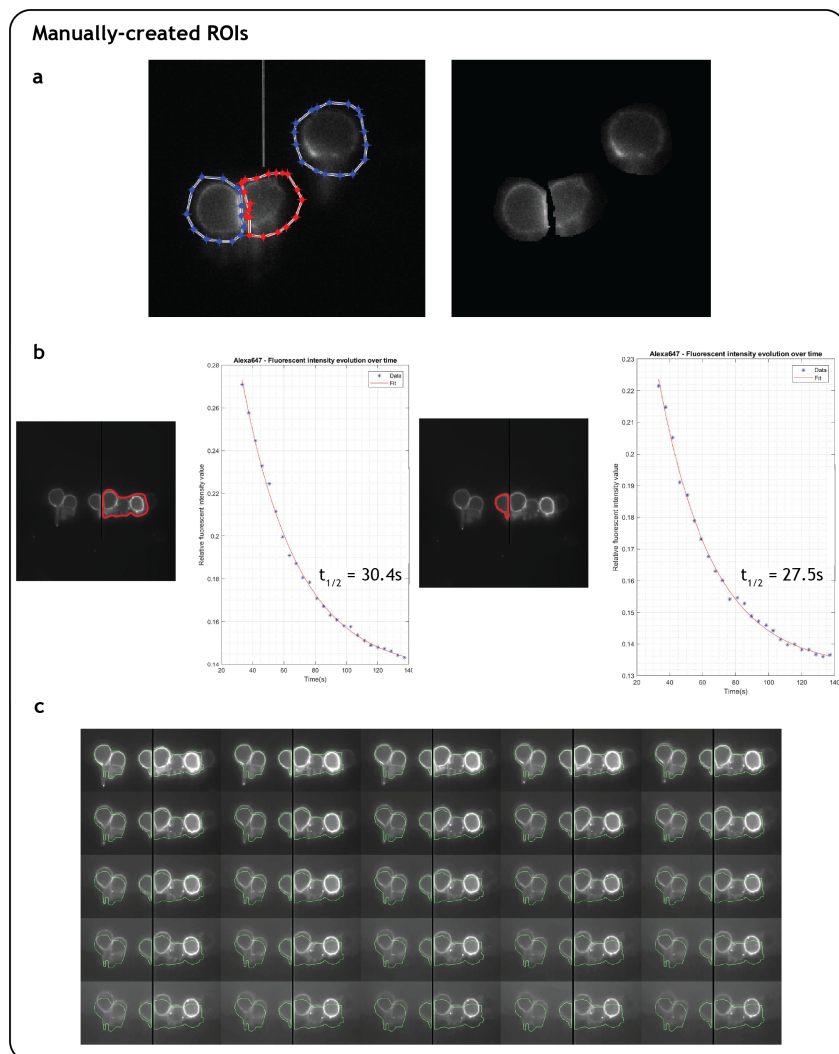
Figure 4.13: **Manually-created ROIs.**

a Images of manually drawn ROIs and the corresponding masks created for analysis. **b** Such generated masks were used to extract the dissociation half-lives of cells. Here WT clones showed half-lives of 30.4s and 27.5s respectively for the two ROIs in red. **c** Montage of frames with cells under buffer exchange. The initial frames were used to create manual ROIs. Cells were observed to move during buffer exchange resulting in inaccurate ROIs at the end of the timelapse.

- **Peak analysis of histogram intensity:** Another dynamic approach was to automatically threshold pixels by analyzing the intensity-derived histogram for each frames. As observed in Figure 4.14b, the majority of pixels are dim and represent the chamber area, by analyzing peaks in the histogram, the threshold can be placed after the first peak, effectively removing

all dim pixels while keeping bright pixels. This resulted in successful creation of cell ROIs, however, distinction between two neighboring cells was often lost.

- **Thresholding by Otsu's method:** Otsu's method for thresholding [174] works by minimizing the variance between black and white pixels in the generated binary image. This method proved quite effective in isolating cells ROIs from background (Fig. 4.14c).

While the idea of thresholding fluorescent images based on intensity for ROI generation proved to be feasible, it was observed that this approach was intensity-biased and tended to favor bright cells. It is worth mentioning that dissociation kinetics should be independent of initial intensity and differentiating cells based on initial intensity was deemed not a valid approach.

4.5.1.3 Automated cell detection based on brightfield images

To avoid any fluorescence intensity-based bias, a different approach was selected by analyzing the brightfield images generated during the timelapse instead of fluorescent images. Reference images of each empty chamber were generated for each prior to cell loading. During the experiment, cell identification and ROI creation were performed by subtracting the reference image of the current chamber from the acquired image. Image registration was applied with same modality of image capture and a geometric *translation* transformation was applied (*imregister* function in MATLAB). The two images were then subtracted and each ROI was identified by connected components analysis. As observed in Figure 4.15a, cells were successfully recognized as independent ROIs when performing reference subtraction. This process was applied to each frame during the timelapse to counteract any potential movements of cells within the chamber. This approach was however greatly dependent on image registration as well as reference image quality. Any shift in the microscope stage that could not be compensated by image registration was harmful and triggered false positive hits (*e.g.* shifted chamber wall with bright pixels). Similarly, as the experiment performed repetitive cycles of cell loading and analysis, chamber morphology changed over time. For instance, accumulation of small debris was often observed around the sieves. While this debris was inconsequential to the cell environments and image acquisition, the difference between the initial reference image and acquired images with small debris was sufficient to return false positive hits. In order to solve that issue, the reference image was updated after washing the cells out of the chamber but the results were still unsatisfactory.
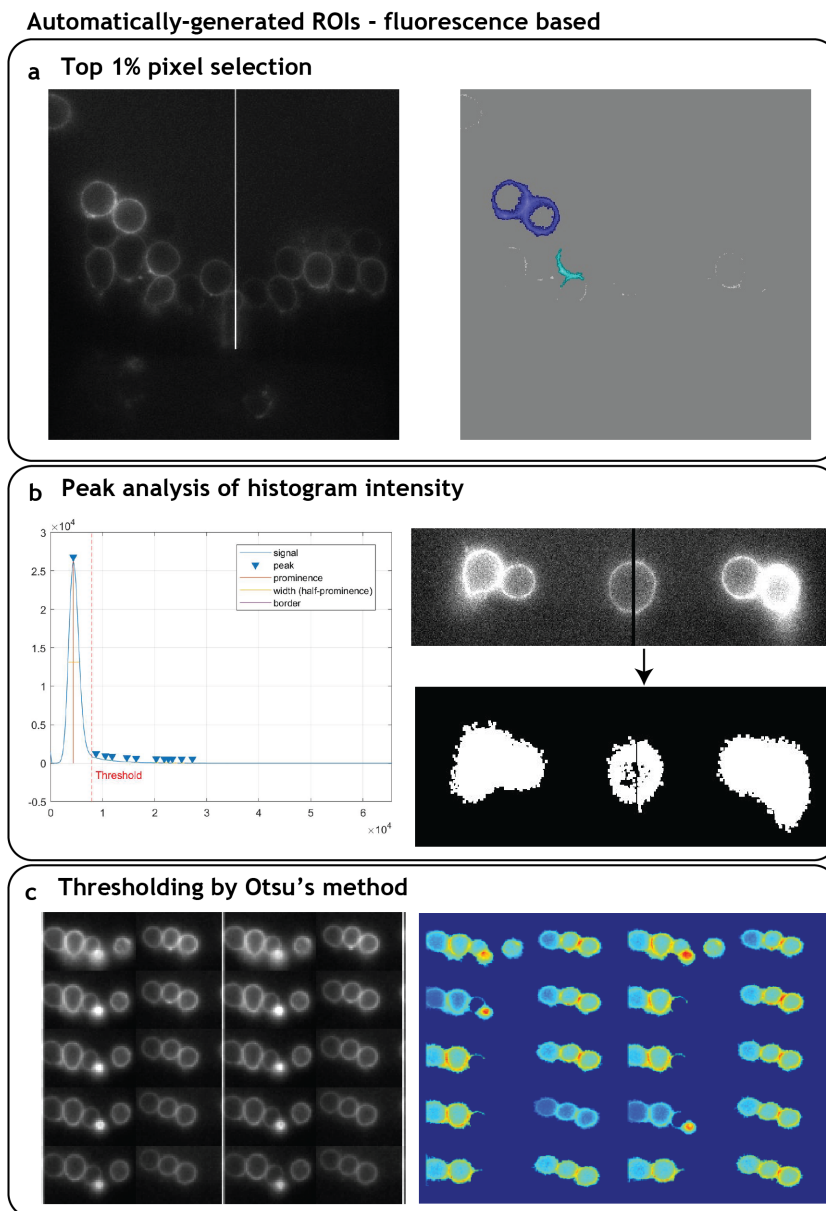
Figure 4.14: **Automated ROIs based on fluorescence.**
a Thresholding by selecting the top 1% brightest pixels for each frames. **b** Thresholding by peak analysis of intensity-derived histogram for each frame. The threshold is placed between the first (main peak with dim pixels of chamber) and second peak. **c** Thresholding by Otsu's method [174].

When the final design of the microfluidic chip was established (see 4.3.4), the chamber layout included five pockets, in the upper part of the chamber, for better cell isolation. Those distinctive

features were used to extract defined localized regions, here the chamber pockets. A reference image of an empty pocket (Fig. 4.15b) was used to identify each of the five pockets in the chamber for each frames. Localized identification was performed on MATLAB by normalized 2-D cross-correlation of the two images (*normxcorr2* function in MATLAB) and selecting the best hits. Once the pockets ROIs were defined, subtracting the reference image allowed identification of pockets with cells in them, similar to the approach just described above. This image analysis process proved to be quite efficient at recognizing cell-containing pockets (Fig. 4.15b). in addition, as the cells did not move extensively within the pockets, the ROIs were in general of good quality to be applied to the fluorescence images for mean fluorescence intensity analysis. However, small debris in the pockets still led to false positive hits (Fig. 4.15b). The recurrence of false positive hits was found to increase over time as the the probability for small debris to accumulate in the chamber increased as well.

4.5.2   Automated cell detection in chamber

Biology is sometimes messy. Despite extensive efforts for filtering cell solution and precise buffer formulation to avoid creation of cell debris, it was observed that over time, small debris had a tendency to accumulate in the chambers as well as dead cells being loaded on-chip. This resulted in frequent false positive hits of cell detection by reference-based analysis. To solve this issue other approaches were sought. Two final cell detection methods were finally selected. The first one consisted in using machine learning and training convolutional neural network (CNN) to develop object detectors specifically tailored for cell detection. The second approach was to use fluorescent tags specifically designed to bind live cells like Calcein AM. Those two approaches had the advantage of recognizing live and/or properly-looking cells as the object detector was trained on selected datasets of good cells and Calcein AM only labeled live cells.

4.5.2.1   Machine learning and neural networks for cell detection

Machine learning was applied for cell detection by training an aggregate channel features (ACF) object detector in MATLAB. A repository of positive and negative images (*(*i.e.) chambers with cells or empty chambers respectively) was manually created. Manual ROIs around brightfield images of cells were drawn in an Image Labeler session in MATLAB to extract cell features. Following ground truth establishment, an ACF object detector was trained to detect cells present in chambers

Automatically-generated ROIs - based on brightfield images

a ROIs by substracting reference frame

b Substracting reference to localized regions

Reference image of chamber pocket

Selected pocket with cell based on reference difference

1 2 3 4 5

i) Identification of 5 pockets
ii) Substracting reference image
iii) Selecting positive hits
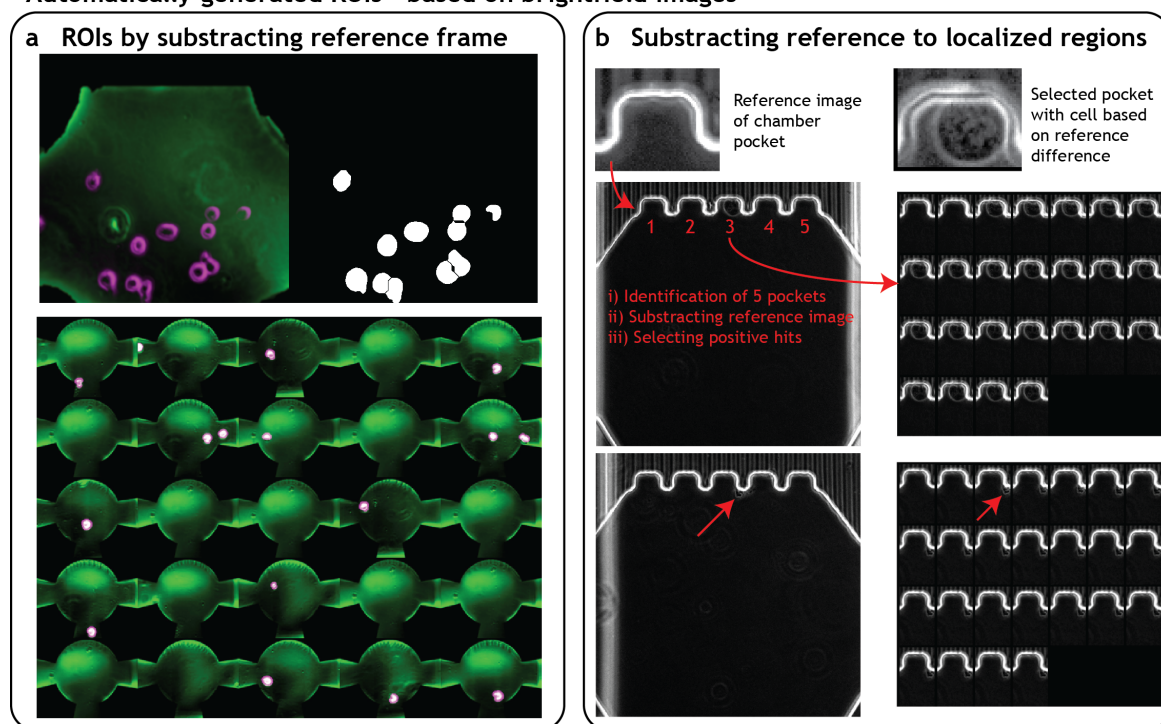
Figure 4.15: **Automated ROIs based brightfield images.**

a Subtracting a reference image of an empty chamber to expose difference with a cell-occupied chamber (common part in green, differences in purple), following by thresholding by Otsu's method to identify cell ROIs. **b** A reference image of a repetitive units like the chamber pocket of the final microfluidic design was used to identify and extract each pockets of the chamber. Subtraction with reference image helped identified positive pockets with cells. However, false positive with debris were often found.

(Fig. 4.16a, left image). The ACF object detector resulted in sensitive and reliable cell detection, even in tricky conditions like when numerous cells were present in a chamber (Fig. 4.16a, image on the right).

Similarly, a convolutional neural network was trained as a backup for the ACF detector. This double utilization of object detectors was employed during experiments to ensure proper cell detection while minimizing false positive occurrence. Details about the model of the trained CNN can be found in Supplementary Figure 7.2.

4.5.2.2 Using live-cell fluorescent tags for cell detection

The second and utterly final approach used for cell detection was to use live-tags such as Calcein Am. It is a cell-permeant dye that can be modified chemically by live cells only into green-fluorescent calcein (FITC channel) after hydrolysis by specific enzymes. Calcein can be found in a blue-fluorescent form with Calcein Blue (DAPI). As both FITC and DAPI were both unused fluorescent channels in the microscope settings, their use were beneficial for cell detection. As observed in Figure 4.16b, the bright signal of Calcein allowed for easy morphological operations to create binary masks around live cells. Moreover, the dual use of Calcein and Calcein Blue allowed for mixing of cell populations, for instance mixing WT and DMBβ cells in the same experiment (more details in Section 5).

4.6 The need of experimental automation

The convergence of the establishment of the final microfluidic design, the determination of how to properly perform buffer exchange on-chip without harming cells, and development of an effective image analysis pipeline for cell detection and analysis triggered us to pursue a higher experimental yield and throughput than could be achieved using manual, user-dependent settings. Cell loading and isolation were observed to be limiting steps for manual experiments. Indeed, in order to avoid more than two cells per chamber, the concentration of loaded cells was reduced, which resulted in a large numbers of empty chambers in each round. Manually scanning each of the 8 chambers, saving cell-positive chambers and triggering buffer exchange and data acquisition for those chambers proved cumbersome when done by a user.

Automating the experimental process was identified as the best solution. In order to properly automate the process, each key step of the experimental flow needed to be defined. This work focused on studying the dissociation kinetics of the TCR-pMHC interactions on live cells with the NTAmers technology, therefore, the experimental flow needed to be designed for this application primarily. The experimental flow is depicted in Figure 4.17 and can be understood as a cyclic flow. Initially, cells would need to be loaded and isolated on-chip. Then, automated cell detection would be performed (via trained CNN/ACF object detectors or live-tags like Calcein). Positive chambers would be registered and the focus would be brought to the first positive chamber, where buffer

Figure 4.16: **Automatically-generated ROIs - Machine learning & Live-tags.**
a Images of generated ROIs by the trained ACF detector for cell detection. Detected ROIs were filtered by area to remove false positive with aberrant sizes. **b** Using Calcein AM (or Calcein Blue) allowed for live cell detection. The signal strength facilitated using morphological operations to create binary masks for the ROIs around cells. The dual use of Calcein AM and Calcein Blue allowed for mixed population distinction on-chip.

exchange with imidazole would be triggered and simultaneously, data acquisition in the form of timelapse imaging would be performed. At the end of the timelapse, analysis of the isolated cell(s) would need to done "real-time", to determine the data of interest, such as half-life of dissociation. Upon extraction of this data, a decision would be made by the program based on user-defined information (*e.g.* half-life thresholding) and the current cell(s) would be pushed out from the chip

in a defined output as the final design presented two distinctive outputs for population subdivision based on half-life of dissociation. Upon the end of the analysis and recovery steps, the process flow brought the focus to the next positive chamber in the current round (Fig. 4.17). In the case where the current chamber is the final positive chamber, the process flow would load cells again for the next cycle of cell detection and analysis. This cyclic flow would allow for complete experimental automation without the need for any user inputs during experiments (the only pre-experimental inputs were for camera settings, chamber registration, and half-life thresholding).

As observed above, the automation would require hardware control, not only with fluidic steps like valve actuation, but also microscope stage moving, image capture, auto-focusing, etc. Furthermore, additional automation would require software control for image analysis, data saving, decision-making processes, etc... Practically speaking, this required the use of one program to handle both hardware and software requirements. Typical software used for microscope handling, like Nikon NIS-Elements, provide great control over camera and microscope but are quite restrictive for extra components like a USB-relay board for valves actuation or advanced image processing. On the other hand, MATLAB provides great data processing capabilities and also allows for simple hardware control for devices such as the USB-relay board. The missing link was having complete control over the microscope setup from within MATLAB. This problem was solved thanks to the use of μManager, which is a software package for control of automated microscopes, like the microscope used in this work (Nikon Ti Eclipse). μManager is open-source software [175] and provides a free imaging platform. The great benefit of μManager is that its core Java API can be controlled by MATLAB, effectively making MATLAB able to control advanced hardware systems like a Nikon Ti Eclipse and an Andor EMCCD camera. A custom MATLAB graphical user interface (GUI) was designed to accommodate user-friendly controls of hardware-related features like valves actuation, camera settings, microscope stage, objectives, focus, as well as triggering custom-made automated processes that handle experimental cycles. The description of this custom MATLAB GUI can be found in Figure 4.18.
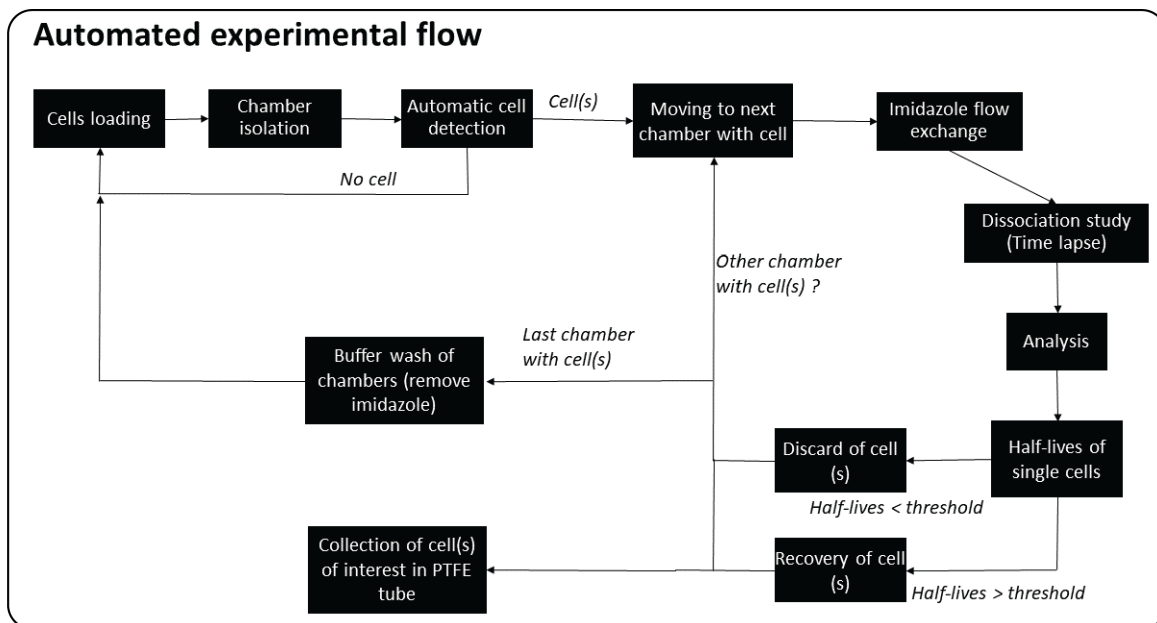
Figure 4.17: **Automated experimental flow.**

Schematics for the automated experimental process flow. Description of the main steps of the experimental flow. This process flow allowed for cycles of experiments in a non-interrupted manner.

4.7 Conclusion

This chapter explored the entire journey from idea to realisation. The initial point of this project was to develop a new innovative technology to solve the limiting of flow cytometry for studying TCR-pMHC interactions at the single-cell level with the NTAmers technology. This work's approach was to use microfluidics technology to isolate single cells and perform quick buffer exchange with an imidazole-rich buffer to trigger dissociation kinetics. The adaption of the NTAmers technology from flow cytometry to fluorescent microscopy was described here in this chapter. The complex journey of designing a microfluidic design able to fulfill all the different requirements has been described in detail here. A microfluidic design with eight independent chambers, able to withstand fast buffer exchange without substantial shear stress on isolated cells was successfully developed. The characterization of this final design was also presented in this section of the thesis. Finally, after the biological and technical side, the creation of an automated, efficient image analysis pipeline, able to autonomously identify cells (via machine learning and morphological operations), extract the signal of interest (fluorescent decay) and perform complex analysis (*e.g.* data fitting
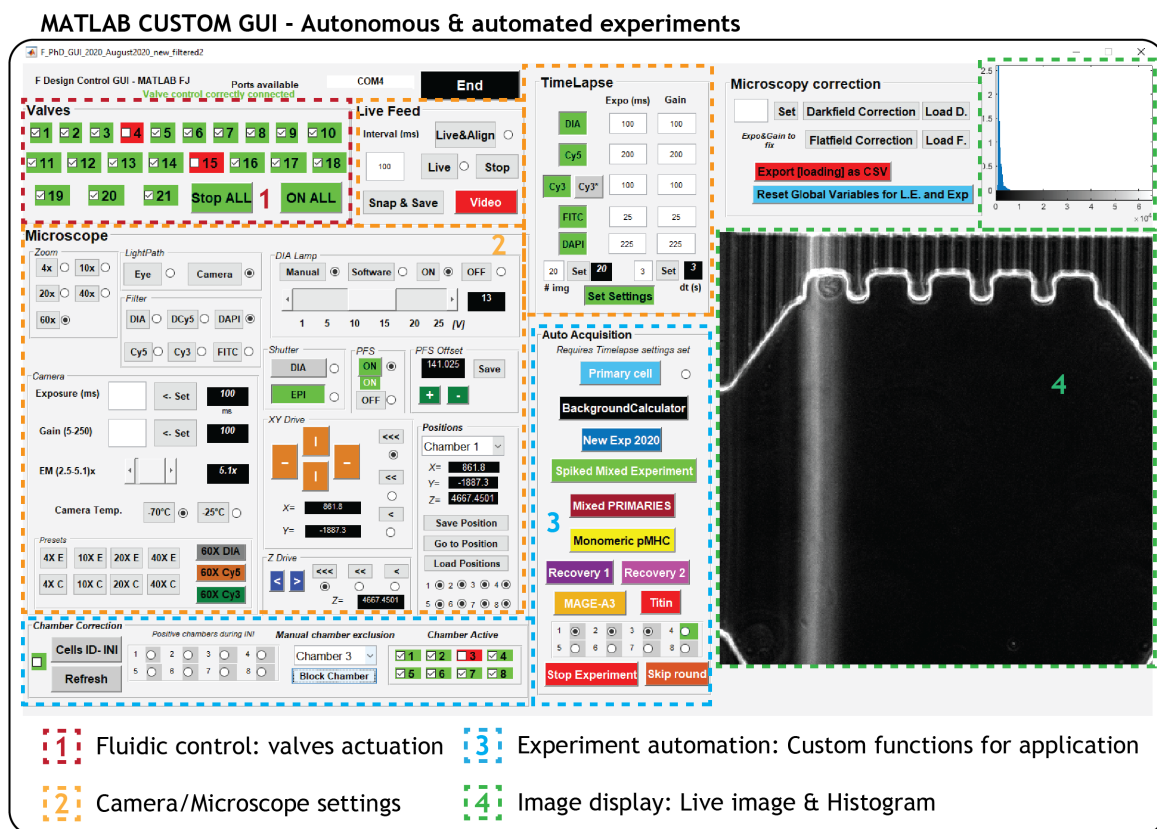
Figure 4.18: **MATLAB CUSTOM GUI - Autonomous & automated experiments.**
This custom GUI is manly divided into four parts. The first handles fluidic controls. The second
is designed for camera/microscope settings. The third contains buttons that trigger custom scripts
for automated experiment handling. The last part is for image display with live imaging, acquired
images, and histogram display.

and decision making) was presented. This entire journey led to the need for experimental automation, which was achieved by allowing precise hardware control by a data-processing software such
as MATLAB. An autonomous and automated experimental cycle was created that would perform
complex biological experiments on single cells in an integrated microfluidic device without the need
of any user inputs during the experiment.

This work demonstrated the feasibility of microfluidics technology for single-cells applications
like cancer immunotherapy. In the next chapter, I will describe the main results obtained for the
biological application selected in this project, mainly, single-cell dissociation kinetics of the TCR-

pMHC interaction. I believe that the technology created here is versatile and can be applied to different applications.

5

Proof-of-concept, characterizations and applications of this innovative platform

This chapter focused on the different applications selected for the innovative microfluidic platform described in this work. This chapter is composed of two sections.

The first section represents the main application selected, which was studying TCR-pMHC dissociation kinetics at the single-cell level for future cancer immunotherapy applications and represents the work that has been submitted for publication. Despite few repetitions with Chapter 4, I believe that this section represents a logical continuity, by representing our contribution to the scientific world. The work submitted here in this section puts an emphasis on the technology developed in this work and its versatility.

The second section describes briefly other leads and potential applications that were explored in this work with primary cells and other uses than NTAmers technology.
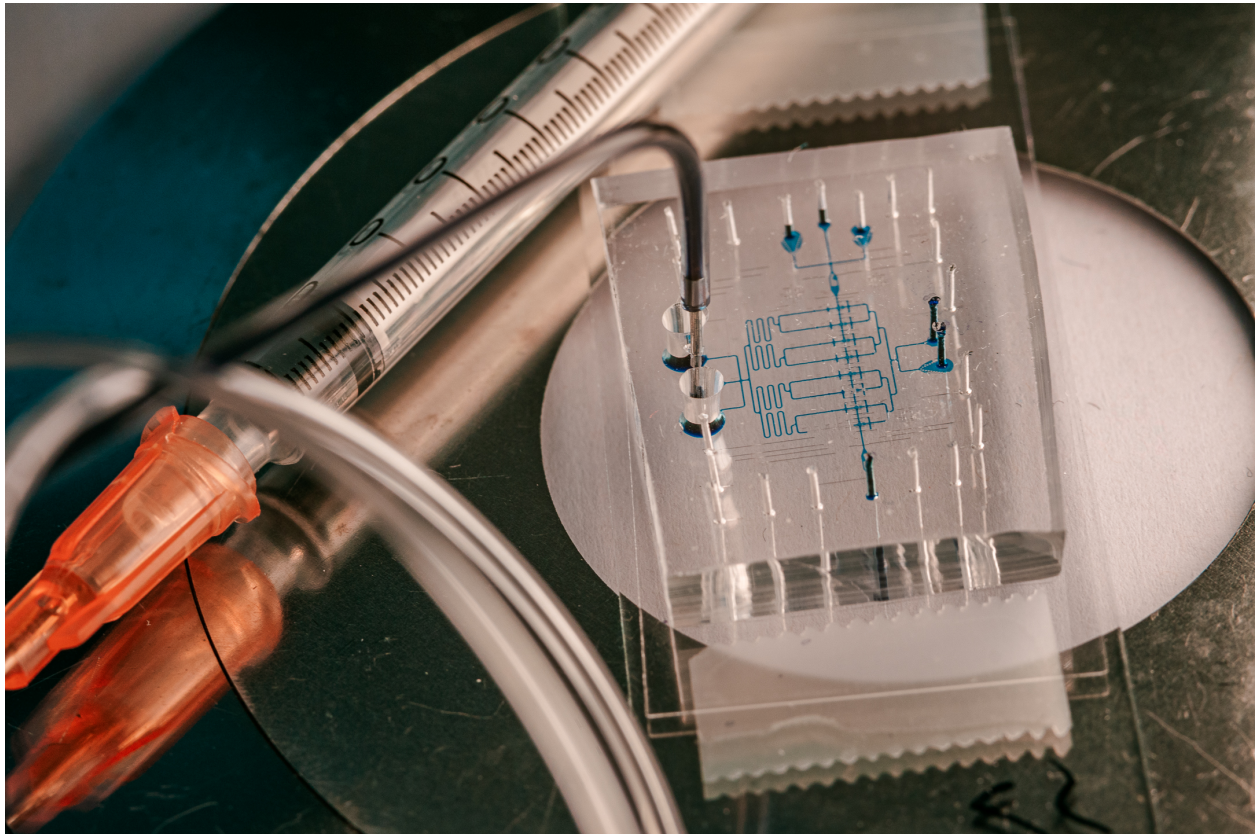
Figure 5.1: **Artistic image of the microfluidic chip.**
Image of the microfluidic device filled with dye for visualization and next to a 1.5mL syringe for size comparison.

5.1 High-throughput single-cell TCR - pMHC dissociation rate measurements performed by an autonomous microfluidic cellular processing unit

The work presented in this section has been made available as a preprint in *bioRXiv*, 2021 [176].

Authors: Fabien Jammes, Julien Schmidt, George Coukos, Sebastian Maerkl

This work was submitted to Nature Methods Brief Communications, 30 June 2021, and it is currently awaiting reviewing and publication.

5.1.1 Abstract

We developed an integrated microfluidic cellular processing unit (mCPU) capable of autonomously isolating single cells, perform, measure, and on-the-fly analyze cell-surface dissociation rates, followed by recovery of selected cells. We performed proof-of-concept, high-throughput single-cell experiments characterizing pMHC-TCR interactions on live CD8+ T cells. The mCPU platform analyzed TCR-pMHC dissociation rates with a throughput of 50 cells per hour and hundreds of cells per run, and we demonstrate that cells can be selected, enriched, and easily recovered from the device.

5.1.2 Main manuscript

Microfluidics, or "lab-on-a-chip" technology has the potential to autonomously perform complex laboratory methods. In mammalian cell applications, microfluidic devices automated tasks such as long-term cell culture [177], transfection [173], cell-secretion analysis [137], chemical cytometry [178, 179], cell sorting [180], and many others. In most if not all applications to date, microfluidic devices are used to scale-down and to automate experimental processes, but data processing and analysis are generally performed off-line after experiments have been completed.

Here we describe a fully-autonomous microfluidic cellular processing unit (mCPU) that performs single-cell surface marker dissociation measurements, and runs all necessary fluid handling, microscope, imaging, image processing, and data analysis steps on-the-fly, creating a closed-loop system (Fig. 5.2a and Supplementary Fig. 7.3). Machine vision and image analysis is used to feedback and control device operation allowing the device to perform complex fluidic processing steps autonomously. We applied this platform to a proof-of-concept, high-throughput measurement determining the dissociation rates between peptide - major histocompatibility complexes (pMHC) and T cell receptors (TCR) on hundreds of cells, and demonstrate that the platform can automatically select cells based on the measured dissociation rate, and recover these cells from the device for downstream applications.

We applied our mCPU concept to single-cell immunology [64, 181]. Contemporary single-cell techniques like flow cytometry acquire single time point measurements. Although useful for a large number of applications, single-time point measurements are not able to provide kinetic information, which is critical in a number of systems including T cell [169], B cell [182], and synthetically engineered surface receptor [183] interactions. We demonstrate that the mCPU can measure the dissociation rate of the interaction between TCRs on CD8+ T cells and pMHCs. This affinity has been shown to be an important parameter and to correlate with T cell function. Current state-of-the-art methods to study single-cell surface receptor dissociation rate measurements are based on cumbersome, non-automated, and low-throughput approaches [169, 58]. There is therefore a need for novel technology to study biological mechanisms that require precise, single-cell control in time and space.
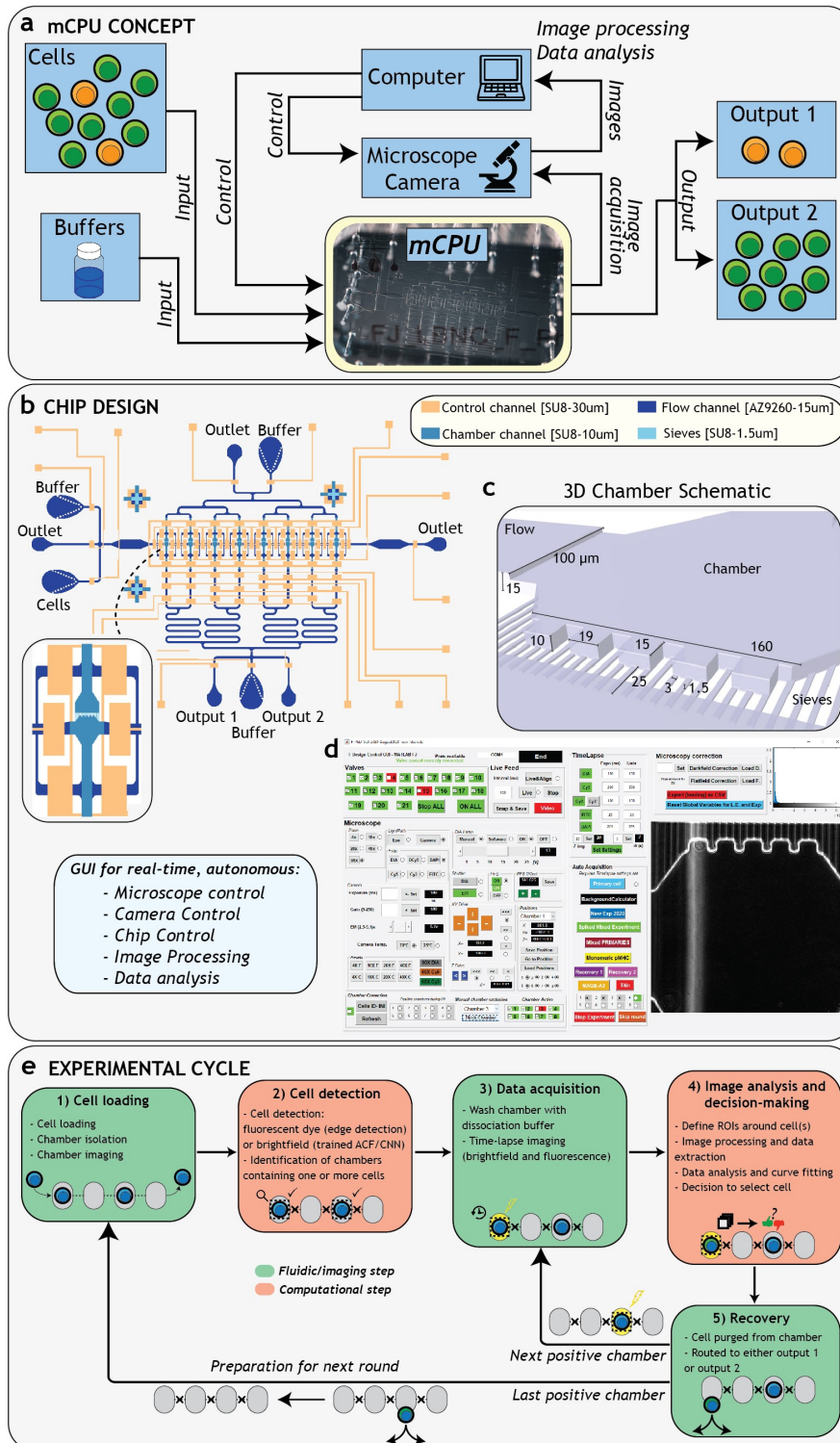
Figure 5.2: Caption on next page

Figure 5.2: **mCPU single-cell analysis**.

a A control chart describing the mCPU platform. A microfluidic device forms the core of the mCPU. **b** The microfluidic device design showing the two-layer channel network consisting of a control (orange) and flow (blue) layer. **c** 3D chamber schematic showing chamber design details. **d** Automation is achieved through a custom MATLAB GUI controlling the chip, camera, and microscope, and performs all image processing and data analysis steps in real-time. **e** The mCPU platform performs sequential experimental rounds that are divided into five discrete steps.

The mCPU design consists of two fluidic layers, 106 micromechanical valves, and 8 cell isolation chambers in which cells are isolated and analyzed individually (Fig. 5.2b and Supplementary Fig. 7.4). Buffer conditions can be changed in each chamber by fast flow exchange without loss of cells by incorporating small sieves and fluidic bypasses in the chamber design (Fig. 5.2c). Complete automation of the experimental process was achieved via a MATLAB program that controls the microfluidic device, camera, and microscope (Fig. 5.2d). To achieve autonomous single-cell experiments, the mCPU platform performs sequential experimental rounds consisting of cell loading and isolation, followed by automatic cell detection in the chambers (Fig. 5.2e). Buffer exchange is triggered in chambers identified to contain a cell, followed by data acquisition through time-lapse imaging. An elaborate analytical pipeline performs image processing, data extraction, and curve-fitting for real-time extraction of single-cell surface marker dissociation rates (Supplementary Figures 7.5 and 7.6). Cells above or below a particular dissociation rate threshold can be selected for recovery. The system then automatically triggers the analysis process in the next cell-containing chamber, or, if no more chambers contain a cell, triggers a new round of cell loading starting the next experimental cycle (Fig. 5.2e).

Here we used NTAmers which are pMHC multimers that can be rapidly dissociated by imidazole (Fig. 5.3a) [62]. To perform dissociation rate measurements of T-cell receptor - pMHC interactions, TCR-transduced CD8+ SUP-T1 cells were pre-stained with NTAmer-pMHC multimers followed by on-chip analysis. Cell containing chambers were identified using either brightfield images with trained convolutional neural network (CNN) and aggregate channel features (ACF) object detectors or via fluorescence using live-cell stains (Fig. 5.3b,c and Supplementary Fig. 7.7). In 6 experimental runs the mCPU achieved an average throughput of ~50 cells per hour and ran

stably and continuously for at least 6 hours (Fig. 5.3d). Acquisition of dissociation kinetics was performed by rapid (≤ 5 seconds) buffer exchange introducing an imidazole containing buffer in the chamber and acquired images over a period of 60 to 90 seconds with a 3 second interval (Fig. 5.3e). Image analysis allowed for automatic determination of the switch from multimeric to monomeric forms by detecting the sudden decrease in PE signal (Fig. 5.3f). Each event was filtered based on multiple parameters described in the methods section (Supplementary Figures 7.8 and 7.9). Monomeric pMHC-TCR dissociation (Alexa647) was then fitted to a one-phase exponential decay model (Supplementary Fig. 7.10). Finally, the cell (or cells) in the chamber was directed to one of two chip outputs depending on whether it met a minimal dissociation rate threshold (Fig. 5.3i).

We focused on characterizing a wild-type (WT), low-affinity patient-derived TCR specific for the NY-ESO-1 tumor antigen and a higher affinity variant (DMβ) that was previously generated [184]. We bench-marked our system by measuring both the WT and DMβ variants, as they cover the physiologically relevant dissociation rates ranging from high for WT (short half-lives) to low for DMβ (long half-lives).

In six mCPU runs a total of 908 cells were analyzed, 447 WT and 461 DMβ expressing cells. We obtained average half-lives of 29.1s and 80.5s for WT and DMβ, respectively (Fig. 5.4a; Supplementary Figures 7.11 & 7.12). These half-lives are similar to those obtained by a clonal population-level FACS measurement requiring at least 200'000 cells (27.1s and 75.8s for WT and DMβ respectively, Supplementary Fig. 7.13) and a previous FACS analysis (17s and 89.7s for WT and DMβ, respectively [185]). The results were repeatable between experiments based on the observed half-life averages (Fig. 5.4b). In this series of experiments 82% of chambers contained a single cell, 14% contained 2 cells, and 4% contained 3 or more cells identified pre-filtering (Fig. 5.4c). These experiments demonstrate that the mCPU is capable of autonomously performing large-scale single-cell surface marker dissociation measurements, which should find uses in characterizing T cell, tumor-infiltrating lymphocyte (TIL), or B cell samples, and synthetically generated surface receptor libraries.

The mCPU integrates cell selection and recovery capabilities to extract cells of interest from the mCPU for downstream processing. To test the mCPU's capability of identifying and enriching rare cells from a mixed population we generated a mixture of WT and DMβ expressing cells. The cells were pre-stained with Calcein Blue and Calcein AM to establish the actual cell identity (Fig.

a NTAmers: REVERSIBLE pMHC MULTIMERS

b CELL LOADING & DETECTION

c Cell detection

d Cells detected over time

e DATA ACQUISITION IN SPECIFIC CHAMBER

f Flow exchange & dissociation kinetics

g DECISION & RECOVERY

h Condition:
$T_{1/2}$ of dissociation larger than threshold ?
If **no**: outlet 1; if **yes**: outlet 2 → *Enriched population*
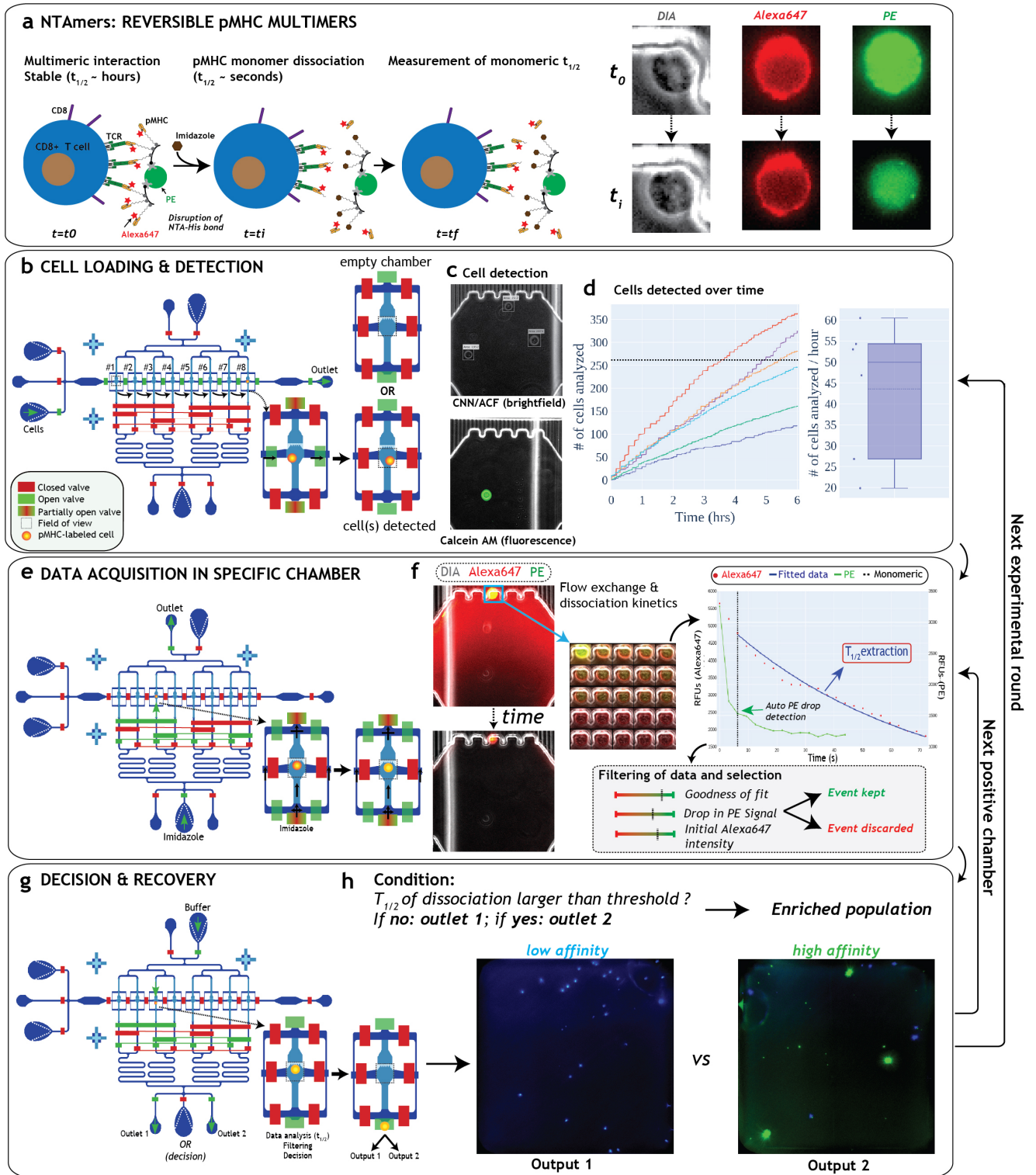
Figure 5.3: Caption on next page

101

Figure 5.3: **mCPU single-cell analysis**.

a We used pMHC NTAmers [62] for dissociation measurements of cell-surface TCR-pMHC interactions. **b-i** The mCPU performs sequential microfluidic processing steps: cell-loading and detection, buffer exchange and single-cell analysis, and cell selection and recovery **b** Cells are loaded and the eight chambers are isolated and imaged to identify chambers containing one or more cells. **c** Cell detection is performed either in brightfield or fluorescence. **d** The cumulative number of cells recorded and analyzed in all chambers per round of cell loading, showing 6 separate experiments. The average analysis rate was ∼50 cells per hour. **e** Chambers containing one or more cells are then imaged via fluorescent time-lapse imaging and washed with imidazole buffer leading to NTAmer dissocation. **f** Time-lapse acquisition is performed on two fluorescent channels: PE (NTAmer dissociation), and Alexa647 (pMHC - TCR dissociation). Image processing, data analysis, and curve fitting is performed to extract TCR-pMHC dissociation half-lives. **g-h** Filtered data are then compared with user-defined thresholds for cell selection and routing to a specific outlet. The process is then repeated in the next cell containing chamber or a new round of cell-loading is triggered.

5.4d). The mixed population was then analyzed on the mCPU measuring the pMHC dissociation rate as well as identifying the cell-type using Calcein staining. The mCPU analyzed a total of 376 single-cells in three mCPU runs (Fig. 5.4e). An initial 90% WT to 10% DMβ target ratio resulted in an average observed ratio of 88% WT to 12% DMβ expressing cells as determined by Calcein dye labelling (Fig. 5.4f). We then sought to identify cells with apparent long half-life pMHC-TCR interactions by setting a half-life threshold of 45s near the lowest observed DMβ half-life, resulting in a sensitivity of 100%. This threshold level in turn yielded a specificity and accuracy of 96%. The mCPU correctly identified all long half-life DMβ clones, as well as a small number of WT clones that also exhibited long half-lives (Fig. 5.4a). With these encouraging results we further increased the input ratio between WT and DMβ clones by an order of magnitude to 99% to 1%, respectively (Fig. 5.4g & Supplementary Fig. 7.14). We let the mCPU run until it detected the first high-affinity cell based on a half-life measurements and were able to identify a DMβ clone after 45 single-cell measurements.

Enabling downstream processing of selected cells requires identification and recovery of selected cells from the device. We performed an experiment on a mixture of WT and DMβ TCR expressing
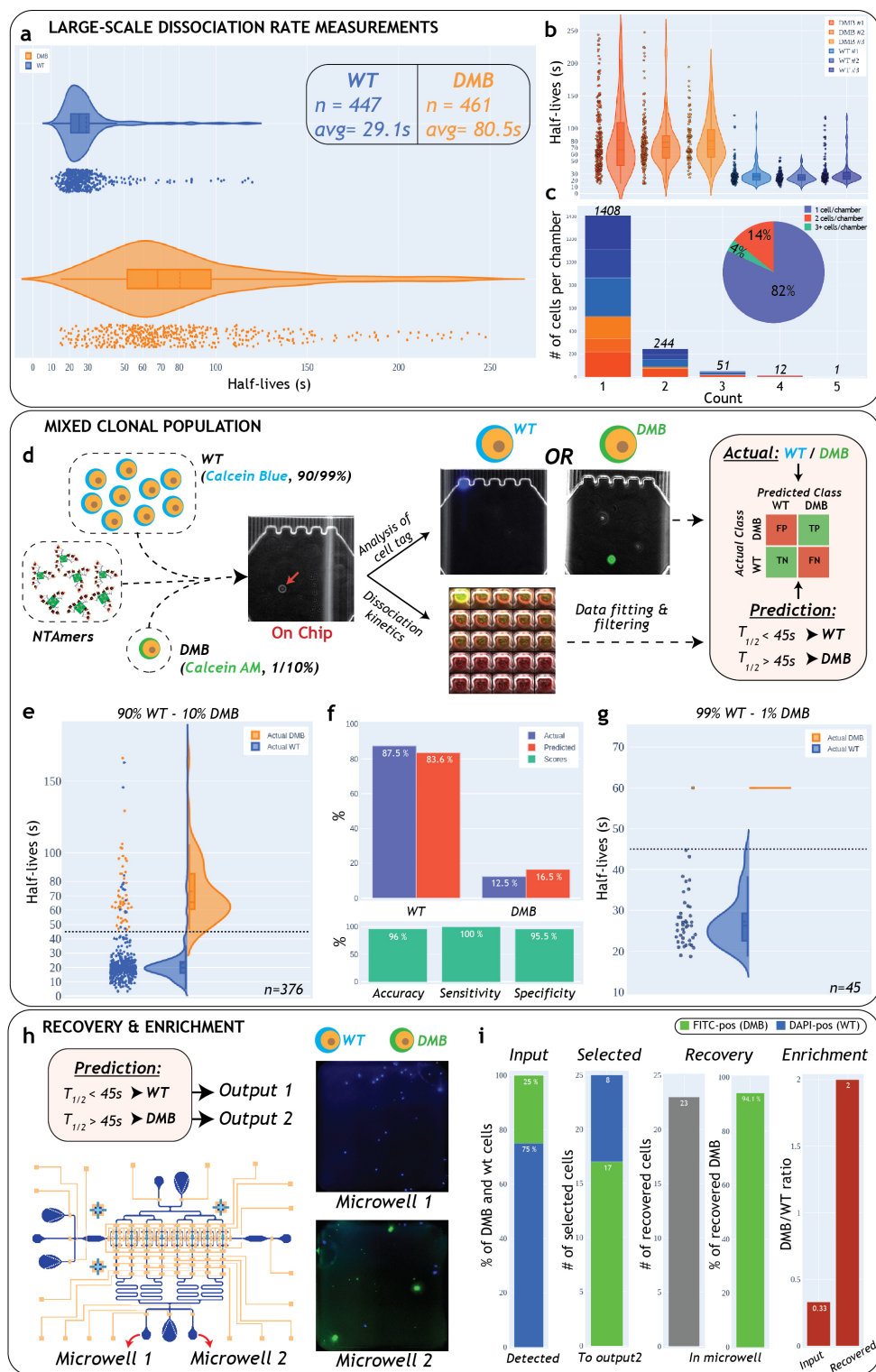
Figure 5.4: Caption on next page

Figure 5.4: **Single-cell TCR-pMHC dissociation measurements**. **a** Large-scale single-cell dissociation rate measurements for WT and DMβ expressing cells (aggregate of 3 independent experiments for each clone). **b** Half-live distributions for each experiment. **c** Distribution of cells detected per chamber. **d** Mixed population experiments. The actual WT to DMβ ratio was determined on-chip via Calcein Blue for WT and Calcein AM for DMβ, followed by dissociation rate measurements. **e** 90% WT to 10% DMβ experiment. Measured half-lives for each cell. Data point color indicates cell-type as determined by calcein staining. A half-life threshold of 45s was used to differentiate between high and low affinity cells. **f** WT to DMβ ratio as determined by calcein (actual) and as determined by using half-life measurements with a 45s half-life threshold (predicted). Accuracy, sensitivity and specificity were determined based on these ratios. **g** Experiment with higher dilution of high-affinity cells (99%WT and 1%DMβ) performed to identify a single-high affinity clone. **h** A recovery and enrichment experiment was performed by routing selected cells to a specific chip outlet. Cells were then transferred into microwells for counting. **i** Recovery and enrichment ratios were determined by comparing on-chip input with counted cells in microwells

cells at a ratio of 77% to 23%, respectively (Fig. 5.4h). We measured half-lives and specifically routed cells with half-lives above a 45s threshold to a recovery outlet. In the outlet we observed a ratio of 33% WT to 67% DMβ expressing cells based on Calcein staining, which represents close to an order of magnitude enrichment, based on the input ratio of DMβ to WT expressing cells of .3 and a post-selection ratio of 2. Cells could be aspirated from the recovery outlet with a pipette and transferred to a multiwell plate and 92% of cells could be successfully transferred with this simple approach (25 cells selected for recovery and 23 cells successfully transferred). We recovered 94% of the selected DMβ cells. Single-cell recovery and transfer to a multiwell plate was also achieved for the single cell identified and selected in the 99% WT and 1%DMβ ratio experiment described above (Supplementary Fig. 7.14).

5.1.3 Conclusion

By enabling complex, time-dependent experiments the mCPU platform fully automates single-cell analysis workflows, and is expected to find applications in areas where precise temporal and spatial control over single-cells is required. For example, promising application areas are basic immunology

such as characterizing T and B cells in response to natural infection and applied immunology including cancer immunotherapy where screening large-numbers of T cells and selection of high-affinity candidates is critical for therapeutic applications. In biotechnology related areas, the mCPU is capable of characterizing native as well as synthetic receptor libraries, which is useful for T cell, B cell, and de novo engineered cell receptor library characterization and screening. In addition to quantifying cell-surface receptor interactions, the mCPU should also be able to measure fast intracellular signaling events, such as calcium dependent signaling. More broadly, we demonstrate the evolution of microfluidic technology towards a truly autonomous "lab-on-a-chip" platform that performs complex fluid handling operations, data acquisition, data analysis, and decision making in a closed-loop system. Such systems could in the near future perform complex and completely unsupervised experiments.

5.1.4 Acknowledgments

5.1.5 Competing interests

The authors declare no competing interests.

5.1.6 Author contributions

J.S, G.C and S.M conceived the idea to perform single-cell pMHC-TCR dissociation rate measurements. J.S provided the NTAmers, cell clones, performed FACS analysis, and contributed to the methods section. S.J.M. and F.J. invented, designed, and optimized the microfluidic device and methods. F.J. implemented the microfluidic design, wrote software, and performed experiments. F.J. and S.J.M analyzed data and wrote the manuscript.

5.2 Other applications & leads

Based on the success of the mCPU platform to study single-cell dissociation kinetics of the TCR-pMHC interaction, we tried to broaden the use of this platform. We believe that the mCPU platform is versatile and can be applied to a wide range of applications.

5.2.1 Primary CD8+ T cells

While the main focus of this work was based on cell clones (SupT1 cell line) for device characterization and proof-of concept, the use of the mCPU platform on patient-derived primary CD8+ T cells was considered as the end goal of this project. Due to a lack of time, the combined use of NTAmers with primary CD8+ T cells on-chip was not explored in this work. However, we did explore the general behavior of primary cells on-chip as preliminary work. Indeed, primary cells are in general more sensitive than cell lines and proper primary cell handling was investigated here. To this end, primary CD8+ T cells (which have an incompatible TCR for the given antigen-specific NTAmers used here) were loaded on-chip and buffer exchange was performed to simulate real experimental conditions. The general behavior of the loaded primary cells were assessed (Fig. 5.5). It was observed that the general size of primary CD8+ T cells was smaller than SupT1 cell clones. Cell deformation or cell squeezing was not observed during buffer exchange. Cells remained mostly intact over time and behaved well during buffer exchange (Fig. 5.5). This preliminary data made us confident that the mCPU platform was adequate and compatible for the use of clinically-relevant samples such as patient-derived primary CD8+ T cells.

5.2.2 Working with conventional dextramers and pMHC monomers

While technologies such as reversible multimers (like the NTAmers technology) can be considered as advanced and niche, dextramers are widely used in immunology. Dextramers are widely used for evaluating the frequency of antigen-specific lymphocytes in a population. However, as they are non-reversible multimers, they do not provide any information about dissociation kinetics in conventional conditions and uses (e.g. flow cytometry).

We postulated that under constant buffer exchange, dissociation kinetics of bound dextramers on cells could be observed and should correlate to the structural affinity of the interaction. To study
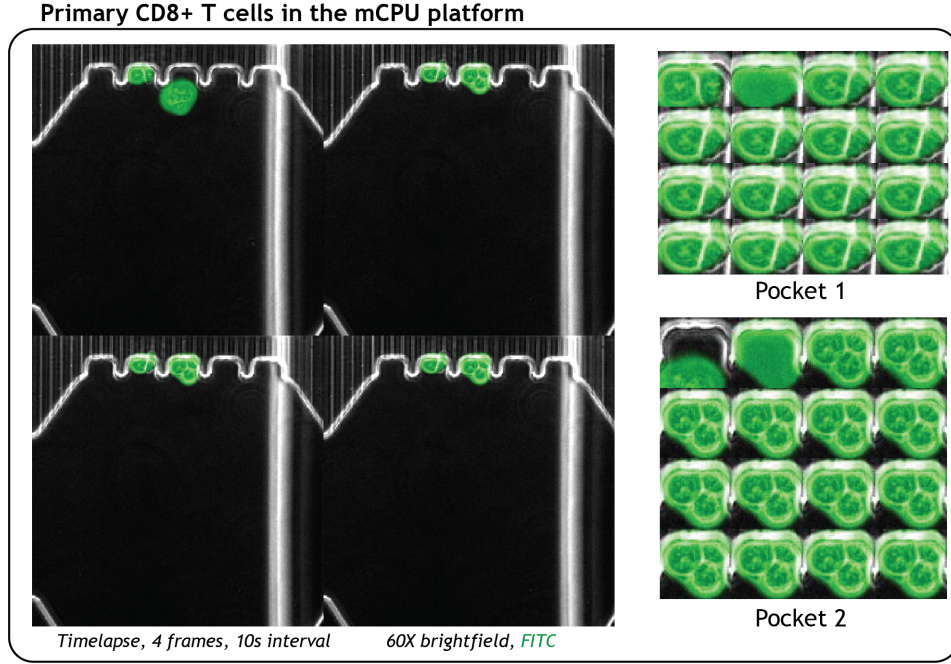
Figure 5.5: **Primary CD8+ T cells in the mCPU platform.**
Example of primary T cells on-chip under buffer exchange. As observed, while generally smaller in size than SupT1 cells, primary cells behaved normally on-chip and buffer exchange was successful without harming the cells.

this hypothesis a collaboration started with Prof. Sai Reddy and Rodrigo Vazquez-Lombardi (Department of Biosystems Science and Engineering, ETH Zurich). Based on their recent preprint [186] on the generation of functional T cell receptors with enhanced specificity while preventing the risk of cross-reactivity. As previously explained, cross-reactivity is a substantial drawback and limitation to TCR engineering therapy (see section 2.3). In their work, they generated a library of cell lines with different functional TCR sequences against the MAGE-A3 tumoral antigen. Typically, their functionality was first assessed by testing binding efficiency through use of dextramers followed by functional testing (often trough co-culture with antigen-producing cells or Calcium signaling) and animal work testing. We postulated that functional predictions could be made by extracting the structural affinity of the different TCR receptors in the cell library towards the same pMHC molecules loaded on the dextramers. The selected antigens in the work of Vazquez-Lombardi was for the MAGE-A3 and Titin antigen. Those antigens were selected based on a recent clinical trial that used TCR-engineered cells against the MAGE-A3 tumoral antigen but exhibited

107

cross-reactivity against the Titin antigen presented on cardiac tissue. This side-effect resulted in the death of two patients [186].

We decided to focus on mainly on 3 clones:

- TCR_{A3}, a melanoma patient-derived TCR receptor

- TCR_{a3a}, an engineered TCR receptor used in the mentioned clinical trial. This TCR showed efficient recognition of the MAGE-A3 antigen but presented cross-reactivity with the Titin antigen.

- TCR_{A3-05}, a newly generated TCR receptor by Vazquez-Lombardi et al., which showed great promise by displaying a high functionality against the MAGE-A3 antigen without cross-reactivity to Titin-antigen.

Independent experiments were performed on each clones. Cells were tagged with Calcein AM (FITC) and loaded on-chip in a buffer saturated with MAGE-A3 dextramers. Buffer exchange was performed to facilitate dissociation of the dextramers, while timelapse acquisition was performed for dextramer dissociation (PE fluorescent channel). As observed in Figure 5.6a, big variations in intensity was observed between clones. We decided to extract half-lives of dissociation for the three main clones against MAGE-A3 dextramers (Fig. 5.6b). Interestingly, the TCR_{A3-05} showed the higher dissociation half life (264s), which would correlate well with functional testing performed by Vazquez-Lombardi et al.[186]. Other clones were tested against the Titin antigen with dextramer dissociation on-chip (data not shown). Unfortunately, due to lack of time, additional experiments and adaptations of the dextramer technology to the mCPU platform were not performed during this thesis. We believe however that this combination of technologies has the potential to help dissociation kinetics studies becoming more mainstream in laboratory settings without the use of expensive and rare reversible multimers such as those used for the NTAmers technology.

Additionally, we explored the feasibility to use directly pMHC monomers for dissociation kinetics on-chip. Indeed, the most expensive component in the NTAmers technology is the multimeric core. Generating fluorescently-labeled target pMHC molecules does not represent the bottleneck cost problem for NTAmers or dextramers. By allowing loading of cells in a buffer saturated with NTAmers or dextramers, we postulated that if the concentration of pMHC monomers was high enough, the mCPU platform could enable direct use of pMHC monomers for structural study of

the TCR-pMHC interactions. Preliminary experiments were performed with inconclusive results (data not shown). Extensive additional work would be required to properly adjust the pMHC monomer concentration and test if this approach is feasible. Unfortunately, due to lack of time in this project, this approach was not studied further.
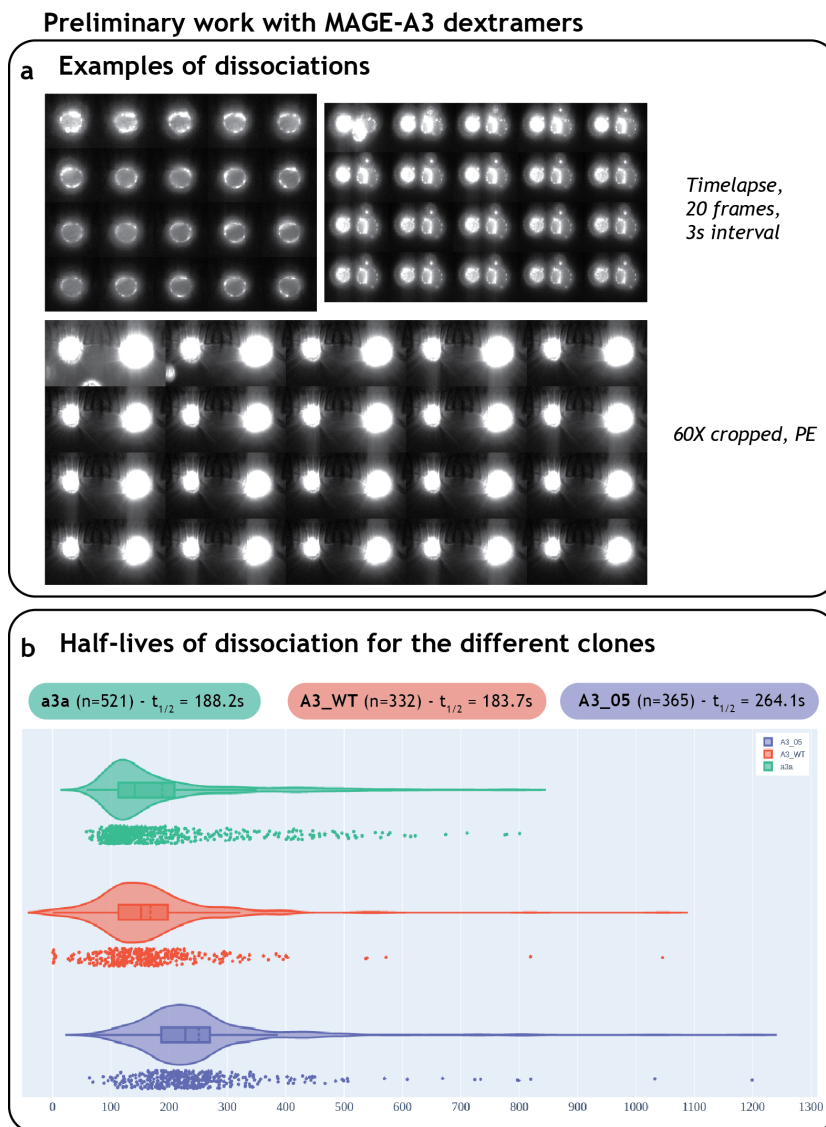

Figure 5.6: **Preliminary work with MAGE-A3 dextramers.**
a Example of dextramer dissociation for the TCR_{A3-05} clone. Variability in initial intensity was observed between clones. **b** Extracted dissociation half-lives of MAGE-A3 dextramers for the three different clones.

5.3 Conclusion

In this chapter, we demonstrated the potential of the mCPU applications for diverse applications. The main application of this work was the study of dissociation kinetics for the TCR-pMHC interaction on single cells and led to a submission for publication. Additionally, we decided to apply our mCPU platform for broader applications. The potential use of primary cells on-chip was explored and their general behavior during buffer exchange showed great promise for future uses. Furthermore, we tried to extend the use of the mCPU platform for the more widely-used dextramers technology (NTAmers technology is restricted to collaboration with the Ludwig Institute for Cancer Research). Encouraging results were found but additional work would be required. Finally, initial work on the use of pMHC monomers for dissociation kinetics was explored. This approach could have a huge impact on the field as an innovative, cost-saving solution enabled by the mCPU platform. Unfortunately, additional work needs to be done to prove the feasibility of this approach. We believe that the mCPU platform fills the requirements described in Section 4.1 by successfully allowing full temporal and spatial control over isolated single cells. The platform was successfully used for the study of single-cells dissociation kinetics, which could represent a major step forward in the clinical identification and use of naturally-occurring high-affinity T cells for cancer immunotherapy. Indeed, the ability to study the structural affinity of T cells at the single-cell level and allowing for selective recovery of cells enables the possibility of enriching high-affinity cells as demonstrated in Section 5.1. We believe that the mCPU can have a wide range of applications ranging from T cell but also to B cell studies for antibody functionality testing, as well as any other applications where time-dependent biological phenomena need to be studied at the single-cell level.

6

Conclusion

In this thesis, we developed an innovative microfluidic device that could handle single-cell dissociation kinetics study of the TCR-pMHC interaction. The different requirements of the technology were established and the different iterations of designs were explained. The final design of the microfluidic device was characterized and tested. Main issues like cell handling on-chip, cell damage during buffer exchange and consistent cell loading were identified, detailed and fixed. The challenges of a robust and automated cell detection and analysis pipeline were described. Machine learning was applied in this project in order to create an efficient object detector and CNN for cell detection, as well as the use of live-cell tags. The need for automation of the experimental process was described as a key element to remove user bias, as well as increasing experimental throughput of the microfluidic device. The integration of the automated image analysis pipeline with precise hardware control allowed for automation of the entire experiment through repetitive experimental cycles of cell loading, isolation, data acquisition and analysis, and finally selective cell recovery. Fully-autonomous, closed-loop microfluidic systems remain rare to this day and we hope that this innovation could help future generations of microfluidic designs to tackle complex biological problems.

In a second part, the established technology was applied to study the single-cell dissociation kinetics of TCR-pMHC interactions on generated cell lines. The technology was validated by obtaining similar results at the single-cell level compared to those previously obtained by flow cytometry, when studying a general population. The distribution of half-lives of dissociation from single cells within a clonal population was observed, which was not possible before with conventional tech-

nologies like flow cytometry. The mCPU platform was then tested for mixed clonal population in order to mimic a complex cell mixture for clinically-relevant applications. The technology showed great accuracy for distinction between low- and high- affinity clones and demonstrated the possibility to enrich a cell population of interest on-chip with a decision based on each cell's observed dissociation half life. We believe this feature to be desirable in clinical settings for future cancer immunotherapy treatments. Indeed, while CAR-T cells and TCR engineering therapy can generate highly-functional cells against tumoral antigens, the risk of cross-reactivity and side effects are also high. We believe that the ability to identify and isolate rare, high-affinity, naturally-occurring T cells has the potential to trigger a new generation of effective, safe, and personalized immunotherapy treatments. The mCPU platform represents a step forward in this direction.

Finally, we believe that the mCPU represents an autonomous platform suited for a broad range of applications. We tried to explore potential other uses of this platform. We explored the possibility to extract information about structural affinity of the TCR-pMHC interaction without the need for expensive and rare reversible multimers like the NTAmers technology. As dextramers are widely used when working with immune cells, we explored the feasibility to use the mCPU and dextramers technologies for identification of high-affinity cells, expanding the use of dextramers to not only binding studies but dissociation studies as well. Despite additional work needed, we believe that this approach is valid and could unlock new applications. Similarly, preliminary work was performed on the potential use of pMHC monomers for dissociation kinetics studies.

In this project we presented and characterized a new technological platform combining an automated, innovative microfluidic design with fluorescence microscopy and an advanced imaging analysis pipeline. This new technology allowed us to perform single-cell dissociation rates of the TCR-pMHC interactions, an established readout of the affinity and activation potential of a given lymphocytes for a given antigen. This project however, mainly focused on the development and characterization of this innovative technology. Further work would be required before implementation of the platform as a potential tool in clinical trial pipelines. While preliminary work was performed on the behavior of primary cells in the mCPU platform, further characterization would be beneficial. We believe that validation experiments involving already characterized primary cells should be the next step. We propose that a mixture of patient-derived antigen-specific lympho-

cytes, which have been characterized by conventional techniques (i.e. clonal isolation and expansion followed by flow cytometry analysis and TCR sequencing), and which show different affinities towards the same antigen, would be loaded onto the mCPU platform and separated into two different populations based on half-life of dissociations. Recovered cells would then be sequenced for their TCR and the results would be compared with known inputs. This type of experiment would ensure that the mCPU platform is able to enrich high-affinity primary cells that have been already characterized. Another potential next step would be to combine the mCPU platform with *in vivo* experiments in murine models. Patient-derived lymphocytes, already screened to be antigen-specific would be loaded on-chip. A threshold would be chosen for distinction and enrichment based on half-lives of dissociation. Cells from the two different populations (low and high-affinity) would then be sequenced for their TCR. A random selection of TCR sequences would then be transfected into murine lymphocytes models and injected into immuno-compromised mice transplanted with the patient tumor. Survival assessment through the form of overall survival (OS) and progression-free survival (PFS) could be then estimated by tumor volume monitoring. The hypothesis would be that transplanted lymphocytes with the TCR sequences originating from high-affinity lymphocytes analyzed by the mCPU platform would provide better tumor volume control and survival rate than low-affinity cells. Those kind of experiments would ensure a proper validation of the potential of the mCPU platform for clinical applications for adoptive cell therapy in cancer immunotherapy.

We believe that the mCPU platform described here could be applied to a wide range of biological applications. The mCPU platform could be used in other immunological applications, for instance, in antibody affinity screening on B cells. Assessing the affinity of antibodies against a given antigen is a key element for monoclonal antibody production. Most techniques nowadays usually involve high-throughput Surface Plasmon Resonance (SPR) or enzyme-linked immunosorbent assays (ELISA) to determine the affinity (e.g. K_D) of antibodies [187]. We propose that the mCPU platform could be adapted for the screening of B cells by studying the affinity of their B-cell receptor (BCR). A library of B cells already selected for recognition of a given antigen of interest could be loaded onto the mCPU platform, followed by the addition of antigen in the chamber for binding with trapped B cells and flow exchange with buffer. Dissociation kinetics of the BCR-antigen interaction could be assessed and B cells of interest could be enriched for BCR sequencing or clonal expansion. This approach could bring the benefits of studying large libraries of B cells,

easily generated through the use of editing tools such as CRISPR, while avoiding the necessity for clonal expansion and antibody production needed by conventional techniques like SPR or ELISA.

In addition to the use for immunoengineering on T cells and B cells, we believe that the mCPU is suited for any single-cell applications where a precise spatial and temporal control is required to study time-dependent phenomena either on the cell surface or even internally. The mCPU platform represents a versatile automated microfluidic device capable of studying complex temporal biological phenomena thanks to an elaborated image analysis pipeline and experimental automation. This platform represents, in our opinion, a good example of the potential of bioengineering in the fight against cancer and more generally for studying biology.

7

Appendix

7.1   Materials and Methods Chapter 4

Most of the Materials and Methods of this chapter are redundant with the Materials and Methods descried in Chapter 5. This applies for NTAmers description, cell origins and culture, all microfluidics microfabrication (from design to wafer and wafer to PDMS chip), microscopy and device setup. Please refer to 7.2 for more details.

Cell viability assessment in glass vial

Cell solution (see 7.2) was prepared and loaded in the glass vial (1.5mL SureStop vials, Chromacol, Thermo Scientific) containing a micro magnetic stir bar (PTFE, 2x7mm, Fisherbrand), which was actuated by a microstrirrer (low speed, Fisherbrand). The cell solution was then kept for several hours (total 19h) and cell viability was assessed by sampling 20μL of cell solution and mixed with 1μL of Trypan blue (Gibco) and cell viability was measured on a automated cell counter (Countess II, Applied Biosystems).

MATLAB-based image analysis

All image analysis strategies were made by custom MATLAB scripts using the main MATLAB functions described in Chapter 4.

Training of the convolutional neural network (CNN)

The CNN model was initially trained as part of a student project with the help of students: Manon Blanche, Theo Nass, and Sylvain Cam. This method section is adapted from their report.

The CNN model was implemented using the Python TensorFlow framework and exported as .json file for use with MATLAB custom scripts. Data consist of 512 x 512 grey-scale images. Each image had been manually associated to a class label, as references for the training data and comparison for the testing data. Two main pipelines were tested: the first model is a network that performs the classifcation over three different categories (referred as cell, empty and trash), whereas the second only classifies two labels (cell and bad).

The classification network was inspired by architecture already used for similar tasks from the literature. Given the large 512 x 512 pixels size of the images, 6 convolutional layers were created, with a kernel size of 3 and a stride of 1. The activation function used is the Rectified Linear Units (ReLU). After each convolution, a max pooling is performed with a kernel size and stride of 2. At the output of these CNN, a fully connected layer flattens the image into a 2304 x 1 dimension vector. To reduce the model complexity and prevent the model from overfitting, a dropout layer is placed after the convolutional layers [5]. The dropout layer ensures a 50% chance that all output of a given hidden neuron will be forced to 0 and thus deactivated. The final output is a 3 x 1 prediction array containing the estimation for each class, activated by the SoftMax function that will re- turn the probability that an image belongs to a class or the other. Since the network was designed to predict classes, the loss function most adapted is categorical cross-entropy. By providing a validation split parameter of 0.2, the model will set apart a 20% fraction of the training data and will evaluate the loss and any model metrics on this validation data at the end of each epoch. This will also give us an insight of the model's tendency to overfit. Overfitting happens when the model starts learning the training images by heart rather than the defining features of a cell. It is characterised by the divergence of the loss function: increase in validation loss while training loss keeps decreasing.
For optimal efficiency, images must be pre- processed before being passed to the model. Pixels were normalized to range from 0 to 1, enabling the model to converge much faster towards a solution.

116

Multiple parameters must be tweaked for model optimization. Amongst them are the pre-processing step, the number of classes, the optimizer function and the number of epochs. The optimization process must consider the fact the dataset is unbalanced, with only 10% of images containing cells. This also affects the metrics used to assess the model's efficiency. The model can easily reach 90% accuracy by classifying every chamber as empty, defeating the purpose of the model. Precision, the percentage of images flagged as containing cells that actually have cells (measure of false positives), and recall, the percentage of cell containing images correctly classified (measure of false negatives), will give a more accurate account of how good the model is at differentiating chambers with and without cells.

7.2 Materials and Methods Chapter 5

Cell lines and culture

The SupT1 cell lines used in this study were developed previously as described here [172]. In this project two clones were used: WT (with the WT TCR sequence) and DMβ with increased affinity compared to WT, within physiological range for cancer neoantigens [58]. Cells were cultured in DMEM media supplemented with L-Glutamine, 10% FBS and 1% Penicillin-Streptomycin (Pen/Strep, Gibco). Cells were passaged once to twice per week at a ratio of 1:20 for 12 maximum passages.

NTAmers production & staining

NTAmers were synthetized by the Peptide and Tetramer Core Facility of the Department of Oncology UNIL/CHUV as described previously [62]. Briefly, NTAmers are composed of Streptavidin-Phycoerythrin (SA-PE, Invitrogen) complexed with biotinylated peptides carrying four $Ni2^+$-nitrilotriacetic acid (NTA4) moieties and non-covalently bound to His-tagged HLA-A*0201 monomers containing an AF647-labeled β2m. Monomers were obtained by refolding of the HLA-A*0201 heavy chain in the presence of AF647-labeled β2m containing the S88C mutation with AF647-maleimide (GE Healthcare) and the analog NY-ESO-1$^{157\text{-}165}$ [SLLMWITQA] tumor antigenic peptide. After purification on a Superdex S75 column, pMHC monomers were mixed at a 10-fold ratio with SA-PE-NTA4 in the presence of $Ni2^+$, aliquoted and kept at -80°C.

For staining, generally 5.10^5 cells were spun down (350g, 5min, 4°C) and re-suspended in 100μL of buffer (PBS with 4% BSA, 1% Pluronic F-127 (Sigma-Aldrich), 2% Pluronic F-68 (Gibco) and 2% Pen/Strep). Cells were tagged with Calcein (Invitrogen) or Calcein Blue (Invitrogen) for live-cell tagging at a concentration of 5μM with an incubation of 30min in the dark at 4°C. Following addition of 1mL of buffer, cells were spun down (350 rcf, 5min at 4°C), re-suspend in 100μL of buffer, and 5μL of pMHC multimers was added with an incubation at 4°C for 30-45min in the dark. Following incubation, 300μL of buffer with 40μL of OptiPrep$^{\text{TM}}$ was added to reduce cell sedimentation. The final solution was loaded in a 1.5mL glass vial (SureStop vials, Chromacol, Thermo Scientific) containing a micro magnetic stir bar (PTFE, 2x7mm, Fisherbrand), which was actuated by a micro-stirrer (low speed, Fisherbrand). The glass vials for cells, imidazole-rich buffer

and washing buffers were kept on ice and placed on top of the magnetic stirrer (Supplementary Fig. 7.3). The chip and microscope stage were enclosed in an environmental chamber kept at 14°C.

Dissociation rate measurements by flow cytometry

To validate the single-cell off-rates measurements performed on-chip, SupT1 cells (WT and DMβ) were analyzed for dissociation measurements by flow cytometry as described previously [58]. Briefly, 200'000 cells were incubated for 40 minutes at 4°C with specific NTAmers (HLA-A*0201/ NY-ESO-1$^{157\text{-}165}$) in 50μL FACS buffer (PBS supplemented with 0.5% BSA, 15 mmol/L HEPES, and 0.02% NaN$_3$). After washing, cells were resuspended in 500μL FACS buffer at 15°C and cell surface-associated mean fluorescence was measured under constant temperature using a thermostat device (15°C) on a SORP-LSRII flow cytometer(BD Biosciences) following gating on living cells. Multimeric PE-NTA$_4$ scaffold and Alexa647-pMHC monomer fluorescence were measured for 30s (baseline). Imidazole was added at 30sec (100 mmol/L) and PE and Alexa647 fluorescence recorded for 10min. Duplicates were used for each cell clones. Data was processed using the FlowJo software (v9.6, Tree Star, Inc.). After gating on living cells, PE or Alexa647 mean fluorescence intensity was derived using the kinetic module of the FlowJo software. Geometric mean fluorescence intensity over time was then plotted using GraphPad Prism software and monomeric TCR-pMHC dissociation kinetics calculated using a one-phase exponential decay equation.

Design and fabrication of the microfluidic device

The device design includes four fluid inputs (with built-in filters) and five fluid outputs. The device features 8 independent chambers that are roughly 150 by 100μm in size. Heights of 10 and 15μm (chambers and flow channel, respectively) were chosen to accommodate the typical cell diameter of lymphocytes (around 12μm). The chambers can be isolated using micromechanical valves (Supplementary Fig. 7.4). Each chamber can be specifically addressed from the bottom buffer inlet via a multiplexer (*e.g* Chamber #2 is addressed individually in Supplementary Fig. 7.4). To reduce shear stress and prevent cell loss during buffer exchange and wash steps, each chamber features small sieves (1.5μm high) to retain cells during fluid exchange operations and two bypass channels to reduce flow velocity in the chamber area. Finally, a partially-closing valve was installed before and after the chamber area. This valve does not fully close when activated, allowing fluid flow while increasing flow resistance.

The microfluidic device was fabricated by standard multilayer soft lithography [128]. The microfluidic device was designed in AutoCAD (Autodesk, California). Molds for the control and flow layers were fabricated on two separate wafers by standard photo-lithographic techniques to obtain microfluidic channels with desired heights. For the control layer, a silicon wafer was primed by oxygen plasma treatment for 7 minutes (TePla 300). SU-8 photoresist (GM 1070, Gersteltec Sarl) was spin-coated to obtain a height of 30μm. After relaxation (30min) and soft bake (3000s ramp to $130°$C, baking for 300s at $130°$C and ramping down to $30°$C for 3000s), the wafer was exposed under a chrome mask for 16s (365 nm wavelength, 20 mW/cm^2 light intensity, Süss MA6 Gen3 mask aligner) followed by a post-exposure bake (2400s ramp to $90°$C, baking at $90°$C for 2400s and ramping down to $30°$C in 2700s). Development of the wafer was performed with propylene glycol monomethyl ether acetate (around 3min) followed by incubation with isopropyl alcohol (2min) to stop the reaction and finally by a hard bake ($130°$C for 2 hours). For the flow layer, a similar procedure was performed on a separate wafer for the first photoresist layer (sieves, 1.5μm height, SU-8 GM 1040, 3.2s illumination). The same wafer was used for patterning of the second layer (chamber area, 10μm height, SU-8 GM 1060, 8.3s illumination). After SU-8 patterning, the wafer was vapor treated with hexamethyldisilazane (HMDS) and AZ 9260 (Microchemical GmbH) was spin-coated to a height of 15μm on a Süss ACS200 GEN3. The wafer was then exposed under a mask for a total of 40 seconds (Süss MA6Gen3). AZ 9260 photoresist (Microchemical GmbH) was spin-coated for a height of 15μm and exposed for a total of 40 seconds. The AZ 9260 photoresist was annealed by ramping the temperature to $135°$C for 2 hours to generate a rounded profile.

For microfluidic chip fabrication, each wafer was treated with trimethylchlorosilane (TMCS) for silanization by vapor deposition in a desiccator for at least 1 hour. For the control layer PDMS (5:1 ratio elastomer to crosslinker) was prepared, poured over the wafer and degassed in a desiccator for 30min. The wafer was then baked in the oven at $80°$C for 25 minutes. Following baking, the PDMS chip was detached by hand from the wafer and punched using a stainless steel punch (OD: 0.65 mm, ID: 0.35 mm, length: 8 mm; Unimed). For the flow layer, PDMS with a 20:1 ratio was spin coated at 1450 rpm (ramping up for 20s, spinning for 35s and ramp down of 20s) onto the wafer and left to sit 15 min before baking for 20 minutes. The layers were then aligned by hand and baked for an additional 90 minutes. The bonded chip was then punched again to create the flow layer interconnects and two output holes were punched with a 2.5cm (OD) manual puncher (Harris

Uni-Core). The final chip was then bonded to a glass cover slip (Thickness No. 1, borosilicate glass, VWR Int.) cleaned using Scotch tape. The cover slip was taped to a glass slide for support. Bonding was performed by oxygen plasma treatment of both the PDMS chip and glass cover slip (Femto plasma oven, duration of 20s at 100% power, flow rate of 25 sscm and 0.1 bar).

Device setup

Pressurization of the control lines on the microfluidic chip was controlled with pneumatic solenoid valve (Pneumadyne manifolds), pressure levels were set with a pressure regulator (Type 10, 2–60 psi, Marsh Bellofram) and a digital gauge (digital manometer, PDC-102N2BFA, Kobold). A USB relay board (USBRELAY32, Numato Lab) was used to control the electric manifold actuation. Control lines were filled with purified, filtered water (Milli-Q water filtered with $0.45\mu m$) and slowly pressurized to 125 kPA. The flow layer was primed with a buffer (PBS with 4% BSA, 1% Pluronic F-127, 2% Pluronic F-68 and 2% Pen/Strep). Tygon tubing (OD 0.0600, ID 0.0200; Cole-Parmer) with stainless steel connecting pins (0.35mm x 8mm, AISI304, Unimed) was used for control lines and buffer solutions. For cell loading, a combination of connecting pin, Tygon tubing and a narrower tubing was used (PEEK, 1/32" OD, .005" ID, Vici) to prevent cell sedimentation in the tube during the experiment. Cells were loaded at desired densities (usually 5.10^5 cells in $400\mu L$) in NTAmer-rich buffer (see above). After initial loading and user-based adjustments (chamber position saving, camera and experimental settings), the custom MATLAB GUI conducted the entirety of the experimental cycle described. Valve actuation sequences are defined for key steps in Supplementary Figure 7.4. Cell recovery was performed from the larger outlet holes (2.5mm), allowing direct pipetting of cells. Recovered cells were transferred into a flat bottom, square-well 384-well plate (Nunclon Delta Surface, Thermo Scientific) and visualized on a microscope.

Data acquisition & analysis

Solenoid valves, microscope, and camera were controlled by the custom Matlab GUI. The chip and microscope stage were enclosed in an environmental chamber kept at 14°C. Imaging of the microfluidics device was performed on a Nikon Ti-E Eclipse automated microscope with an epifluorescence illuminator (C-HGFI Intensilight, Nikon). Images were acquired with an Ixon DU-888 camera (EMCCD camera, Andor Technology), using a 60x oil objective (CFI Plan Apo Lambda 60X Oil, Nikon). Time-lapses of fluorescent signals were recorded for two fluorescent labels. The

first fluorescent tag uses Alexa647 probes linked to the pMHC monomers. The second fluorescent tag is a PE probe linked to the core unit maintaining the pMHC monomers in a multimeric form. After addition of imidazole-rich buffer (200 mM of imidazole in PBS with 4% BSA, 1% Pluronic F-127, 2% Pluronic F-68 and 2% Pen/Strep), the His-Tag links between the PE core and the Alexa647-fluorescent pMHC monomers is disrupted by competitive inhibition and only the monomeric signal is kept and recorded. This dual use of fluorescent tags allows to determine the time component of the switch from multimeric to monomeric form. Brightfield images (exposure time: 50ms, 50 gain, EM gain x5.1, temperature at -70°C) as well as fluorescent images for both the Alexa647 fluorophores (Nikon filter cube: Cy5, HC 620/60, HC 700/75, BS 660; exposure time: 250ms, 250 gain, EM gain x5.1, temperature at -70°C) and PE fluorophores (Nikon filter cube: Cy3 HC 535/40, HC 590/40, BS 565; exposure time: 250ms, 250 gain, EM gain x5.1, temperature at -70°C) were recorded during time-lapses for a total of 60 to 90 seconds with a fixed interval of 3s for each channel for a total of 20 to 30 frames acquired per channel. Fluorescent images were corrected by dark frame subtraction and flat-field correction. Timeseries images were analyzed using custom MATLAB code. Briefly, cells were identified as ROIs. ROIs were defined using Calcein tag (FITC channel, exposure time: 25ms, 25 gain, EM gain x5.1, temperature at -70°C), Calcein Blue (DAPI channel, exposure time: 125ms, 125 gain, EM gain x5.1, temperature at -70°C) or brightfield images (via trained CNN or ACF object detectors) around cells of interest and around background regions (Supplementary Fig. 7.5). The mean intensity of the ROIs was calculated over the different frames, the background mean intensity was subtracted from the mean signal intensity and the signal over time was plotted and fitted to a one-phase exponential decay corrected for bleaching. Bleaching rates were established for both fluorophores by performing flow exchange with buffer lacking imidazole. This allowed to extract bleaching rates for Alexa647 and PE of 245s and 123s respectively, Supplementary Fig. 7.6. The bleaching rate of Alexa647 was used to compensate bleaching during experiments by adapting dissociation rates accordingly $(A*e^{(-(k+k_{bleaching})*t)}+B)$.

After fitting, key parameters were extracted for event filtering. The key parameters included goodness of fit (R^2) keeping events with a minimum of 0.95 to ensure proper fitting of the data. Other key parameters were initial intensity (A, maximum level of 45'000 RFUs) and background level (B, maximum level of 15'000 RFUs). Finally, a drop in PE signal (difference between initial and final intensity) higher than 32% . In addition of those key parameters, the half-lives of dissociation

were extracted after filtering and fitting (Supplementary Figures 7.8, 7.11 & 7.12). The extracted half-lives were used to trigger the decision on cell selection for output and recovery.

7.3 Supplementary Figures Chapter 4
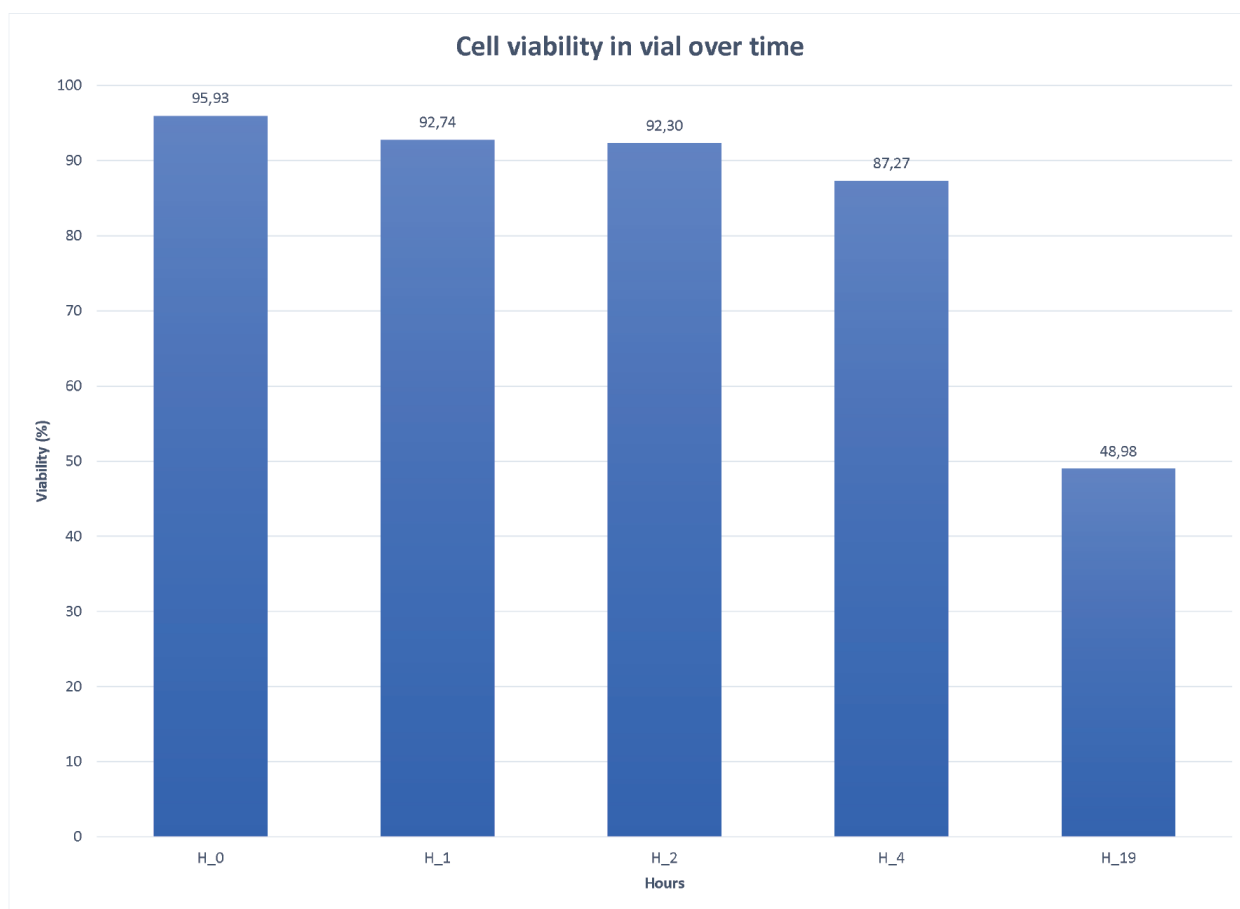
Figure 7.1: **Cell viability in glass vial over time.**

Cell viability in buffer (PBS with 4% BSA, 1% Pluronic F-127, 2% Pluronic F-68 and 2% Pen/Strep) was assessed over time at 14°C under stirring with micro-magnet and micro-stirrer.

Figure 7.2: **Training a CNN model for cell detection in chamber.**
a Description of the chosen CNN model. **b** Examples of classification between the two categories: *cell* and *bad*. **c** Confusion matrix for score assessment of the generated CNN model.

7.4 Supplementary Figures Chapter 5

In this section we present supplementary figures that were included in the submitted manuscript that represent the Chapter 5, first section.
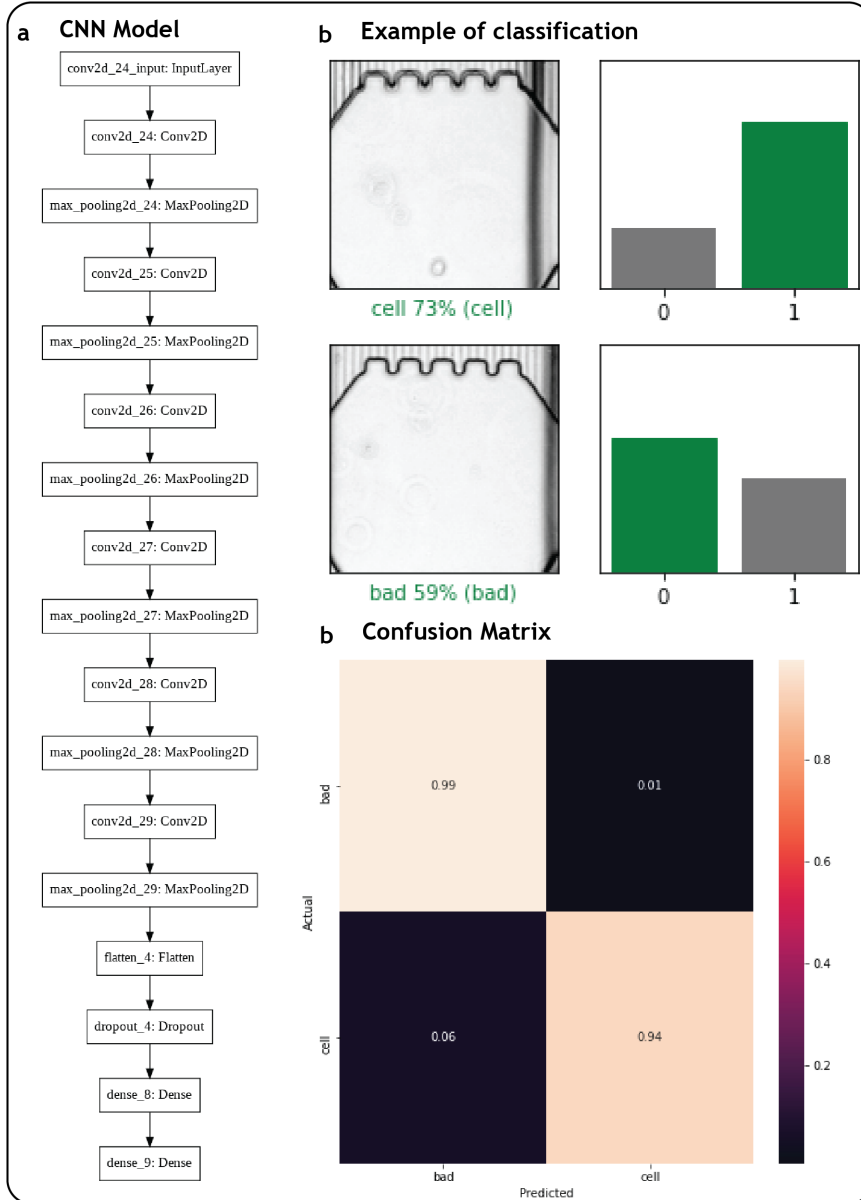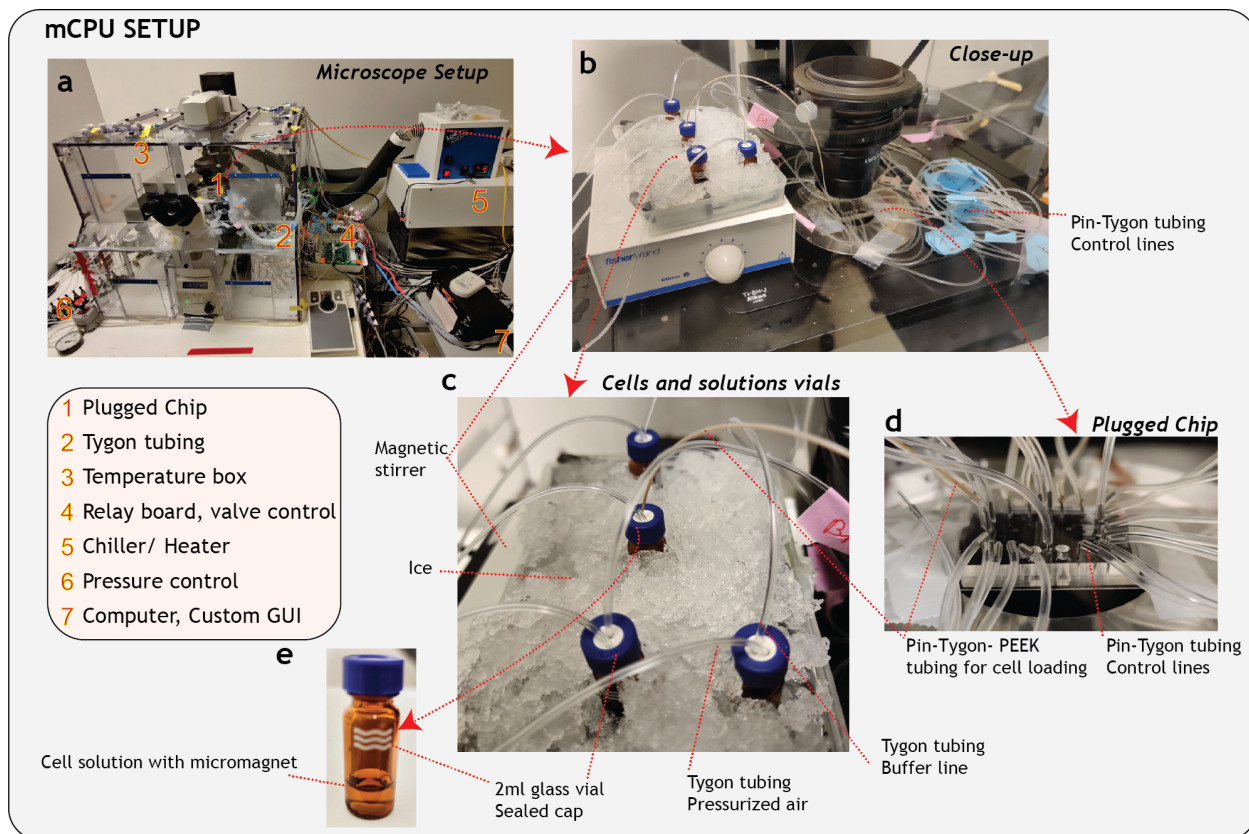

Figure 7.3: **mCPU setup**.

a Microscope setup with connected mCPU, temperature control, pneumatic valve and computer control. **b** Close-up view of the mCPU device and connected buffer and cell vials. **c** Vials with buffers and cells were kept on ice to prevent temperatures to reach above 15°C. Tygon and PEEK tubing is used to connect the vials to the chip. **d** Image of the mCPU with larger punched outlets for Outputs 1 and 2 for cell recovery. **e** Images of a glass vial used for buffers and cells. The cell vial includes a micromagnet for stirring.

Figure 7.4: **Pneumatic valve actuation states and sequences during the various experimental round**.

For each major step of the experimental cycle, valves are actuated in a specific sequence and for a given time. Each chamber is addressed independently by a multiplexer for flow exchange and cell recovery (here, chamber #2 is addressed).
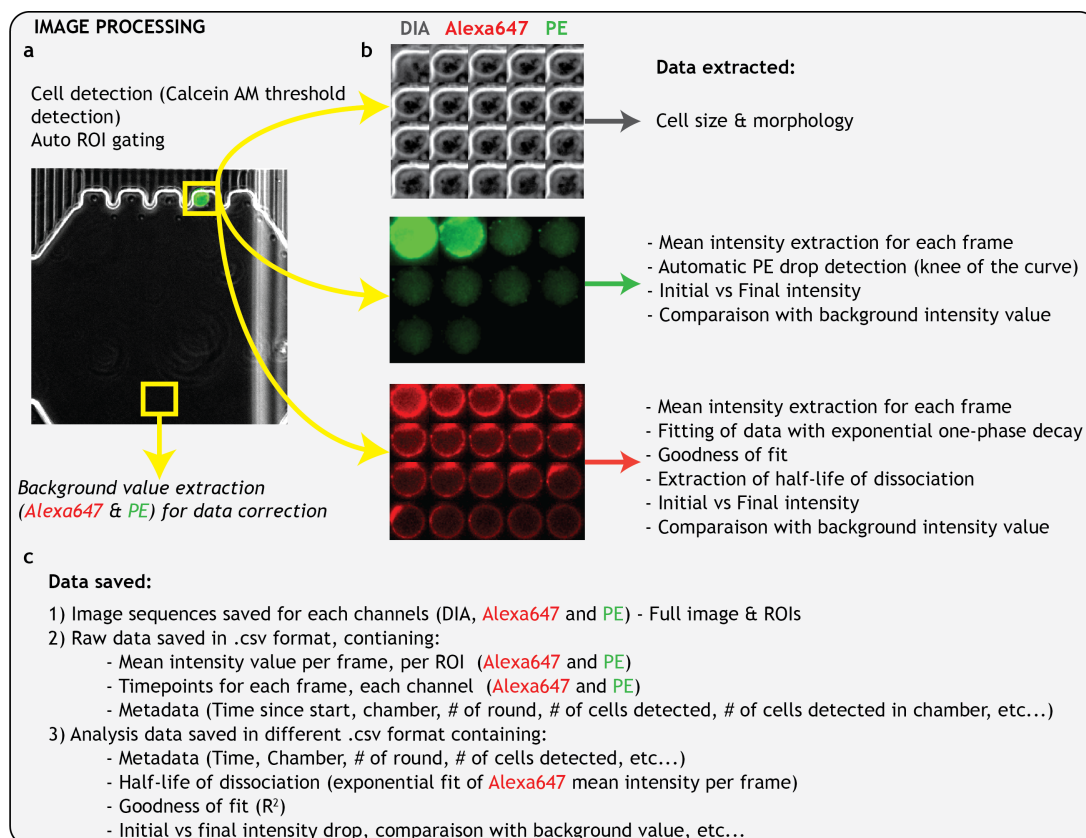
Figure 7.5: "Real-time" image processing.
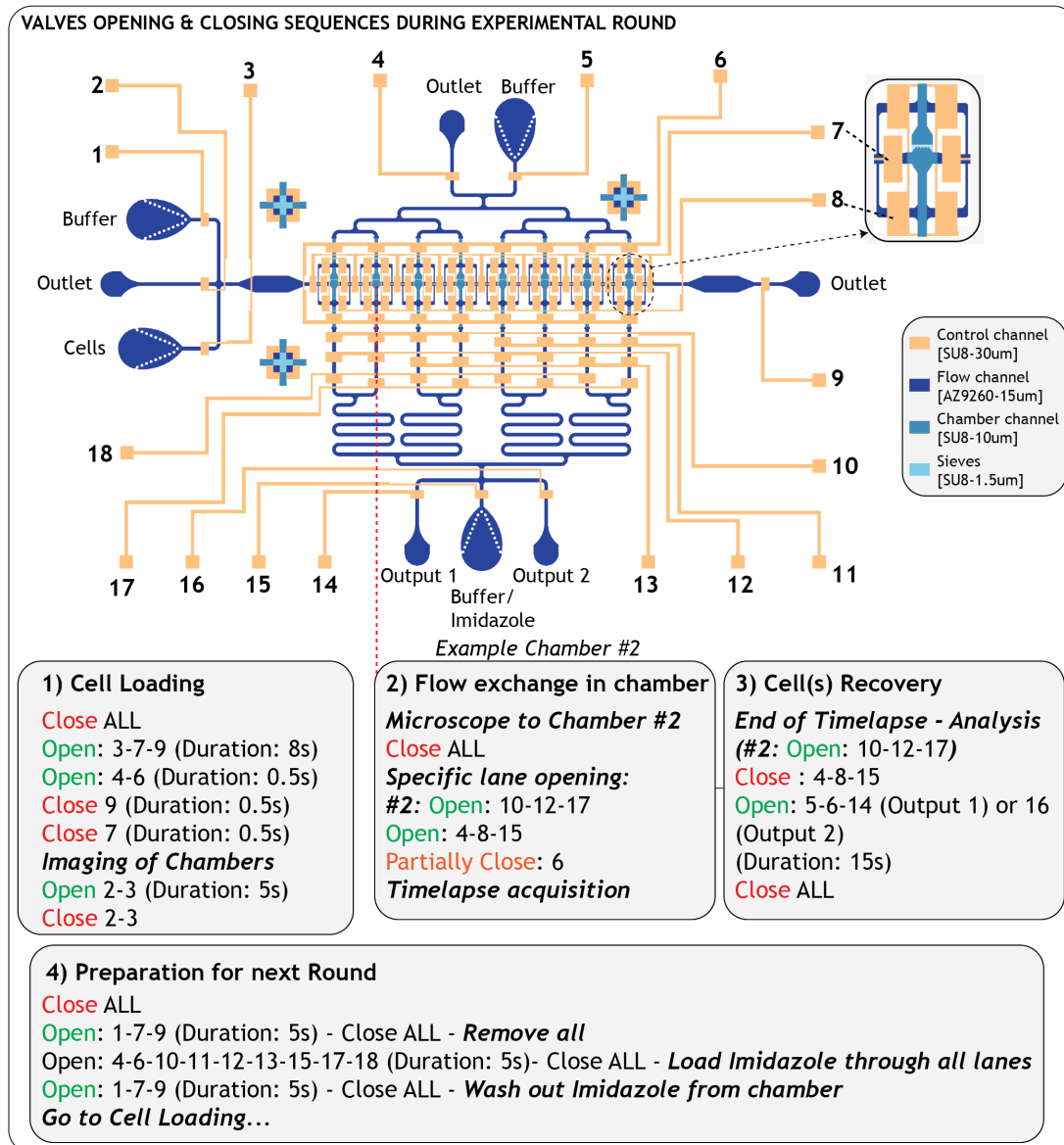**a** Automated cell detection is performed either via brightfield detection (CNN/ACF) or via fluorescent live-cell tags (*e.g.* Calcein AM). Automatic ROIs are created for each detected cell and one background ROI at the bottom of the chamber for background subtraction. **b** After ROI creation, each frame is automatically analyzed and data is extracted for each channel. Brightfield channel provides cell size and morphology information. The mean intensity of the PE channel (multimeric core of the *NTAmers* technology) is analyzed to automatically detect the sudden drop in signal, indicating a switch from multimeric to monomeric states of the NTAmer (code automatically identifies knee of curve). After the monomeric switch timepoint is identified, the analysis of the mean intensity of the Alexa647 channel is cropped accordingly and the data is fitted with an exponential one-phase decay to extract the dissociation half-life of the cell analyzed. Additional data such as goodness of fit (R^2), initial intensities, background level intensity, etc..., are also recorded. **c** All images and data generated are saved in either .tiff or .csv format.
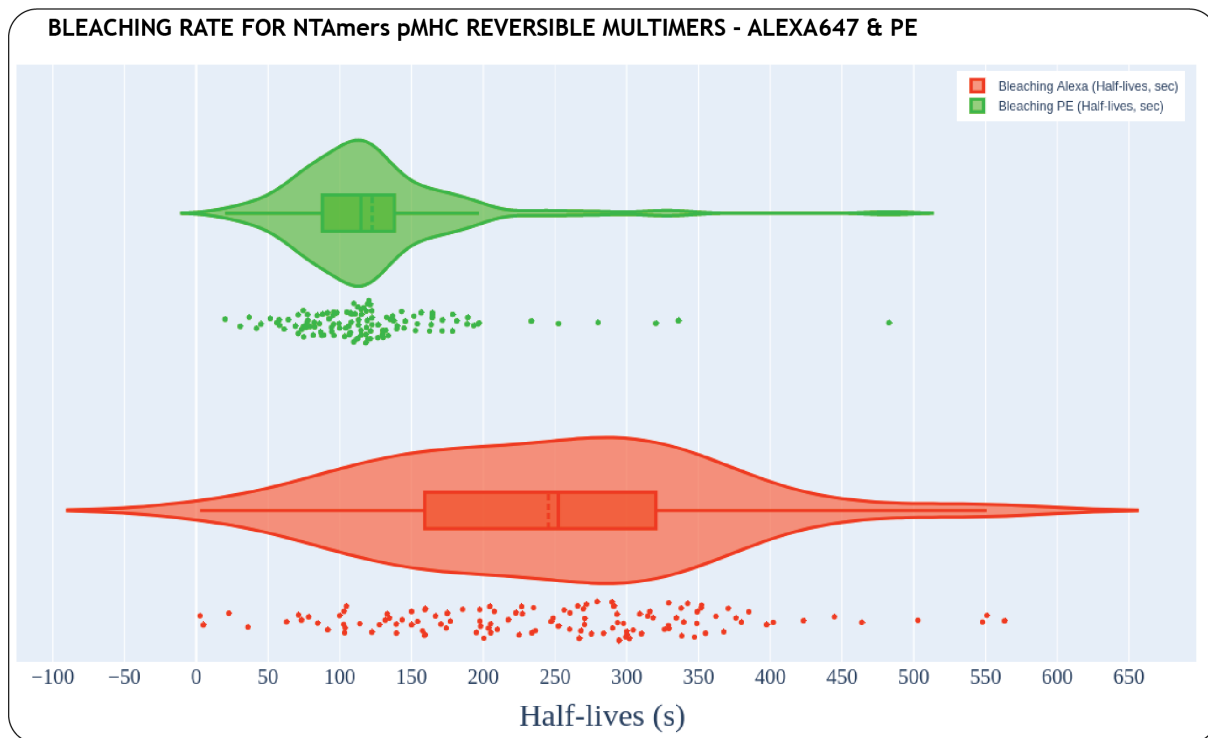
Figure 7.6: **Bleaching rates for NTAmers Alexa647 and PE fluorophores**.

Bleaching rates were established on the mCPU by performing flow exchange with buffer without imidazole with same parameters (camera, time-lapse duration, etc...) as normal experimental conditions. The obtained bleaching rate for Alexa647 was used for bleaching correction during fitting $(A * e^{(\text{-}(\text{k}+\text{k}_{\text{bleaching}})^{*}\text{t})} + B)$.

ASSESSMENT OF CELL DETECTION ACCURACY

	1 event	2 events	3 events	4 events	5 events
Incorrect	6.17% (47)	9.04% (15)	3.45% (1)	0% (0)	0% (0)
Correct	93.83% (715)	90.96% (151)	96.55% (28)	100% (13)	100% (3)
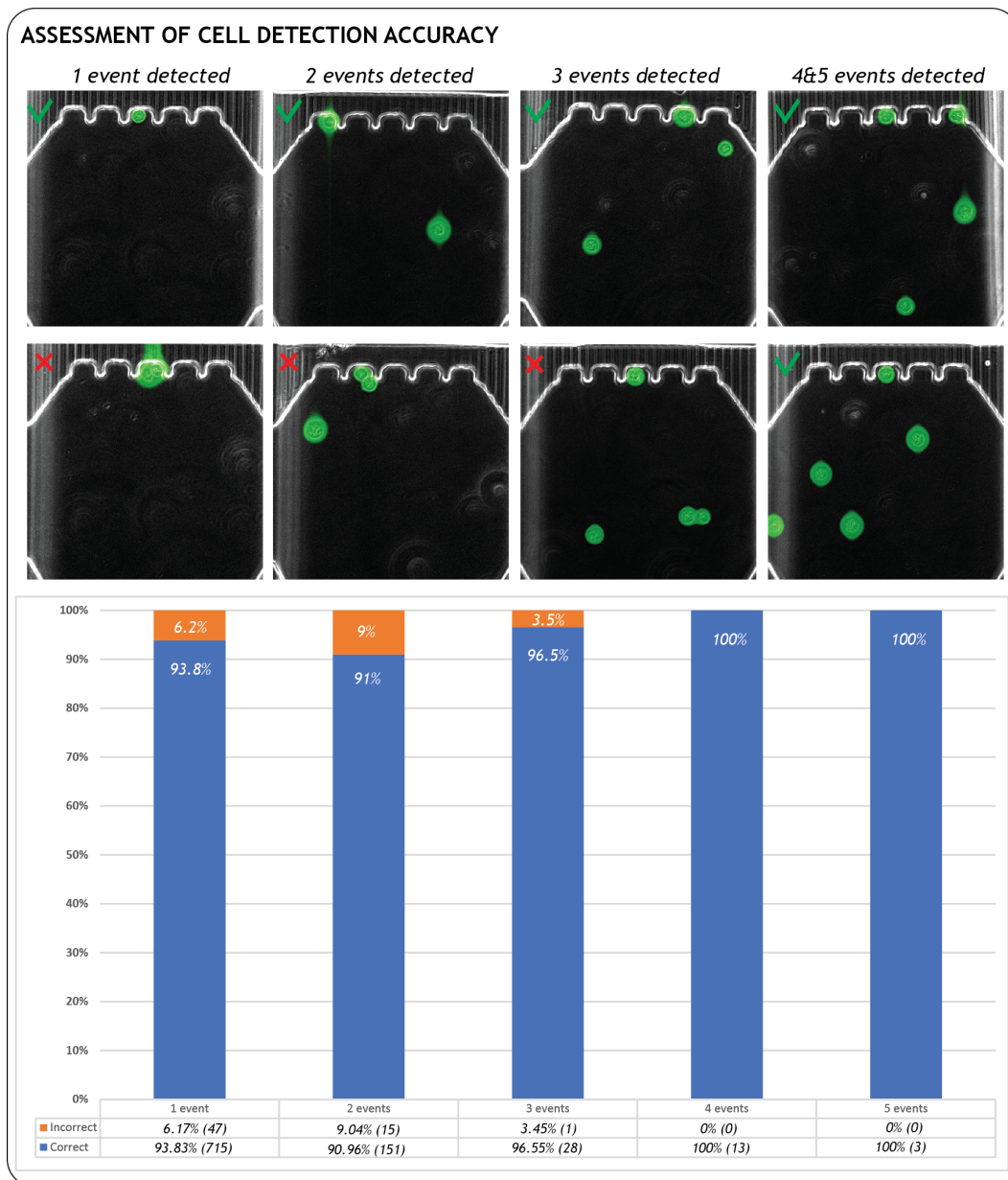
Figure 7.7: **Assessment of cell detection accuracy**

Saved images with Calcein AM hits were analyzed to detect errors in cell detection in comparison with saved metadata. The recurrence of errors in calculated events per chambers (*e.g.* 2 cells touching triggering a 1-cell detection event) was assessed over the different experiments performed.
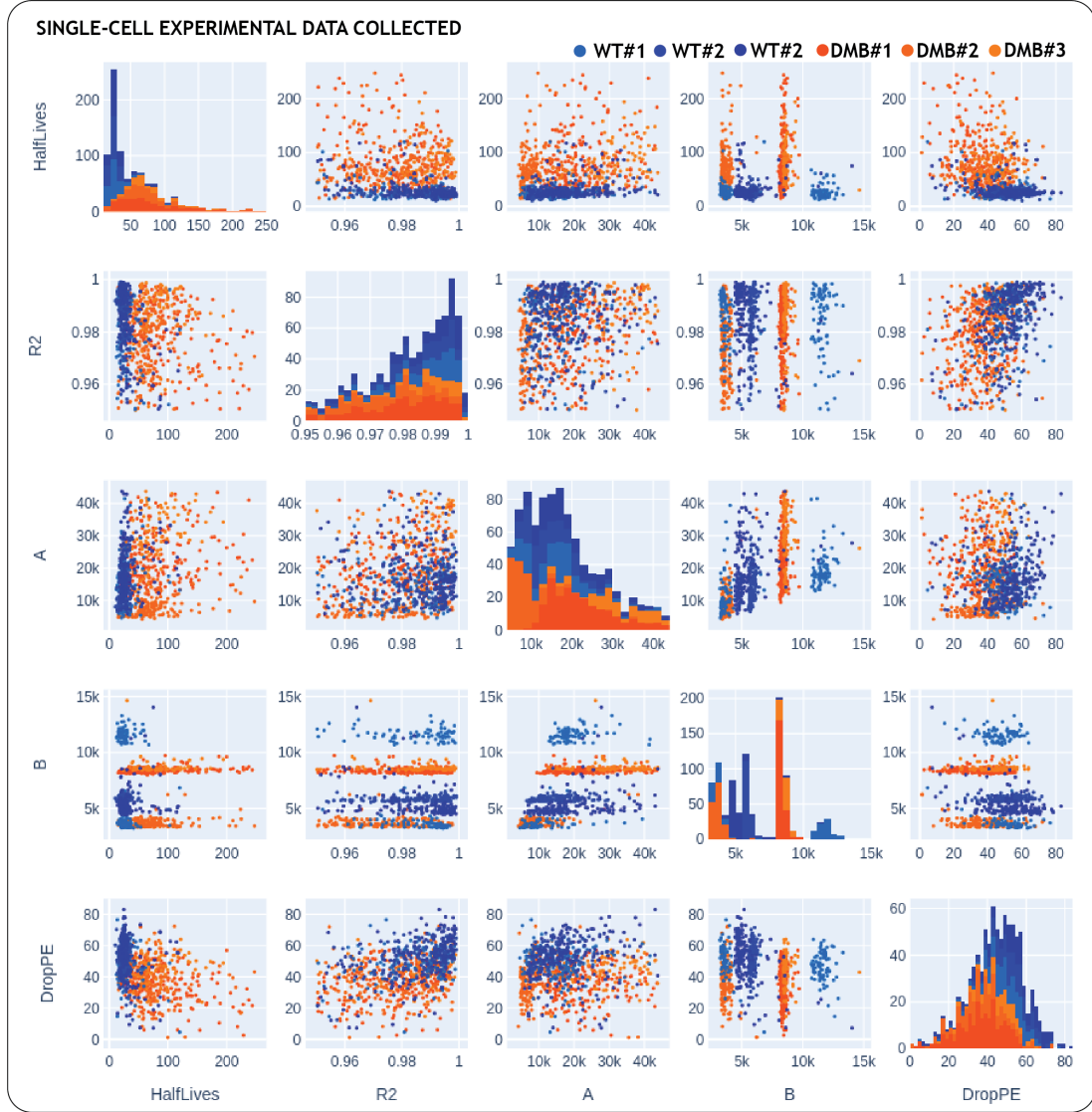
Figure 7.8: **Single-cell experimental data collected**

Scatter plot of single-cell events collected during 6 experiments (3 on WT clones, 3 on DMβ clones). Data points are shown for events that passed the filter criteria. Key parameters extracted and used for fitting and filtering are goodness of fit (R^2), A (initial Alexa intensity), B (background level), and drop in PE, which represents the difference between initial and final PE intensity levels.

Figure 7.9: **Parameter distributions after filtering of single-cell experimental data**
a Goodness of fit (R^2 distribution post-filtering for the different experimental replicates. **b** Initial intensity (A) distribution. **c** Distribution of drop in PE, the difference between initial and final intensity in PE. **d** Background intensity (B) distribution.
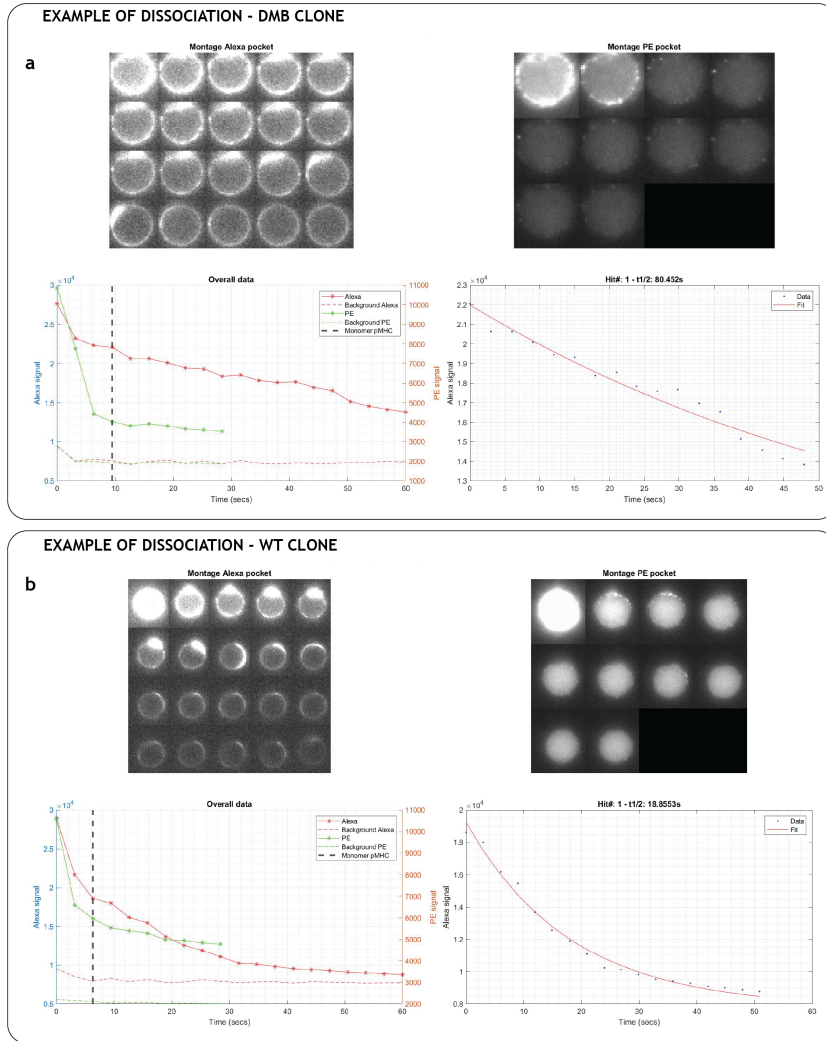
Figure 7.10: **Examples of automatically-generated data of single-cell pMHC-TCR dissociation measurements**.

Data are automatically generated and plotted during experimental cycle for a single event. **a** Example of dissociation kinetics of a single DMβ cell with image timeseries of both Alexa647 and PE signals and overall mean intensity plots (bottom left plot). The sharp decrease in PE signal is automatically detected and is shown by the vertical black dotted line. The mean intensity of the Alexa647 is cropped accordingly and then fitted with a one-phase exponential decay to extract half-life of dissociation (here, around 80 seconds). **b** Similar example for a single WT cell ($t_{1/2} = 19$ seconds).
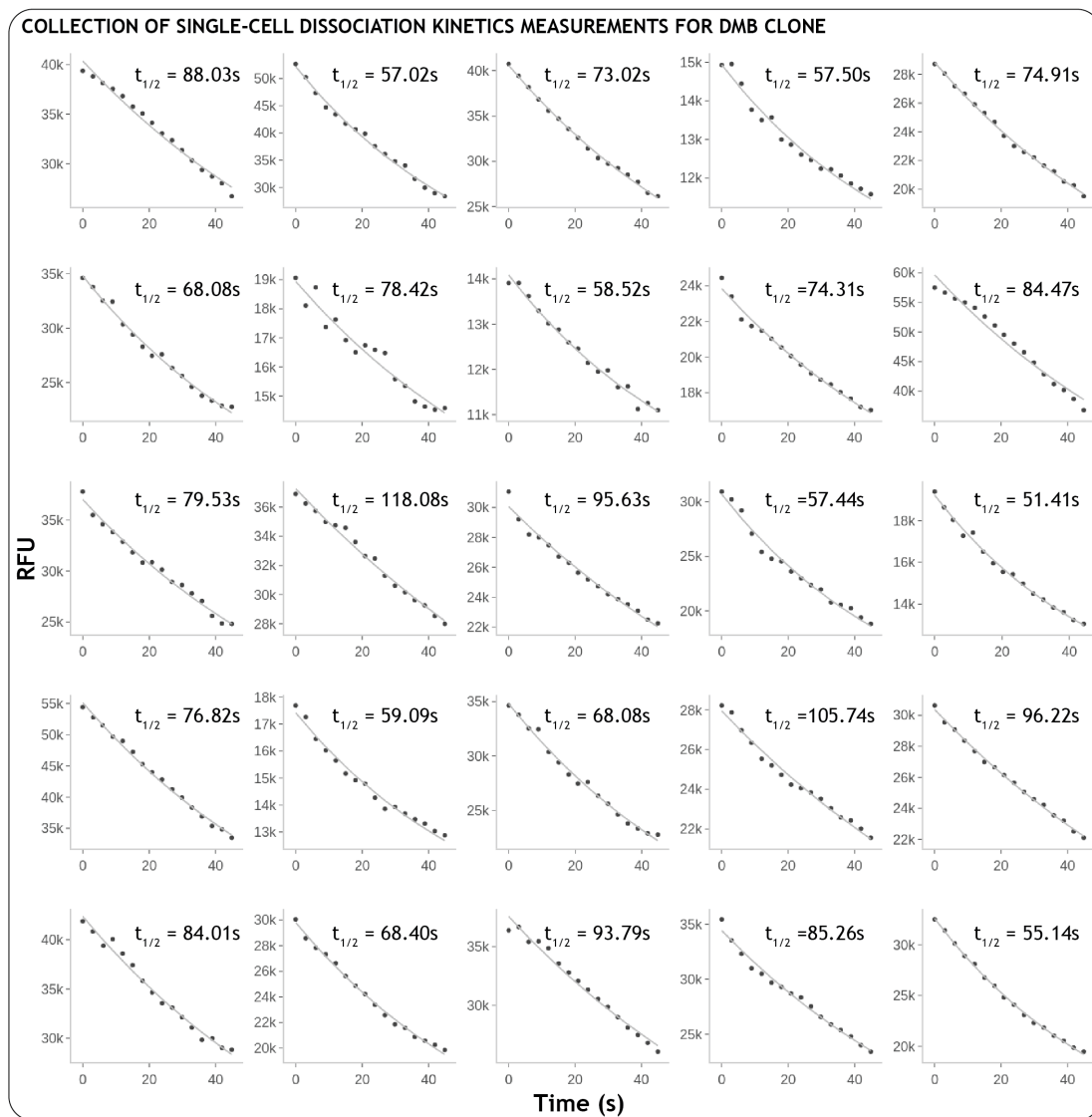
Figure 7.11: **Examples of single-cell dissociation kinetics measurements for DMβ cells**. Random selection of 25 filtered events during DMβ dissociation measurements. Data was automatically cropped to the time when the switch to monomer (PE drop) occurred.
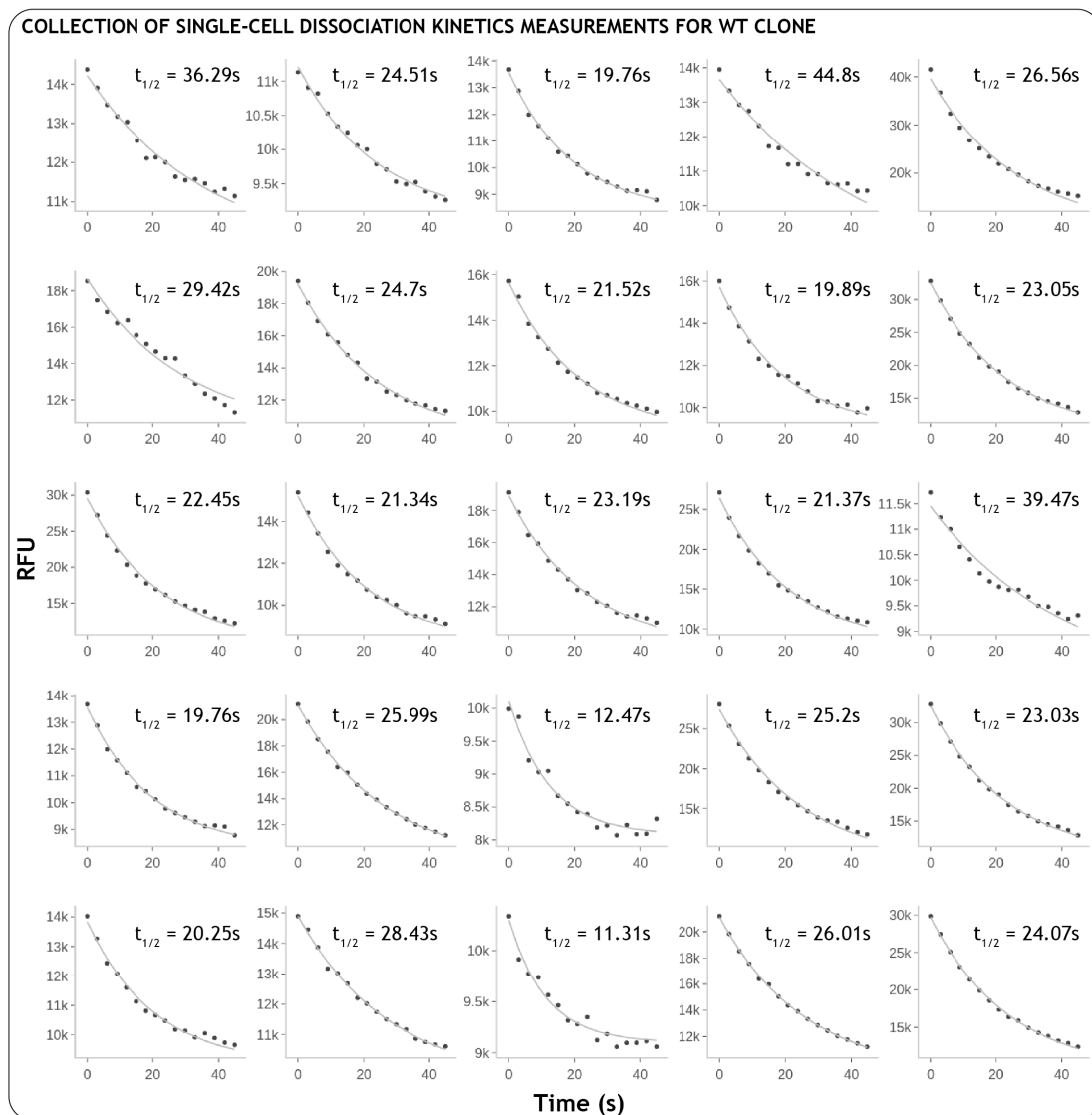
Figure 7.12: **Examples of single-cell dissociation kinetics measurements for WT cells** Random selection of 25 filtered events during WT dissociation measurements. Data was automatically cropped to the time when the switch to monomer (PE drop) occurred.
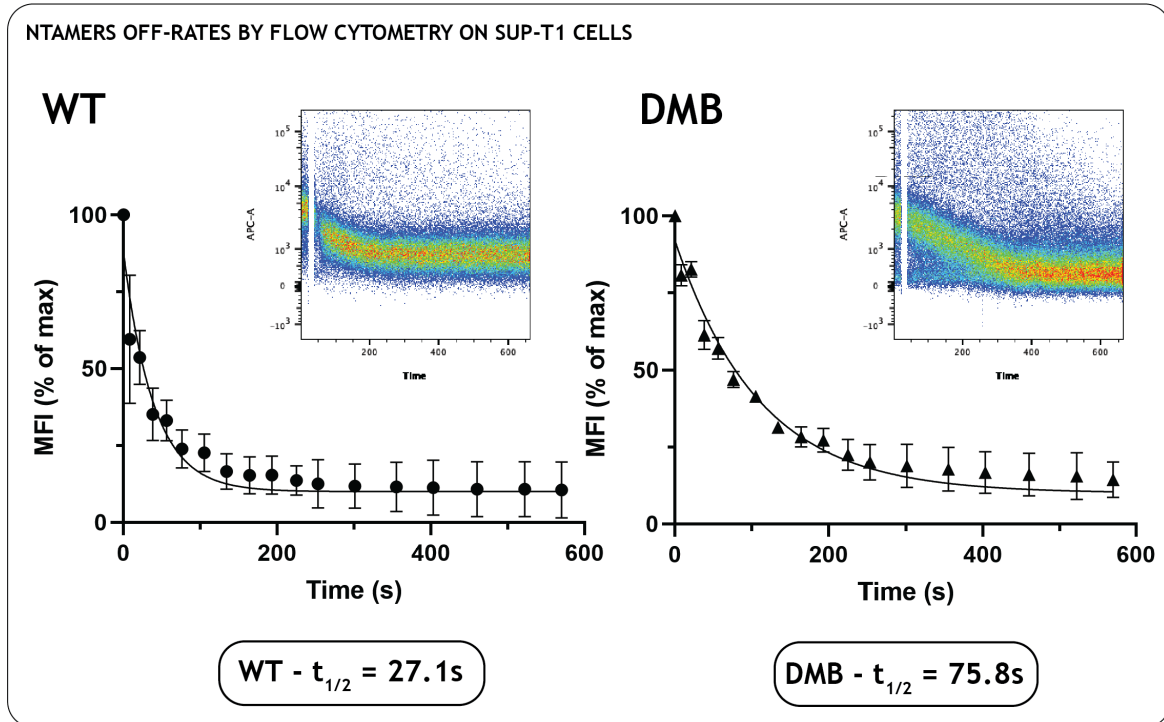
Figure 7.13: **pMHC-NTAmers dissociation rates determined by flow cytometry**.
Sup-T1 cells from same batch as the clones used during single-cell experiments on-chip were analyzed by flow cytometry for off-rates measurements. The extracted half-lives were compared with values obtained on-chip for validation. WT clones showed a half-life of dissociation of 27.1s and DMβ clones showed an average half-life of 75.8s by flow cytometry.
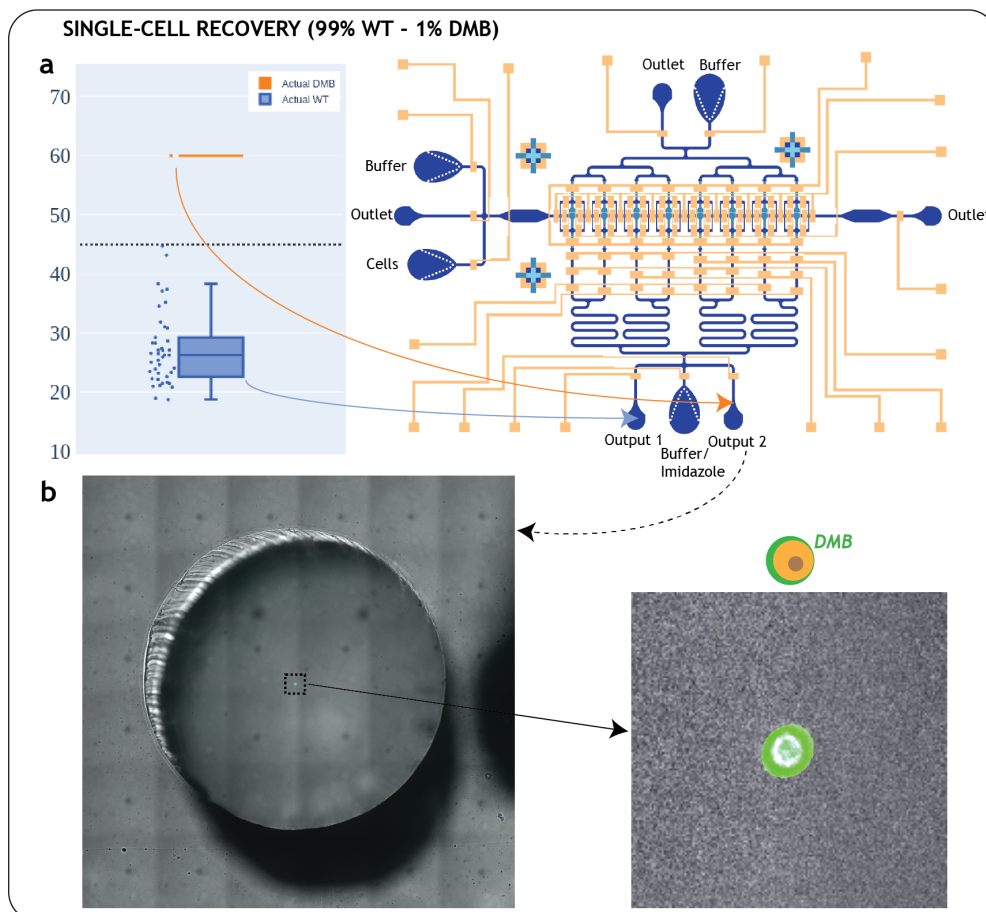
Figure 7.14: **Single-cell recovery**

a A mixed cell population (99% WT - 1%DMβ) was tagged with Calcein Blue and Calcein AM respectively and differentiated by half-life thresholding. The first cell encountered with half-life superior than 45s was pushed to Output 2. **b** Image of single recovered cell. Imaging confirmed the cell to be a DMβ clone.

Preliminary work with MAGE-A3 dextramers
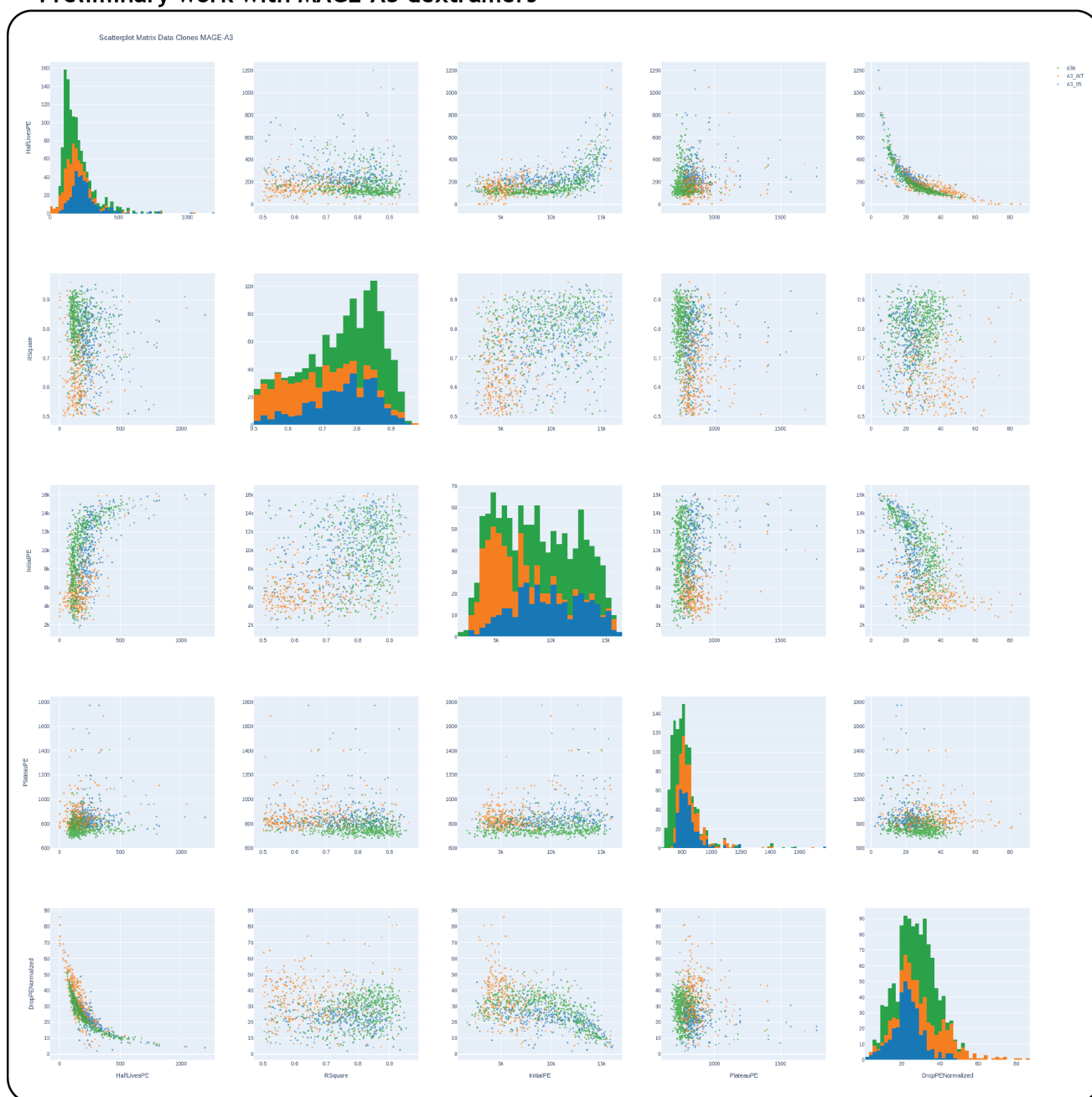
Figure 7.15: **Preliminary work with MAGE-A3 dextramers**

Scatter plot of all key parameters for dissociation kinetics for the three clones tested against the MAGE-A3 dextramers.

Bibliography

[1] G. B. Faguet, "A brief history of cancer: Age-old milestones underlying our current knowledge database," *International Journal of Cancer*, vol. 136, no. 9, pp. 2022–2036, 2015.

[2] S. I. Hajdu, "A note from history: Landmarks in history of cancer, part 1," *Cancer*, vol. 117, no. 5, pp. 1097–1102, 2011.

[3] L. Falzone, S. Salomone, and M. Libra, "Evolution of cancer pharmacological treatments at the turn of the third millennium," *Frontiers in Pharmacology*, vol. 9, no. NOV, 2018.

[4] F. Bray, J. Ferlay, I. Soerjomataram, R. L. Siegel, L. A. Torre, and A. Jemal, "Global cancer statistics 2018: GLOBOCAN estimates of incidence and mortality worldwide for 36 cancers in 185 countries," *CA: A Cancer Journal for Clinicians*, vol. 68, no. 6, pp. 394–424, 2018.

[5] D. Hanahan and R. A. Weinberg, "Hallmarks of cancer: The next generation," *Cell*, vol. 144, no. 5, pp. 646–674, 2011.

[6] R. Kim, M. Emi, and K. Tanabe, "Cancer immunoediting from immune surveillance to immune escape," *Immunology*, vol. 121, no. 1, pp. 1–14, 2007.

[7] M. D. Vesely, M. H. Kershaw, R. D. Schreiber, and M. J. Smyth, "Natural innate and adaptive immunity to cancer," *Annual Review of Immunology*, vol. 29, pp. 235–271, 2011.

[8] D. Ribatti, "The concept of immune surveillance against tumors: The first theories," *Oncotarget*, vol. 8, no. 4, pp. 7175–7180, 2017.

[9] M. J. Scanlan, A. O. Gure, A. A. Jungbluth, L. J. Old, and Y. T. Chen, "Cancer/testis antigens: An expanding family of targets for cancer immunotherapy," *Immunological Reviews*, vol. 188, no. 3, pp. 22–32, 2002.

[10] A. SUDHAKAR, "History of Cancer, Ancient and Modern Treatment Methods Akulapalli," *Journal of Cancer Science & Therapy*, vol. 1, no. 2, pp. 1–4, 2009.

[11] B. A. Chabner and T. G. Roberts, "Chemotherapy and the war on cancer," *Nature Reviews Cancer*, vol. 5, no. 1, pp. 65–72, 2005.

[12] A. M. Tsimberidou, "Targeted therapy in cancer," *Cancer Chemotherapy and Pharmacology*, vol. 76, no. 6, pp. 1113–1132, 2015.

[13] C. Köhler, G., Milstein, "Continuous cultures of fused cells secreting antibody of predefined specificity," *Nature*, vol. 256, no. Mopc 21, pp. 495–497, 1975.

[14] R. Rosell, N. Karachaliou, D. Morales-Espinosa, C. Costa, M. A. Molina, I. Sansano, A. Gasco, S. Viteri, B. Massuti, J. Wei, M. G. Cao, and A. M. Bueno, "Adaptive resistance to targeted therapies in cancer," *Translational Lung Cancer Research*, vol. 2, no. 3, pp. 152–159, 2013.

[15] F. H. Groenendijk and R. Bernards, "Drug resistance to targeted therapies: Déjà vu all over again," *Molecular Oncology*, vol. 8, no. 6, pp. 1067–1083, 2014.

[16] S. Al-Dimassi, T. Abou-Antoun, and M. El-Sibai, "Cancer cell resistance mechanisms: A mini review," *Clinical and Translational Oncology*, vol. 16, no. 6, pp. 511–516, 2014.

[17] N. Vasan, J. Baselga, and D. M. Hyman, "A view on drug resistance in cancer," *Nature*, vol. 575, no. 7782, pp. 299–309, 2019.

[18] M. Schuster, A. Nechansky, H. Loibner, and R. Kircheis, "Cancer immunotherapy," *Biotechnology Journal*, vol. 1, no. 2, pp. 138–147, 2006.

[19] S. J. Oiseth and M. S. Aziz, "Cancer immunotherapy: a brief review of the history, possibilities, and challenges ahead," *Journal of Cancer Metastasis and Treatment*, vol. 3, no. 10, p. 250, 2017.

[20] P. Dobosz and T. Dzieciątkowski, "The Intriguing History of Cancer Immunotherapy," *Frontiers in Immunology*, vol. 10, no. December, 2019.

[21] A. D. Waldman, J. M. Fritz, and M. J. Lenardo, "A guide to cancer immunotherapy: from T cell basic science to clinical practice," *Nature Reviews Immunology*, vol. 20, no. 11, pp. 651–668, 2020.

[22] K. Esfahani, L. Roudaia, N. Buhlaiga, S. V. Del Rincon, N. Papneja, and W. H. Miller, "A review of cancer immunotherapy: From the past, to the present, to the future," *Current Oncology*, vol. 27, no. S2, pp. 87–97, 2020.

[23] P. Sharma, S. Hu-Lieskovan, J. A. Wargo, and A. Ribas, "Primary, Adaptive, and Acquired Resistance to Cancer Immunotherapy," *Cell*, vol. 168, no. 4, pp. 707–723, 2017.

[24] A. Shimabukuro-Vornhagen, P. Gödel, M. Subklewe, H. J. Stemmler, H. A. Schlößer, M. Schlaak, M. Kochanek, B. Böll, and M. S. von Bergwelt-Baildon, "Cytokine release syndrome," *Journal for ImmunoTherapy of Cancer*, vol. 6, no. 1, 2018.

[25] L. Tang, Y. Zheng, M. B. Melo, L. Mabardi, A. P. Castaño, Y. Q. Xie, N. Li, S. B. Kudchodkar, H. C. Wong, E. K. Jeng, M. V. Maus, and D. J. Irvine, "Enhancing T cell therapy through TCR-signaling-responsive nanoparticle drug delivery," *Nature Biotechnology*, vol. 36, no. 8, 2018.

[26] D. L. Porter, B. L. Levine, M. Kalos, A. Bagg, and C. H. June, "Chimeric Antigen Receptor–Modified T Cells in Chronic Lymphoid Leukemia," *New England Journal of Medicine*, vol. 365, pp. 725–733, aug 2011.

[27] R. J. Brentjens, M. L. Davila, I. Riviere, J. Park, X. Wang, L. G. Cowell, S. Bartido, J. Stefanski, C. Taylor, M. Olszewska, O. Borquez-Ojeda, J. Qu, T. Wasielewska, Q. He, Y. Bernal, I. V. Rijo, C. Hedvat, R. Kobos, K. Curran, P. Steinherz, J. Jurcic, T. Rosenblat, P. Maslak, M. Frattini, and M. Sadelain, "CD19-targeted T cells rapidly induce molecular remissions in adults with chemotherapy-refractory acute lymphoblastic leukemia," *Science Translational Medicine*, vol. 5, pp. 177ra38–177ra38, mar 2013.

[28] J. H. Park, I. Rivière, M. Gonen, X. Wang, B. Sénéchal, K. J. Curran, C. Sauter, Y. Wang, B. Santomasso, E. Mead, M. Roshal, P. Maslak, M. Davila, R. J. Brentjens, and M. Sadelain, "Long-Term Follow-up of CD19 CAR Therapy in Acute Lymphoblastic Leukemia," *New England Journal of Medicine*, vol. 378, pp. 449–459, feb 2018.

[29] M. A. Fischbach, J. A. Bluestone, and W. A. Lim, "Cell-based therapeutics: The next pillar of medicine," *Science Translational Medicine*, vol. 5, apr 2013.

[30] J. N. Brudno and J. N. Kochenderfer, "Toxicities of chimeric antigen receptor T cells: Recognition and management," *Blood*, vol. 127, no. 26, pp. 3321–3330, 2016.

[31] L. A. Johnson and C. H. June, "Driving gene-engineered T cell immunotherapy of cancer," *Cell Research*, vol. 27, no. 1, pp. 38–58, 2017.

[32] M. E. Sharpe, "T-cell Immunotherapies and the Role of Nonclinical Assessment: The Balance between Efficacy and Pathology," *Toxicologic Pathology*, vol. 46, no. 2, pp. 131–146, 2018.

[33] R. B. Di Roberto, R. Castellanos-Rueda, S. Frey, D. Egli, R. Vazquez-Lombardi, E. Kapetanovic, J. Kucharczyk, and S. T. Reddy, "A Functional Screening Strategy for Engineering Chimeric Antigen Receptors with Reduced On-Target, Off-Tumor Activation," *Molecular Therapy*, vol. 28, no. 12, pp. 2564–2576, 2020.

[34] U. Sahin and Ö. Türeci, "Personalized vaccines for cancer immunotherapy," *Science*, vol. 359, pp. 1355–1360, mar 2018.

[35] J. Schmidt, P. Guillaume, D. Dojcinovic, J. Karbach, G. Coukos, and I. Luescher, "In silico and cell-based analyses reveal strong divergence between prediction and observation of T-cell-recognized tumor antigen T-cell epitopes," *Journal of Biological Chemistry*, vol. 292, pp. 11840–11849, jul 2017.

[36] E. Alspach, D. M. Lussier, A. P. Miceli, I. Kizhvatov, M. DuPage, A. M. Luoma, W. Meng, C. F. Lichti, E. Esaulova, A. N. Vomund, D. Runci, J. P. Ward, M. M. Gubin, R. F. Medrano, C. D. Arthur, J. M. White, K. C. Sheehan, A. Chen, K. W. Wucherpfennig, T. Jacks, E. R. Unanue, M. N. Artyomov, and R. D. Schreiber, "MHC-II neoantigens shape tumour immunity and response to immunotherapy," *Nature*, vol. 574, pp. 696–701, oct 2019.

[37] G. Gaud, R. Lesourne, and P. E. Love, "Regulatory mechanisms in T cell receptor signalling," *Nature Reviews Immunology*, vol. 18, no. 8, pp. 485–497, 2018.

[38] L. Klein, B. Kyewski, P. M. Allen, and K. A. Hogquist, "Positive and negative selection of the T cell repertoire: What thymocytes see (and don't see)," *Nature Reviews Immunology*, vol. 14, no. 6, pp. 377–391, 2014.

[39] Q. Qi, Y. Liu, Y. Cheng, J. Glanville, D. Zhang, J. Y. Lee, R. A. Olshen, C. M. Weyand, S. D. Boyd, and J. J. Goronzy, "Diversity and clonal selection in the human T-cell repertoire," *Proceedings of the National Academy of Sciences of the United States of America*, vol. 111, no. 36, pp. 13139–13144, 2014.

[40] P. C. de Greef, T. Oakes, B. Gerritsen, M. Ismail, J. M. Heather, R. Hermsen, B. Chain, and R. J. de Boer, "The naive t-cell receptor repertoire has an extremely broad distribution of clone sizes," *eLife*, vol. 9, pp. 1–24, 2020.

[41] M. Wieczorek, E. T. Abualrous, J. Sticht, M. Álvaro-Benito, S. Stolzenberg, F. Noé, and C. Freund, "Major histocompatibility complex (MHC) class I and MHC class II proteins: Conformational plasticity in antigen presentation," *Frontiers in Immunology*, vol. 8, no. MAR, pp. 1–16, 2017.

[42] M. A. Garstka, A. Fish, P. H. Celie, R. P. Joosten, G. M. Janssen, I. Berlin, R. Hoppes, M. Stadnik, L. Janssen, H. Ovaa, P. A. Van Veelen, A. Perrakis, and J. Neefjes, "The first step of peptide selection in antigen presentation by MHC class I molecules," *Proceedings of the National Academy of Sciences of the United States of America*, vol. 112, no. 5, pp. 1505–1510, 2015.

[43] M. G. Rudolph and I. A. Wilson, "The specificity of TCR/pMHC interaction," *Current Opinion in Immunology*, vol. 14, pp. 52–65, feb 2002.

[44] A. H. Kalergis, N. Boucheron, M. A. Doucey, E. Palmieri, E. C. Goyarts, Z. Vegh, I. F. Luescher, and S. G. Nathenson, "Efficient T cell activation requires an optimal dwell-time of interaction between the TCR and the pMHC complex," *Nature Immunology*, vol. 2, pp. 229–234, mar 2001.

[45] L. J. Carreño, P. A. González, and A. M. Kalergis, "Modulation of T cell function by TCR/pMHC binding kinetics," *Immunobiology*, vol. 211, pp. 47–64, feb 2006.

[46] J. D. Stone, A. S. Chervin, and D. M. Kranz, "T-cell receptor binding affinities and kinetics: impact on T-cell activity and specificity," *Immunology*, vol. 126, no. 2, pp. 165–176, 2009.

[47] J. Huang, V. I. Zarnitsyna, B. Liu, L. J. Edwards, N. Jiang, B. D. Evavold, and C. Zhu, "The kinetics of two-dimensional TCR and pMHC interactions determine T-cell responsiveness," *Nature*, vol. 464, pp. 932–936, apr 2010.

[48] P. G. Coulie, B. J. Van Den Eynde, P. Van Der Bruggen, and T. Boon, "Tumour antigens recognized by T lymphocytes: At the core of cancer immunotherapy," *Nature Reviews Cancer*, vol. 14, no. 2, pp. 135–146, 2014.

[49] M. M. Hoffmann and J. E. Slansky, "T-cell receptor affinity in the age of cancer immunotherapy," *Molecular Carcinogenesis*, vol. 59, pp. 862–870, jul 2020.

[50] A. V. Joglekar and G. Li, "T cell antigen discovery," *Nature Methods*, vol. 18, no. 8, pp. 873–880, 2021.

[51] M. E. Birnbaum, J. L. Mendoza, D. K. Sethi, S. Dong, J. Glanville, J. Dobbins, E. Özkan, M. M. Davis, K. W. Wucherpfennig, and K. C. Garcia, "Deconstructing the peptide-MHC specificity of t cell recognition," *Cell*, vol. 157, no. 5, pp. 1073–1087, 2014.

[52] J. D. Altman, P. A. Moss, P. J. Goulder, D. H. Barouch, M. G. McHeyzer-Williams, J. I. Bell, A. J. McMichael, and M. M. Davis, "Phenotypic analysis of antigen-specific T lymphocytes," *Science*, vol. 274, no. 5284, pp. 94–96, 1996.

[53] P. Batard, D. A. Peterson, E. Devêvre, P. Guillaume, J. C. Cerottini, D. Rimoldi, D. E. Speiser, L. Winther, and P. Romero, "Dextramers: New generation of fluorescent MHC class I/peptide multimers for visualization of antigen-specific CD8+ T cells," *Journal of Immunological Methods*, vol. 310, pp. 136–148, mar 2006.

[54] M. T. Bethune, B. Comin-Anduix, Y.-H. H. Fu, A. Ribas, and D. Baltimore, "Preparation of peptide–MHC and T-cell receptor dextramers by biotinylated dextran doping," *BioTechniques*, vol. 62, pp. 123–130, mar 2017.

[55] A. K. Bentzen and S. R. Hadrup, "Evolution of MHC-based technologies used for detection of antigen-responsive T cells," *Cancer Immunology, Immunotherapy*, vol. 66, no. 5, pp. 657–666, 2017.

[56] P. D. Holler and D. M. Kranz, "Quantitative analysis of the contribution of TCR/pepMHC affinity and CD8 to T cell activation," *Immunity*, vol. 18, no. 2, pp. 255–264, 2003.

[57] J. D. Stone, W. E. Demkowicz, and L. J. Stern, "HLA-restricted epitope identification and detection of functional T cell responses by using MHC-peptide and costimulatory microarrays," *Proceedings of the National Academy of Sciences of the United States of America*, vol. 102, no. 10, pp. 3744–3749, 2005.

[58] M. Hebeisen, M. Allard, P. O. Gannon, J. Schmidt, D. E. Speiser, and N. Rufer, "Identifying individual T cell receptors of optimal avidity for tumor antigens," *Frontiers in Immunology*, vol. 6, no. NOV, 2015.

[59] M. P. Tan, A. B. Gerry, J. E. Brewer, L. Melchiori, J. S. Bridgeman, A. D. Bennett, N. J. Pumphrey, B. K. Jakobsen, D. A. Price, K. Ladell, and A. K. Sewell, "T cell receptor binding affinity governs the functional profile of cancer-specific CD8 ¡sup¿+¡/sup¿ T cells," *Clinical & Experimental Immunology*, vol. 180, no. 2, pp. 255–270, 2015.

[60] M. Allard, B. Couturaud, L. Carretero-Iglesia, M. N. Duong, J. Schmidt, G. C. Monnot, P. Romero, D. E. Speiser, M. Hebeisen, and N. Rufer, "TCR-ligand dissociation rate is a robust and stable biomarker of CD8+ T cell potency," *JCI Insight*, vol. 2, jul 2017.

[61] M. Knabel, T. J. Franz, M. Schiemann, A. Wulf, B. Villmow, B. Schmidt, H. Bernhard, H. Wagner, and D. H. Busch, "Reversible MHC multimer staining for functional isolation of T-cell populations and effective adoptive transfer," *Nature Medicine*, vol. 8, no. 6, pp. 631–637, 2002.

[62] J. Schmidt, P. Guillaume, M. Irving, P. Baumgaertner, D. Speiser, and I. F. Luescher, "Reversible major histocompatibility complex I-peptide multimers containing Ni 2+-nitrilotriacetic acid peptides and histidine tags improve analysis and sorting of CD8 + T cells," *Journal of Biological Chemistry*, vol. 286, pp. 41723–41735, dec 2011.

[63] J. Schmidt, D. Dojcinovic, P. Guillaume, and I. Luescher, "Analysis, isolation, and activation of antigen-specific CD4+ and CD8+ T cells by soluble MHC-peptide complexes," *Frontiers in Immunology*, vol. 4, no. JUL, pp. 1–14, 2013.

[64] F. C. Jammes and S. J. Maerkl, "How single-cell immunology is benefiting from microfluidic technologies," *Microsystems and Nanoengineering*, vol. 6, no. 1, 2020.

[65] A. T. Woolley and R. A. Mathies, "Ultra-high-speed DNA fragment separations using microfabricated capillary array electrophoresis chips," *Proceedings of the National Academy of Sciences of the United States of America*, vol. 91, no. 24, pp. 11348–11352, 1994.

[66] G. M. Whitesides, "The origins and the future of microfluidics," *Nature*, vol. 442, pp. 368–373, jul 2006.

[67] G. J. Sommer, D. S. Chang, A. Jain, S. M. Langelier, J. Park, M. Rhee, W. Fang, R. Zeitoun, and M. Burns, "Introduction to Microfluidics," 2009.

[68] D. T. Chiu, A. J. DeMello, D. Di Carlo, P. S. Doyle, C. Hansen, R. M. Maceiczyk, and R. C. Wootton, "Small but Perfectly Formed? Successes, Challenges, and Opportunities for Microfluidics in the Chemical and Biological Sciences," *Chem*, vol. 2, no. 2, pp. 201–223, 2017.

[69] N. Convery and N. Gadegaard, "30 years of microfluidics," *Micro and Nano Engineering*, vol. 2, pp. 76–91, mar 2019.

[70] J. C. McDonald, D. C. Duffy, J. R. Anderson, D. T. Chiu, H. Wu, O. J. Schueller, and G. M. Whitesides, "Fabrication of microfluidic systems in poly(dimethylsiloxane)," *Electrophoresis*, vol. 21, no. 1, pp. 27–40, 2000.

[71] D. B. Weibel, W. R. DiLuzio, and G. M. Whitesides, "Microfabrication meets microbiology," *Nature Reviews Microbiology*, vol. 5, no. 3, pp. 209–218, 2007.

[72] E. Fung, L. Esposito, J. A. Todd, and L. S. Wicker, "Multiplexed immunophenotyping of human antigen-presenting cells in whole blood by polychromatic flow cytometry," *Nature Protocols*, vol. 5, no. 2, pp. 357–370, 2010.

[73] M. Doan, I. Vorobjev, P. Rees, A. Filby, O. Wolkenhauer, A. E. Goldfeld, J. Lieberman, N. Barteneva, A. E. Carpenter, and H. Hennig, "Diagnostic Potential of Imaging Flow Cytometry," *Trends in Biotechnology*, vol. 36, no. 7, pp. 649–652, 2018.

[74] P. K. Chattopadhyay, T. M. Gierahn, M. Roederer, and J. C. Love, "Single-cell technologies for monitoring immune systems," *Nat Immunol*, vol. 15, no. 2, pp. 128–135, 2014.

[75] D. R. Gossett, W. M. Weaver, A. J. MacH, S. C. Hur, H. T. K. Tse, W. Lee, H. Amini, and D. Di Carlo, "Label-free cell separation and sorting in microfluidic systems," *Analytical and Bioanalytical Chemistry*, vol. 397, no. 8, pp. 3249–3267, 2010.

[76] H. Miao Ji, V. Samper, Y. Chen, C. Kiat Heng, T. Meng Lim, and L. Yobas, "Silicon-based microfilters for whole blood cell separation," *Biomedical Microdevices*, vol. 10, no. 2, pp. 251–257, 2008.

[77] X. Jiang, K. H. K. Wong, A. H. Khankhel, M. Zeinali, E. Reategui, M. J. Phillips, X. Luo, N. Aceto, F. Fachin, A. N. Hoang, W. Kim, A. E. Jensen, L. V. Sequist, S. Maheswaran, D. A. Haber, S. L. Stott, and M. Toner, "Microfluidic isolation of platelet-covered circulating tumor cells," *Lab on a Chip*, vol. 17, no. 20, pp. 3498–3503, 2017.

[78] A. F. Sarioglu, N. Aceto, N. Kojic, M. C. Donaldson, M. Zeinali, B. Hamza, A. Engstrom, H. Zhu, T. K. Sundaresan, D. T. Miyamoto, X. Luo, A. Bardia, B. S. Wittner, S. Ramaswamy, T. Shioda, D. T. Ting, S. L. Stott, R. Kapur, S. Maheswaran, D. A. Haber, and M. Toner, "A microfluidic device for label-free, physical capture of circulating tumor cell clusters," *Nature Methods*, 2015.

[79] A. Tripathi, J. Riddell Iv, and N. Chronis, "A Biochip with a 3D microfluidic architecture for trapping white blood cells," *Sensors and Actuators B*, vol. 186, pp. 244–251, 2013.

[80] A. Mohd Noor, T. Masuda, W. Lei, K. Horio, Y. Miyata, M. Namatame, Y. Hayase, T. I. Saito, and F. Arai, "A microfluidic chip for capturing, imaging and counting CD3+ T-lymphocytes and CD19+ B-lymphocytes from whole blood," *Sensors and Actuators, B: Chemical*, vol. 276, no. August, pp. 107–113, 2018.

[81] B. Turan, T. Masuda, W. Lei, A. M. Noor, K. Horio, T. I. Saito, Y. Miyata, and F. Arai, "A pillar-based microfluidic chip for T-cells and B-cells isolation and detection with machine learning algorithm," *ROBOMECH Journal*, vol. 5, p. 27, 2018.

[82] M. Yamada, M. Nakashima, and M. Seki, "Pinched flow fractionation: Continuous size separation of particles utilizing a laminar flow profile in a pinched microchannel," *Analytical Chemistry*, vol. 76, no. 18, pp. 5465–5471, 2004.

[83] A. Karimi, S. Yazdi, and A. M. Ardekani, "Hydrodynamic mechanisms of cell and particle trapping in microfluidic," *Biomicrofluidics*, vol. 7, p. 21501, apr 2013.

[84] M. Yamada and M. Seki, "Hydrodynamic filtration for on-chip particle concentration and classification utilizing microfluidics," *Lab on a Chip*, vol. 5, no. 11, p. 1233, 2005.

[85] J. Takagi, M. Yamada, M. Yasuda, and M. Seki, "Continuous particle separation in a microchannel having asymmetrically arranged multiple branches," *Lab on a Chip*, vol. 5, no. 7, pp. 778–784, 2005.

[86] Siyang Zheng, Yu-Chong Tai, and H. Kasdan, "A Micro Device for Separation of Erythrocytes and Leukocytes in Human Blood," in *2005 IEEE Engineering in Medicine and Biology 27th Annual Conference*, pp. 1024–1027, IEEE, 2005.

[87] J. A. Davis, D. W. Inglis, K. J. Morton, D. A. Lawrence, L. R. Huang, S. Y. Chou, J. C. Sturm, and R. H. Austin, "Deterministic hydrodynamics: Taking blood apart," *Proceedings of the National Academy of Sciences of the United States of America*, vol. 103, no. 40, pp. 14779–14784, 2006.

[88] J. Nilsson, M. Evander, B. Hammarström, and T. Laurell, "Review of cell and particle trapping in microfluidic systems," *Analytica Chimica Acta*, vol. 649, pp. 141–157, 2009.

[89] V. Lecault, A. K. White, A. Singhal, and C. L. Hansen, "Microfluidic single cell analysis: From promise to practice," *Current Opinion in Chemical Biology*, vol. 16, no. 3-4, pp. 381–390, 2012.

[90] W. M. Weaver, P. Tseng, A. Kunze, M. Masaeli, A. J. Chung, J. S. Dudani, H. Kittur, R. P. Kulkarni, and D. Di Carlo, "Advances in high-throughput single-cell microtechnologies," *Current Opinion in Biotechnology*, vol. 25, pp. 114–123, 2014.

[91] A. Reece, B. Xia, Z. Jiang, B. Noren, R. McBride, and J. Oakey, "Microfluidic techniques for high throughput single cell analysis," *Current Opinion in Biotechnology*, vol. 40, pp. 90–96, aug 2016.

[92] Q. Huang, S. Mao, M. Khan, and J. M. Lin, "Single-cell assay on microfluidic devices," *Analyst*, vol. 144, no. 3, pp. 808–823, 2019.

[93] W. Wei, Y. S. Shin, C. Ma, J. Wang, M. Elitas, R. Fan, and J. R. Heath, "Microchip platforms for multiplex single-cell functional proteomics with applications to immunology and cancer research," *Genome Medicine*, vol. 5, no. 8, 2013.

[94] S. Baratchi, K. Khoshmanesh, C. Sacristán, D. Depoil, D. Wlodkowic, P. McIntyre, and A. Mitchell, "Immunology on chip: Promises and opportunities," *Biotechnology Advances*, vol. 32, no. 2, pp. 333–346, 2014.

[95] M. Junkin and S. Tay, "Microfluidic single-cell analysis for systems immunology," *Lab on a Chip*, vol. 14, no. 7, pp. 1246–1260, 2014.

[96] Y. F. S. Seah, H. Hu, and C. A. Merten, "Microfluidic single-cell technology in immunology and antibody screening," *Molecular Aspects of Medicine*, vol. 59, pp. 47–61, 2018.

[97] N. Sinha, N. Subedi, and J. Tel, "Integrating immunology and microfluidics for single immune cell analysis," *Frontiers in Immunology*, vol. 9, no. OCT, pp. 1–16, 2018.

[98] J. R. Rettig and A. Folch, "Large-Scale Single-Cell Trapping And Imaging Using Microwell Arrays," *Analytical Chemistry*, vol. 77, no. 17, pp. 5628–5634, 2005.

[99] D. Di Carlo, L. Y. Wu, and L. P. Lee, "Dynamic single cell culture array," *Lab on a chip*, vol. 6, pp. 1445–9, nov 2006.

[100] S. L. Faley, M. Copland, D. Wlodkowic, W. Kolch, K. T. Seale, J. P. Wikswo, and J. M. Cooper, "Microfluidic single cell arrays to interrogate signalling dynamics of individual, patient-derived hematopoietic stem cells," *Lab on a Chip*, vol. 9, no. 18, pp. 2659–2664, 2009.

[101] H. Chen, F. Ye, and G. Guo, "Revolutionizing immunology with single-cell RNA sequencing," *Cellular and Molecular Immunology*, vol. 16, pp. 242–249, mar 2019.

[102] Y. Gong, A. O. Ogunniyi, and J. C. Love, "Massively parallel detection of gene expression in single cells using subnanolitre wells," *Lab on a Chip*, vol. 10, no. 18, pp. 2334–2337, 2010.

[103] B. J. Dekosky, G. C. Ippolito, R. P. Deschner, J. J. Lavinder, Y. Wine, B. M. Rawlings, N. Varadarajan, C. Giesecke, T. Dörner, S. F. Andrews, P. C. Wilson, S. P. Hunicke-Smith, C. G. Willson, A. D. Ellington, and G. Georgiou, "High-throughput sequencing of the paired

human immunoglobulin heavy and light chain repertoire," *Nature Biotechnology*, vol. 31, pp. 166–9, feb 2013.

[104] J. Yuan and P. A. Sims, "An Automated Microwell Platform for Large-Scale Single Cell RNA-Seq," *Scientific Reports*, vol. 6, 2016.

[105] R. J. Kimmerling, G. Lee Szeto, J. W. Li, A. S. Genshaft, S. W. Kazer, K. R. Payer, J. de Riba Borrajo, P. C. Blainey, D. J. Irvine, A. K. Shalek, and S. R. Manalis, "A microfluidic platform enabling single-cell RNA-seq of multigenerational lineages," *Nature Communications*, vol. 7, p. 10220, jan 2016.

[106] Q. Han, E. M. Bradshaw, B. Nilsson, D. A. Hafler, and J. C. Love, "Multidimensional analysis of the frequencies and rates of cytokine secretion from single cells by quantitative microengraving," *Lab on a Chip*, vol. 10, no. 11, pp. 1391–1400, 2010.

[107] Q. Han, N. Bagheri, E. M. Bradshaw, D. A. Hafler, D. A. Lauffenburger, and J. C. Love, "Polyfunctional responses by human T cells result from sequential release of cytokines," *Proceedings of the National Academy of Sciences*, vol. 109, pp. 1607–1612, jan 2011.

[108] Y. J. Yamanaka, G. L. Szeto, T. M. Gierahn, T. L. Forcier, K. F. Benedict, M. S. Brefo, D. A. Lauffenburger, D. J. Irvine, and J. C. Love, "Cellular barcodes for efficiently profiling single-cell secretory responses by microengraving," *Analytical Chemistry*, vol. 84, no. 24, pp. 10531–10536, 2012.

[109] N. Varadarajan, D. S. Kwon, K. M. Law, A. O. Ogunniyi, M. N. Anahtar, J. M. Richter, B. D. Walker, and J. C. Love, "Rapid, efficient functional characterization and recovery of HIV-specific human CD8 + T cells using microengraving," *Proceedings of the National Academy of Sciences of the United States of America*, vol. 109, pp. 3885–3890, mar 2012.

[110] A. J. Torres, R. L. Contento, S. Gordo, K. W. Wucherpfennig Cd, J. C. Love, K. W. Wucherpfennig, and J. C. Love, "Functional single-cell analysis of T-cell activation by supported lipid bilayer-tethered ligands on arrays of nanowells," *Lab Chip*, vol. 13, no. 1, 2013.

[111] J. C. Love, J. L. Ronan, G. M. Grotenbreg, A. G. van der Veen, and H. L. Ploegh, "A microengraving method for rapid selection of single cells producing antigen-specific antibodies," *Nature Biotechnology*, vol. 24, pp. 703–707, jun 2006.

[112] C. M. Story, E. Papa, C. C. A. Hu, J. L. Ronan, K. Herlihy, H. L. Ploegh, and J. C. Love, "Profiling antibody responses by multiparametric analysis of primary B cells," *Proceedings of the National Academy of Sciences of the United States of America*, vol. 105, pp. 17902–17907, nov 2008.

[113] A. O. Ogunniyi, C. M. Story, E. Papa, E. Guillen, and J. C. Love, "Screening individual hybridomas by microengraving to discover monoclonal antibodies," *Nature Protocols*, vol. 4, no. 5, pp. 767–782, 2009.

[114] A. Jin, T. Ozawa, K. Tajiri, T. Obata, S. Kondo, K. Kinoshita, S. Kadowaki, K. Takahashi, T. Sugiyama, H. Kishi, and A. Muraguchi, "A rapid and efficient single-cell manipulation method for screening antigen-specific antibody-secreting cells from human peripheral blood," *Nature Medicine*, vol. 15, no. 9, pp. 1088–1092, 2009.

[115] Y. Lu, Q. Xue, M. R. Eisele, E. S. Sulistijo, K. Brower, L. Han, E. A. D. Amir, D. Pe'er, K. Miller-Jensen, and R. Fan, "Highly multiplexed profiling of single-cell effector functions reveals deep functional heterogeneity in response to pathogenic ligands," *Proceedings of the National Academy of Sciences of the United States of America*, vol. 112, no. 7, pp. E607–E615, 2015.

[116] I. Zaretsky, M. Polonsky, E. Shifrut, S. Reich-Zeliger, Y. Antebi, G. Aidelberg, N. Waysbort, and N. Friedman, "Monitoring the dynamics of primary T cell activation and differentiation using long term live cell imaging in microwell arrays," *Lab on a Chip*, vol. 12, pp. 5007–5015, dec 2012.

[117] B. Dura, Y. Liu, and J. Voldman, "Deformability-based microfluidic cell pairing and fusion," *Lab on a Chip*, vol. 14, pp. 2783–2790, aug 2014.

[118] B. Dura, S. K. Dougan, M. Barisa, M. M. Hoehl, C. T. Lo, H. L. Ploegh, and J. Voldman, "Profiling lymphocyte interactions at the single-cell level by microfluidic cell pairing," *Nature Communications*, vol. 6, no. 1, pp. 1–13, 2015.

[119] M. M. Hoehl, S. K. Dougan, H. L. Ploegh, and J. Voldman, "Massively parallel microfluidic cell-pairing platform for the statistical study of immunological cell-cell interactions," in *15th International Conference on Miniaturized Systems for Chemistry and Life Sciences 2011, MicroTAS 2011*, vol. 3, pp. 1508–1510, Chemical and Biological Microsystems Society, 2011.

[120] B. Dura, M. M. Servo, R. M. Barry, H. L. Ploeghf, S. K. Dougand, and J. Voldman, "Longitudinal multiparameter assay of lymphocyte interactions from onset by microfluidic cell pairing and culture," *Proceedings of the National Academy of Sciences of the United States of America*, vol. 113, pp. E3599–E3608, jun 2016.

[121] F. Lin and E. C. Butcher, "T cell chemotaxis in a simple microfluidic device," *Lab on a Chip*, vol. 6, no. 11, pp. 1462–1469, 2006.

[122] N. G. Jain, E. A. Wong, A. J. Aranyosi, L. Boneschansker, J. F. Markmann, D. M. Briscoe, and D. Irimia, "Microfluidic mazes to characterize T-cell exploration patterns following activation in vitro," *Integrative Biology (United Kingdom)*, vol. 7, no. 11, pp. 1423–1431, 2015.

[123] E. Agliari, E. Biselli, A. De Ninno, G. Schiavoni, L. Gabriele, A. Gerardino, F. Mattei, A. Barra, and L. Businaro, "Cancer-driven dynamics of immune cells in a microfluidic environment," *Scientific Reports*, vol. 4, pp. 11–13, 2014.

[124] A. Boussommier-Calleja, R. Li, M. B. Chen, S. C. Wong, and R. D. Kamm, "Microfluidics: A New Tool for Modeling Cancer–Immune Interactions," *Trends in Cancer*, vol. 2, no. 1, pp. 6–19, 2016.

[125] A. Pavesi, A. T. Tan, S. Koh, A. Chia, M. Colombo, E. Antonecchia, C. Miccolis, E. Ceccarello, G. Adriani, M. T. Raimondi, R. D. Kamm, and A. Bertoletti, "A 3D microfluidic model for preclinical evaluation of TCR-engineered T cells against solid tumors," *JCI insight*, vol. 2, jun 2017.

[126] S. Parlato, A. De Ninno, R. Molfetta, E. Toschi, D. Salerno, A. Mencattini, G. Romagnoli, A. Fragale, L. Roccazzello, M. Buoncervello, I. Canini, E. Bentivegna, M. Falchi, F. R. Bertani, A. Gerardino, E. Martinelli, C. Natale, R. Paolini, L. Businaro, and L. Gabriele, "3D Microfluidic model for evaluating immunotherapy efficacy by tracking dendritic cell behaviour toward tumor cells," *Scientific Reports*, vol. 7, dec 2017.

[127] M. A. Unger, "Monolithic Microfabricated Valves and Pumps by Multilayer Soft Lithography," *Science*, vol. 288, pp. 113–116, apr 2000.

[128] T. Thorsen, S. J. Maerkl, and S. R. Quake, "Microfluidic Large-Scale Integration," *Science*, vol. 298, pp. 580–4, oct 2002.

[129] J. S. Marcus, W. F. Anderson, and S. R. Quake, "Microfluidic single-cell mRNA isolation and analysis," *Analytical Chemistry*, vol. 78, pp. 3084–3089, may 2006.

[130] N. Bontoux, L. Dauphinot, T. Vitalis, V. Studer, Y. Chen, J. Rossier, and M. C. Potier, "Integrating whole transcriptome assays on a lab-on-a-chip for single cell gene profiling," *Lab on a Chip*, vol. 8, no. 3, pp. 443–450, 2008.

[131] J. F. Zhong, Y. Chen, J. S. Marcus, A. Scherer, S. R. Quake, C. R. Taylor, and L. P. Weiner, "A microfluidic processor for gene expression profiling of single human embryonic stem cells," *Lab on a Chip*, vol. 8, no. 1, pp. 68–74, 2007.

[132] N. M. Toriello, E. S. Douglas, N. Thaitrong, S. C. Hsiao, M. B. Francis, C. R. Bertozzi, and R. A. Mathies, "Integrated microfluidic bioprocessor for single-cell gene expression analysis," *Proceedings of the National Academy of Sciences of the United States of America*, vol. 105, no. 51, pp. 20173–20178, 2008.

[133] A. K. White, M. Vaninsberghe, O. I. Petriv, M. Hamidi, D. Sikorski, M. A. Marra, J. Piret, S. Aparicio, and C. L. Hansen, "High-throughput microfluidic single-cell RT-qPCR," *Proceedings of the National Academy of Sciences of the United States of America*, vol. 108, pp. 13999–14004, aug 2011.

[134] C. Ma, R. Fan, H. Ahmad, Q. Shi, B. Comin-Anduix, T. Chodon, R. C. Koya, C.-C. C. Liu, G. A. Kwong, C. G. Radu, A. Ribas, and J. R. Heath, "A clinical microchip for evaluation of single immune cells reveals high functional heterogeneity in phenotypically similar T cells," *Nature Medicine*, vol. 17, pp. 738–743, jun 2011.

[135] A. Singhal, C. A. Haynes, and C. L. Hansen, "Microfluidic measurement of antibody-antigen binding kinetics from low-abundance samples and single cells," *Analytical Chemistry*, vol. 82, pp. 8671–8679, oct 2010.

[136] M. Junkin, A. J. Kaestli, Z. Cheng, C. Jordi, C. Albayrak, A. Hoffmann, and S. Tay, "High-Content Quantification of Single-Cell Immune Dynamics," *Cell Reports*, vol. 15, pp. 411–422, apr 2016.

[137] A. J. Kaestli, M. Junkin, and S. Tay, "Integrated platform for cell culture and dynamic quantification of cell secretion," *Lab on a Chip*, vol. 17, no. 23, pp. 4124–4133, 2017.

[138] S. J. Maerkl and S. R. Quake, "A systems approach to measuring the binding energy landscapes of transcription factors," *Science*, vol. 315, no. 5809, pp. 233–237, 2007.

[139] M. Geertz, D. Shore, and S. J. Maerkl, "Massively parallel measurements of molecular interaction kinetics on a microfluidic platform," *Proceedings of the National Academy of Sciences of the United States of America*, vol. 109, pp. 16540–16545, oct 2012.

[140] J. L. Garcia-Cordero, C. Nembrini, A. Stano, J. A. Hubbell, and S. J. Maerkl, "A high-throughput nanoimmunoassay chip applied to large-scale vaccine adjuvant screening," *Integrative Biology (United Kingdom)*, vol. 5, no. 4, pp. 650–658, 2013.

[141] F. Volpetti, J. Garcia-Cordero, and S. J. Maerkl, "A microfluidic platform for high-throughput multiplexed protein quantitation," *PLoS ONE*, vol. 10, feb 2015.

[142] J. L. Garcia-Cordero and S. J. Maerkl, "Multiplexed surface micropatterning of proteins with a pressure-modulated microfluidic button-membrane," *Chemical Communications*, vol. 49, no. 13, pp. 1264–1266, 2013.

[143] M. Mehling, T. Frank, C. Albayrak, and S. Tay, "Real-time tracking, retrieval and gene expression analysis of migrating human T cells," *Lab on a Chip*, vol. 15, no. 5, pp. 1276–1283, 2015.

[144] J. Schwarz, V. Bierbaum, J. Merrin, T. Frank, R. Hauschild, T. Bollenbach, S. Tay, M. Sixt, and M. Mehling, "A microfluidic device for measuring cell migration towards substrate-bound and soluble chemokine gradients," *Scientific Reports*, vol. 6, nov 2016.

[145] T. Thorsen, R. W. Roberts, F. H. Arnold, and S. R. Quake, "Dynamic Pattern Formation in a Vesicle-Generating Microfluidic Device," *Physical Review Letters*, vol. 86, pp. 4163–4166, apr 2001.

[146] A. Rakszewska, J. Tel, V. Chokkalingam, and W. T. S. Huck, "One drop at a time: toward droplet microfluidics as a versatile tool for single-cell analysis," *NPG Asia Materials*, vol. 6, jan 2014.

[147] T. P. Lagus and J. F. Edd, "A review of the theory, methods and recent applications of high-throughput single-cell droplet microfluidics," *Journal of Physics D: Applied Physics*, 2013.

[148] N. Wen, Z. Zhao, B. Fan, D. Chen, D. Men, J. Wang, and J. Chen, "Development of droplet microfluidics enabling high-throughput single-cell analysis," *Molecules*, vol. 21, no. 7, pp. 1–13, 2016.

[149] F. Tang, C. Barbacioru, Y. Wang, E. Nordman, C. Lee, N. Xu, X. Wang, J. Bodeau, B. B. Tuch, A. Siddiqui, K. Lao, and M. A. Surani, "mRNA-Seq whole-transcriptome analysis of a single cell," *Nature Methods*, vol. 6, no. 5, pp. 377–382, 2009.

[150] A. M. Klein, L. Mazutis, I. Akartuna, N. Tallapragada, A. Veres, V. Li, L. Peshkin, D. A. Weitz, and M. W. Kirschner, "Droplet barcoding for single-cell transcriptomics applied to embryonic stem cells.," *Cell*, vol. 161, no. 5, pp. 1187–1201, 2015.

[151] E. Z. Macosko, A. Basu, R. Satija, J. Nemesh, K. Shekhar, M. Goldman, I. Tirosh, A. R. Bialas, N. Kamitaki, E. M. Martersteck, J. J. Trombetta, D. A. Weitz, J. R. Sanes, A. K. Shalek, A. Regev, and S. A. McCarroll, "Highly parallel genome-wide expression profiling of individual cells using nanoliter droplets," *Cell*, vol. 161, pp. 1202–1214, may 2015.

[152] G. X. Zheng, J. M. Terry, P. Belgrader, P. Ryvkin, Z. W. Bent, R. Wilson, S. B. Ziraldo, T. D. Wheeler, G. P. McDermott, J. Zhu, M. T. Gregory, J. Shuga, L. Montesclaros, J. G. Underwood, D. A. Masquelier, S. Y. Nishimura, M. Schnall-Levin, P. W. Wyatt, C. M. Hindson, R. Bharadwaj, A. Wong, K. D. Ness, L. W. Beppu, H. J. Deeg, C. McFarland, K. R. Loeb, W. J. Valente, N. G. Ericson, E. A. Stevens, J. P. Radich, T. S. Mikkelsen, B. J. Hindson, and J. H. Bielas, "Massively parallel digital transcriptional profiling of single cells," *Nature Communications*, vol. 8, jan 2017.

[153] X. Zhang, T. Li, F. Liu, Y. Chen, J. Yao, Z. Li, Y. Huang, and J. Wang, "Comparative Analysis of Droplet-Based Ultra-High-Throughput Single-Cell RNA-Seq Systems," *Molecular Cell*, vol. 73, pp. 130–142.e5, jan 2019.

[154] J. R. Mcdaniel, B. J. DeKosky, H. Tanno, A. D. Ellington, and G. Georgiou, "Ultra-high-throughput sequencing of the immune receptor repertoire from millions of lymphocytes," *Nature Protocols*, vol. 11, pp. 429–442, mar 2016.

[155] V. Chokkalingam, J. Tel, F. Wimmers, X. Liu, S. Semenov, J. Thiele, C. G. Figdor, and W. T. Huck, "Probing cellular heterogeneity in cytokine-secreting immune cells using droplet-based microfluidics," *Lab on a Chip*, vol. 13, pp. 4740–4744, dec 2013.

155

[156] T. Konry, M. Dominguez-Villar, C. Baecher-Allan, D. A. Hafler, and M. L. Yarmush, "Droplet-based microfluidic platforms for single T cell secretion analysis of IL-10 cytokine," *Biosensors and Bioelectronics*, vol. 26, pp. 2707–2710, jan 2011.

[157] T. Konry, A. Golberg, and M. Yarmush, "Live single cell functional phenotyping in droplet nano-liter reactors.," *Scientific reports*, vol. 3, p. 3179, 2013.

[158] L. Qiu, F. Wimmers, J. Weiden, H. A. Heus, J. Tel, and C. G. Figdor, "A membrane-anchored aptamer sensor for probing IFNγ secretion by single cells," *Chemical Communications*, vol. 53, no. 57, pp. 8066–8069, 2017.

[159] K. Eyer, R. C. Doineau, C. E. Castrillon, L. Briseño-Roa, V. Menrath, G. Mottet, P. England, A. Godina, E. Brient-Litzler, C. Nizak, A. Jensen, A. D. Griffiths, J. Bibette, P. Bruhns, and J. Baudry, "Single-cell deep phenotyping of IgG-secreting cells for high-resolution immune monitoring," *Nature Biotechnology*, vol. 35, pp. 977–982, oct 2017.

[160] S. Sarkar, "T Cell Dynamic Activation and Functional Analysis in Nanoliter Droplet Microarray," *Journal of Clinical & Cellular Immunology*, vol. 06, no. 03, 2015.

[161] S. Sarkar, P. Sabhachandani, D. Stroopinsky, K. Palmer, N. Cohen, J. Rosenblatt, D. Avigan, and T. Konry, "Dynamic analysis of immune and cancer cell interactions at single cell level in microfluidic droplets," *Citation: Biomicrofluidics*, vol. 10, p. 54115, sep 2016.

[162] A. I. Segaliny, G. Li, L. Kong, C. Ren, X. Chen, J. K. Wang, D. Baltimore, G. Wu, and W. Zhao, "Functional TCR T cell screening using single-cell droplet microfluidics," *Lab on a Chip*, vol. 18, no. 24, pp. 3733–3749, 2018.

[163] T. Gomes, S. A. Teichmann, and C. Talavera-lo, "Immunology Driven by Large-Scale Single-Cell Sequencing," *Trends in Immunology*, pp. 1–11, 2019.

[164] H. J. Jackson, S. Rafiq, and R. J. Brentjens, "Driving CAR T-cells forward," *Nature Reviews Clinical Oncology*, vol. 13, pp. 370–383, jun 2016.

[165] A. Salmaninejad, S. F. Valilou, A. G. Shabgah, S. Aslani, M. Alimardani, A. Pasdar, and A. Sahebkar, "PD-1/PD-L1 pathway: Basic biology and role in cancer immunotherapy.," *Journal of cellular physiology*, vol. 234, pp. 16824–16837, aug 2019.

[166] C. H. June, R. S. O'Connor, O. U. Kawalekar, S. Ghassemi, and M. C. Milone, "CAR T cell immunotherapy for human cancer," *Science*, vol. 359, no. 6382, pp. 1361–1365, 2018.

[167] R. C. Sterner and R. M. Sterner, "CAR-T cell therapy: current limitations and potential strategies," *Blood Cancer Journal*, vol. 11, no. 4, 2021.

[168] R. C. Larson and M. V. Maus, "Recent advances and discoveries in the mechanisms and functions of CAR T cells," *Nature Reviews Cancer*, vol. 21, no. 3, pp. 145–161, 2021.

[169] M. Nauerth, B. Weißbrich, R. Knall, T. Franz, G. Dössinger, J. Bet, P. J. Paszkiewicz, L. Pfeifer, M. Bunse, W. Uckert, R. Holtappels, D. Gillert-Marien, M. Neuenhahn, A. Krackhardt, M. J. Reddehase, S. R. Riddell, and D. H. Busch, "TCR-Ligand k off Rate Correlates with the Protective Capacity of Antigen-Specific CD8 + T Cells for Adoptive Transfer," *Science Translational Medicine*, vol. 5, no. 192, 2013.

[170] S. Bobisse, R. Genolet, A. Roberti, J. L. Tanyi, J. Racle, B. J. Stevenson, C. Iseli, A. Michel, M.-A. Le Bitoux, P. Guillaume, J. Schmidt, V. Bianchi, D. Dangaj, C. Fenwick, L. Derré, I. Xenarios, O. Michielin, P. Romero, D. S. Monos, V. Zoete, D. Gfeller, L. E. Kandalaft, G. Coukos, and A. Harari, "Sensitive and frequent identification of high avidity neo-epitope specific CD8+ T cells in immunotherapy-naive ovarian cancer," *Nature Communications*, vol. 9, no. 1, p. 1092, 2018.

[171] M. Hebeisen, S. G. Oberle, D. Presotto, D. E. Speiser, D. Zehn, and N. Rufer, "Molecular insights for optimizing T cell receptor specificity against cancer," *Frontiers in Immunology*, vol. 4, pp. 1–10, jun 2013.

[172] D. A. Schmid, M. B. Irving, V. Posevitz, M. Hebeisen, A. Posevitz-Fejfar, J.-C. F. Sarria, R. Gomez-Eerland, M. Thome, T. N. M. Schumacher, P. Romero, D. E. Speiser, V. Zoete, O. Michielin, and N. Rufer, "Evidence for a TCR Affinity Threshold Delimiting Maximal CD8 T Cell Function," *The Journal of Immunology*, vol. 184, no. 9, pp. 4936–4946, 2010.

[173] K. Woodruff and S. J. Maerkl, "A High-Throughput Microfluidic Platform for Mammalian Cell Transfection and Culturing," *Scientific Reports*, vol. 6, p. 23937, mar 2016.

[174] N. Otsu, "A Threshold Selection Method from Gray-Level Histograms," *IEEE Transactions on Systems, Man, and Cybernetics*, vol. C, no. 1, pp. 62–66, 1979.

157

[175] A. Edelstein, N. Amodaj, K. Hoover, R. Vale, and N. Stuurman, "Computer control of microscopes using manager," *Current Protocols in Molecular Biology*, vol. 92, pp. 14.20.1–14.20.17, oct 2010.

[176] F. Jammes, J. Schmidt, G. Coukos, and S. J. Maerkl, "High-throughput single-cell tcr - pmhc dissociation rate measurements performed by an autonomous microfluidic cellular processing unit," *bioRxiv*, 2021.

[177] R. Gómez-Sjöberg, A. A. Leyrat, D. M. Pirone, C. S. Chen, and S. R. Quake, "Versatile, fully automated, microfluidic cell culture system," *Analytical Chemistry*, vol. 79, no. 22, pp. 8557–8563, 2007.

[178] T. Sun and H. Morgan, "Single-cell microfluidic Impedance cytometry: A review," *Microfluidics and Nanofluidics*, vol. 8, no. 4, pp. 423–443, 2010.

[179] X.-D. Zhu, J. Chu, and Y.-H. Wang, "Advances in Microfluidics Applied to Single Cell Operation," *Biotechnology Journal*, 2017.

[180] L. Mazutis, J. Gilbert, W. L. Ung, D. A. Weitz, A. D. Griffiths, and J. A. Heyman, "Single-cell analysis and sorting using droplet-based microfluidics," *Nature Protocols*, vol. 8, no. 5, pp. 870–891, 2013.

[181] J. R. Choi, "Advances in single cell technologies in immunology," *BioTechniques*, vol. 69, no. 3, pp. 227–236, 2020.

[182] A. Gérard, A. Woolfe, G. Mottet, M. Reichen, C. Castrillon, V. Menrath, S. Ellouze, A. Poitou, R. Doineau, L. Briseno-Roa, P. Canales-Herrerias, P. Mary, G. Rose, C. Ortega, M. Delincé, S. Essono, B. Jia, B. Iannascoli, O. Richard-Le Goff, R. Kumar, S. N. Stewart, Y. Pousse, B. Shen, K. Grosselin, B. Saudemont, A. Sautel-Caillé, A. Godina, S. McNamara, K. Eyer, G. A. Millot, J. Baudry, P. England, C. Nizak, A. Jensen, A. D. Griffiths, P. Bruhns, and C. Brenan, "High-throughput single-cell activity-based screening and sequencing of antibodies using droplet microfluidics," *Nature Biotechnology*, vol. 38, pp. 715–721, jun 2020.

[183] S. Rafiq, C. S. Hackett, and R. J. Brentjens, "Engineering strategies to overcome the current roadblocks in CAR T cell therapy," *Nature Reviews Clinical Oncology*, vol. 17, pp. 147–167, mar 2020.

[184] M. Irving, V. Zoete, M. Hebeisen, D. Schmid, P. Baumgartner, P. Guillaume, P. Romero, D. Speiser, I. Luescher, N. Rufer, and O. Michielin, "Interplay between T cell receptor binding kinetics and the level of cognate peptide presented by major histocompatibility complexes governs CD8+ T cell responsiveness," *Journal of Biological Chemistry*, vol. 287, pp. 23068–23078, jun 2012.

[185] M. Hebeisen, J. Schmidt, P. Guillaume, P. Baumgaertner, D. E. Speiser, I. Luescher, and N. Rufer, "Identification of Rare High-Avidity, Tumor- Reactive CD8+ T Cells by Monomeric TCR–Ligand Off-Rates Measurements on Living Cells," *American Association for Cancer Research*, 2015.

[186] R. Vazquez-Lombardi, J. S. Jung, F. Bieberich, E. Kapetanovic, E. Aznauryan, C. R. Weber, and S. T. Reddy, "Crispr-targeted display of functional t cell receptors enables engineering of enhanced specificity and prediction of cross-reactivity," *bioRxiv*, 2020.

[187] J. Boonyaratanakornkit and J. J. Taylor, "Techniques to Study Antigen-Specific B Cell Responses," *Frontiers in immunology*, vol. 10, no. July, p. 1694, 2019.

Fabien Jammes

Avenue Du Tir Fédéral 48 | 1024 Ecublens, Switzerland
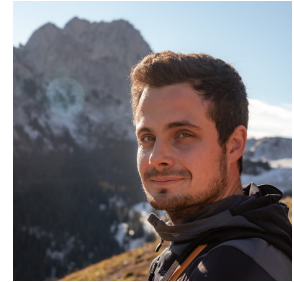+41 78 909 06 25
jammes.fab@gmail.com

in jammesfabien

STRENGTHS

- Microfluidics devices fabrication & characterization
- Programming, data analysis & visualization
- Project management in multi-cultural environment

EDUCATION

2017 – 2021 **Swiss Federal Institute of Technology, Lausanne (EPFL)**
PhD in Biotechnology & Bioengineering

2014 – 2017 **Swiss Federal Institute of Technology, Lausanne (EPFL)**
Master of Science in Life Sciences Engineering
- Academic exchange year at Massachusetts Institute of Technology (MIT), Boston

2011 – 2014 **Swiss Federal Institute of Technology, Lausanne (EPFL)**
Bachelor of Science in Life Sciences Engineering

CORE EXPERIENCE

03.2017 – 08.2021 **Laboratory of Biological Network Characterization (LBNC), EPFL** *Lausanne, Switzerland*
RESEARCH ASSISTANT
"A novel microfluidic platform for single-cell analysis of lymphocytes for cancer immunotherapy"
Development of an innovative, fully autonomous microfluidic platform for single-cell analysis of immune cells for cancer immunotherapy. This technology could lead to new, more effective immunotherapy treatments. Collaboration between EPFL, Ludwig Cancer Research Institute and CHUV, mixing biologists, clinicians and engineers.
- Development of an innovative microfluidic technology, its automation and integration (Clean room, microfabrication)
- Data and image analysis, data classification & visualization, machine learning (CNN, Tenserflow, Python & Matlab)
- Project management (timeline & budget, PRINCE 2) ; scientific publications & patent pending

03.2016 – 12.2016 **Langer Lab, Koch Institute for Integrative Cancer Research, MIT** *Boston, MA USA*
VISITING STUDENT
"Stem cell-derived extracellular matrices as cell culture substrates"
Innovative proteomics study of extracellular matrices from human mesenchymal stem cells as potential novel cell culture substrates. This approach helped identifying key extracellular proteins for stem cell culture in vitro.
- Stem-cell culture & manipulation; Proteomics; fluorescent microscopy
- Multicultural and interdisciplinary experience

09.2015 – 02.2016 **Stemedica International** *Lausanne, Switzerland*
RESEARCH INTERNSHIP
"The implication of mesenchymal stem cells and microbiota for Alzheimer's disease"
Study of the role of microbiota for Alzheimer's disease and the role of mesenchymal stem cells with inflammation. Establishment of new laboratory including price negotiation, budget management, chemical storage management.
- Setup of a new laboratory with instruments acquisition & budget management
- Animal work (mice)

ADDITIONAL EXPERIENCE

03.2017 – 08.2021 **Laboratory of Biological Network Characterization (LBNC), EPFL** *Lausanne, Switzerland*
SAFETY OFFICER *(CONCURRENT WITH RESEARCH ASSISTANT)*
In charge of coordinating safety procedures and direct correspondance with the safety department at EPFL. Stock and waste management in the laboratory. Received safety training (EPFL, FOBS 1 & 2).

09.2014 – 06.2015 **De Palma's lab (ISREC), EPFL** *Lausanne, Switzerland*
RESEARCH INTERNSHIP
"The role of miRNA in macrophages regulation in tumor microenvironment"
- Flow cytometry; IHC/IF; Cell culture; Animal work (mice); Image analysis

Sgouros's lab, Johns Hopkins *Baltimore, MD, USA*
RESEARCH INTERNSHIP
"Anti-PD-L1 antibody radioconjugates for Imaging and Radiopharmaceutical therapy (RPT)"
  ● Flow cytometry; Cell culture; Animal work (mice); Cytotoxicity studies; Data analysis

PROFESSIONAL EXPERTISE

■ **Data analysis & Programming**
  ● Data classification (Python Scikit, Numpy, Pandas)
  ● Data Visualization / Image analysis (Matlab, Python Plotly, Dash, Matplotlib, Seaborn)
  ● Object detection (ACF detector, CNN; Matlab, Python, Tenserflow)
  ● Statistics (Matlab, Python, GraphPad Prism)

■ **Microfabrication, Microtechnology & Medical devices**
  ● Design of microfluidic devices (AutoCAD, Clewin, KLayout)
  ● Microfabrication (Clean room, photolithography processes, PDMS)
  ● Microfluidics implementation & integration (hardware-software interface, MATLAB GUI)
  ● Fluorescence microscopy (integration with microfluidics and coupled image analysis)

■ **Wet lab**
  ● Mammalian cell culture (primary, stem cells) ; cell transfection
  ● Flow cytometry / FACS
  ● IF/IHC ; DNA/RNA extraction ; Western Blot ; qPCR
  ● Animal work (mice, IP/IV injection)
  ● Safety training & Chemical/Waste management (EPFL training FOBS 1&2)

■ **Project management**
  ● Prince 2 certification (2019)
  ● Interdisciplinary/multicultural collaboration (EPFL/CHUV/Ludwig Cancer Research Institute)
  ● Budget & timeline management (PhD thesis grant & project execution)
  ● Supervision of MSc students (introduction to clean room, machine learning projects)

■ **Science communication**
  ● Technical writing (report, review & publication)
 ● Presentation skills (target audience both specialist & general public)

■ **IT**
  ● Programming & Data analysis: Matlab; Python; good notion in C/C++; GraphPad Prism
  ● Microfabrication: AutoCAD, Clewin, KLayout
  ● Adobe Illustrator, InDesign, Lightroom, Photoshop
  ● Microsoft Office (Excel, Powerpoint, Word)

EXTRACURRICULAR ACTIVITIES

■ **Sport** Climbing; Skiing (Ski teacher 2010-2011); Hiking; Yoga; Swimming (competition); Basketball (competition)

■ **Nature** Traveling, marine wildlife conservation, whale watching

■ **Photo** Landscape photography, astrophotography

■ **Student life** Committee member of a student sport association «PolyBeach» & involved in different student activities

LANGUAGES

FRENCH **ENGLISH** **GERMAN**
Native *Fluent (C2)* *Notion (A2/B1)*
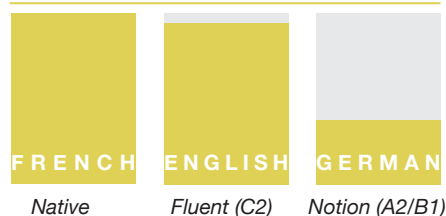
PERSONAL INFORMATION

● 27
● Single
● French citizenship
● Swiss Resident (B permit, since 2011)
● Swiss driver's licence (Type B)

2